IONOSPHERIC HEATING ANALYSIS

William E. Gordor, et al

Rice University

Prepared for:

Rome Air Development Center
Advanced Research Projects Agency

April 1974

RADC-TR-74-124
Final Technical Report
April 1974

IONOSPHERIC HEATING ANALYSIS

William Marsh Rice University

Sponsored By;
Defense Advanced Research Projects Agency
ARPA Order No. 1423

Approved for public release:
distribution unlimited.

The views and conclusions contained in this document are those of the authors and should not be interpreted as necessarily representing the official policies, either expressed or implied, of the Defense Advanced Research Projects Agency or the U. S. Government.

Rome Air Development Center
Air Force Systems Commond
Griffiss Air Force Bose, New York

ib

UNCLASSIFIED

SECURITY CLASSIFICATION OF THIS PAGE *(When Data Entered)*

AD-781 178

REPORT DOCUMENTATION PAGE

READ INSTRUCTIONS BEFORE COMPLETING FORM

1. REPORT NUMBER: RADC-TR-74-124	2. GOVT ACCESSION NO.
3. RECIPIENT'S CATALOG NUMBER	
4. TITLE *(and Subtitle)*: IONOSPHERIC HEATING ANALYSIS	5. TYPE OF REPORT & PERIOD COVERED: Final Technical Report
6. PERFORMING ORG. REPORT NUMBER: N/A	
7. AUTHOR(s): William E. Gordon, Herbert C. Carlson	8. CONTRACT OR GRANT NUMBER(s): F30602-72-C-0278
9. PERFORMING ORGANIZATION NAME AND ADDRESS: William Marsh Rice University, Houston, TX 77001	10. PROGRAM ELEMENT, PROJECT, TASK AREA & WORK UNIT NUMBERS: 62301E, 14233001
11. CONTROLLING OFFICE NAME AND ADDRESS: Advanced Research Projects Agency, 1400 Wilson Boulevard, Arlington, VA 22209	12. REPORT DATE: April 1974 13. NUMBER OF PAGES: 107
14. MONITORING AGENCY NAME & ADDRESS *(if different from Controlling Office)*: Rome Air Development Center (OCSE), Griffiss Air Force Base, New York 13441	15. SECURITY CLASS. *(of this report)*: UNCLASSIFIED 15a. DECLASSIFICATION/DOWNGRADING SCHEDULE: N/A

16. DISTRIBUTION STATEMENT *(of this Report)*

Approved for public release; distribution unlimited.

17. DISTRIBUTION STATEMENT *(of the ebstract entered in Block 20, if different from Report)*

Same

18. SUPPLEMENTARY NOTES

Monitored by;
Frederick C. Wilson (OCSE)
RADC, GAFB, NY 13441

19. KEY WORDS *(Continue on reverse side if necessary and identify by block number)*

Ionosphere
Electron Density
Wave Propagation
Plasma Temperature
Ionospheric Heating
Plasma Instabilities
Radio Heating of the Ionosphere

20. ABSTRACT *(Continue on reverse side if necessary and identify by block number)*

Enhancements of various features of the incoherent scatter spectrum are observed when the ionosphere is illuminated with powerful, high-frequency radio waves. The radio waves excite plasma instabilities producing lines or more complex spectral features near the local plasma frequency, at the local ion-acoustic frequency, near the local gyrofrequency and twice the gyrofrequency. The enhancements occur in a thin slab as observed by the incoherent scatter

DD FORM 1 JAN 73 1473 EDITION OF 1 NOV 65 IS OBSOLETE

UNCLASSIFIED

SECURITY CLASSIFICATION OF THIS PAGE *(When Data Entered)*

radar and at both upshifted and downshifted frequencies with respect to the probing radar frequency. The enhancements are observed to vary with time when the high frequency transmitter that produces the radio wave excitation is held at constant power, and to vary with time as the high frequency transmitter is turned on or off.

The powerful radio waves are produced by a 160 kilowatt transmitter feeding a logperiodic set of curtains mounted at the focus of the 1000-foot reflector in the frequency range 5 to 12 megahertz. The effects are observed with the incoherent scatter radar using the same reflector, by ionosondes nearby, and by photometers.

The frequencies of the plasma line and the ion line and their relation to the pump (high frequency radio wave) frequency were predictable from available parametric instability theory. Other spectral features are being explained as the theory develops with the help of the observations. There remain some discrepancies, in particular the asymmetries in intensity, width, fluctuations and decay rates of the upshifted compared to the downshifted plasma lines.

The Appendix contains a collection of spectra observed under various conditions.

IONOSPHERIC HEATING ANALYSIS

William E. Gordon
Herbert C. Carlson

Contractor: William Marsh Rice University
Contract Number: F30602-72-C-0278
Effective Date of Contract: 1 December 1971
Contract Expiration Date: 31 May 1973
Amount of Contract: $112,113.00
Program Code Number: 2E20

Principal Investigator: William E. Gordon
Phone: 713 528-4141, Ext 475

Project Engineer: Vincent J. Coyne
Phone: 315 330-3141

Contract Engineer: Frederick C. Wilson
Phone: 315 330-3085

This research was supported by the Defense Advanced Research Projects Agency of the Department of Defense and was monitored by Frederick C. Wilson RADC (OCSE), GAFB, NY 13441 under Contract F30602-72-C-0278

PUBLICATION REVIEW

This technical report has been reviewed and is approved.

Frederick C Wilson

RADC Project Engineer

FOREWORD

The ionospheric heating experiments described in this report were conducted at the Arecibo Observatory operated by Cornell University at Arecibo. They have been performed by W. E. Gordon and H. C. Carlson with the scientific collaboration of R. A. Behnke, T. Hagfors and J. F. Rowe from the Arecibo Observatory; I. J. Kantor, D. M. Kim, A. R. Laird, L. Dias and F. Schwab from Rice University; R. L. Showen from the University of Puerto Rico, Mayaguez; M. Biondi and D. Sipler from the University of Pittsburgh; and V. B. Wickwar from Yale University and Rice University. Engineering and technical support was provided by D. Albino, R. B. Dyce, M. A. Feyjoo, D. VanWinkle, J. Maldonado and R. Towers from the Arecibo Observatory; L. M. LaLonde, D. T. Farley, J. Hagen, G. Ioannides and C. Zamlutti from Cornell University; W. Utlaut and J. Carroll from the National Oceanic and Atmospheric Administration in Boulder; and R. Tanner from Technology for Communications International. The observations summarized here would not have been possible without the cooperation and assistance of all of the above people as well as those at Rome Air Development Center and the Advanced Research Projects Agency. Mr. A. Van Every at ARPA provided the encouragement and the support over many years that produced these results.

IONOSPHERIC HEATING ANALYSIS

SUMMARY

Enhancements of various features of the incoherent scatter spectrum are observed when the ionosphere is illuminated with powerful, high-frequency radio waves. The radio waves excite plasma instabilities producing lines or more complex spectral features near the local plasma frequency, at the local ion-acoustic frequency, near the local gyrofrequency and twice the gyrofrequency. The enhancements occur in a thin slab as observed by the incoherent scatter radar and at both upshifted and downshifted frequencies with respect to the probing radar frequency. The enhancements are observed to vary with time when the high frequency transmitter that produces the radio wave excitation is held at constant power, and to vary with time as the high frequency transmitter is turned on or off.

The powerful radio waves are produced by a 160 kilowatt transmitter feeding a log-periodic set of curtains mounted at the focus of the 1000-foot reflector in the frequency range 5 to 12 megahertz. The effects are observed with the incoherent scatter radar using the same reflector, by ionosondes nearby, and by photometers.

The frequencies of the plasma line and the ion line and their relation to the pump (high frequency radio wave) frequency were predictable from available parametric instability theory. Other spectral features are being explained as the theory develops with the help of the observations. There remain some discrepancies, in particular the asymmetries in intensity, width, fluctuations and decay rates of the upshifted compared to the downshifted plasma lines.

The Appendix contains a collection of spectra observed under various conditions.

IONOSPHERIC HEATING ANALYSIS

INTRODUCTION

The heating experiments at Arecibo have yielded a number of interesting results derived from the normal absorption of radio waves in the ionosphere[1-3] and from the anomalous absorption of the high-frequency (5-10 MHz) waves and the excitation of plasma instabilities.[4-6] The results are summarized below.

O-mode heating of the ambient electrons has been detected. Deviative absorption ray tracing, and heat-balance calculations are consistent with: the magnitude of the increase, typically peaking at 150° to 400°K, with the higher values at night; the location, typically 4° to 9° north of the Observatory; the volume, matched to the beam when mapped in two or three dimensions; and thermal relaxation times of a few tens of seconds. The ion temperature is unchanged within error bars of tens of degrees K.

The HF excited plasma line exhibits spectral features (decay-mode line, growing-mode line, image of decay-mode line), most of which can be explained by linear parametric theory. Observation of an additional broad spectral feature has led to extension of the nonlinear theory. Some features are not as yet explained. The decay times are consistent with the wave-damping theory and offer a new tool for collision frequency and photoelectron studies. Airy structure in the vicinity of HF reflection has been observed, consistent with theory. Fluctuations of the plasma-line intensities over two orders of magnitude show distribution functions suggesting upper-threshold saturation in the ionospheric plasma for higher HF transmitted power levels. Ion-component spectra have been measured and seem to be consistent with the theory. Additional spectra are available for study in the Appendix.

Red-line enhancement and suppression in the airglow have been observed. Suppression of roughly one percent is observed in association with extraordinary-mode excitation of the plasma, implying a temperature-dependent reduction in the recombination rate. Enhancement of one to ten rayleighs is observed in association with ordinary-mode excitation of the plasma, implying an increase through energetic-electron-impact excitation of the airglow. The rise and fall times of these enhancements are substantially less than the O^1D-state lifetime, so quenching rates of the airglow emission can be found.

The Boulder and Arecibo ionograms during heating experiments exhibit the same general characteristics, although the details vary and are probably related to field-line geometry and incident-power differences.

In addition to enhancements of the plasma at and near the plasma-line frequency and at the ion-line frequency, enhancements have been observed at the electron gyrofrequency and at twice this frequency[7] (see Table 1).

NORMAL ABSORPTION

Heating Effects

The effects of the deposition of radio-wave energy on electron temperature, ion-temperature, electron number density, and velocity are discussed here. Parameters important in determining heating effects are the transmitted power, polarization, HF frequency, ionospheric critical frequency, temperature, altitude, and time of day (HF absorption in D and E region).

Table 1

HF EXCITATION

Ionospheric Effects Observed	Ordinary Mode	Extraordinary Mode	Interpretation
Electron heating			
Temperature increase	R	W	A
Time constants	R	N	A
Ionograms (n=night, d=day)	O-echo X-echo	O-echo X-echo	
Split traces	R R	R R	
Attenuation	R S	R(n),S(d) R(n),S(d)	
Branched penetrating freq.	R R(n),S(d)	R R	
F-region enhancements			
Plasma lines	R	S	A
Features near plasma lines	R	S	T
Ion Line	W	S	T
Gyroline	W	N	T
Asymmetries of up/down shifted plasma lines	R	S	U
Rise times of plasma lines	R	N	T
Fall times of plasma lines	R	N	A
Threshold of instability	R	N	T
Ringing of plasma line	R	N	T
Bernstein mode		W?	T
E-region enhancements			
Sporadic-E plasma line	W	N	T
Photometer			
Enhancement of 6300-Å line	R	S	A
Suppression of 6300-Å line	N	W	A

R = Regularly observed
W = Observed weakly
S = Searched for but not observed
N = No search

A = Agrees with generally accepted theory
T = Theoretical explanation available
U = Explanation unavailable

Figure 1 shows contours of electron temperatures when the ordinary mode was reflected. The backscatter data begins after the heater has been on for half an hour. Notice that the electrons are heated at and below the altitude where the heating wave reflects. After the heater is turned off, the electrons relax to their ambient temperature of 850° to 950°K. The time resolution here is 8 minutes, the altitude resolution is 30 km, and the accuracy in the electron measurement is better than 30°K. The plasma velocity was measured, but no velocity changes could be correlated with the temperature effects.

There is some danger that backscatter data presented for the O-mode reflecting case will be contaminated by the presence of the parametric instability generated at the reflection altitude. However, the instability comes from an exceedingly narrow altitude range (less than 300m), and the interrogating pulse lengths of 30 or 45 km normally used for temperature analysis usually cause the power from the instability to be swamped with a large backscatter echo.

An example of the difference in heating effect between penetrating and reflecting cases is given in Figure 2. For the penetrating case on the left, the F layer is heated near the peak, while on the right, only electrons at and below the reflection altitude of 294 km are significantly heated. The cubes show several items simultaneously. The front face graphs heater power for each time block, as well as the heater frequency and f_oF_2 versus time. The top face gives the electron temperature for each time block integrated in altitude over the entire F layer. The right face of each cube shows two plots: the lowest temperature plot is the time average of all the unheated data blocks, and the other plot is the average of the heated blocks. The most striking result here is the abrupt cutoff of the heating above the

reflection altitude, and also the fact that the heating is greater for the reflecting case.

An experiment was made with the heater power changed from zero to half to full power. The results are given in Figures 3 and 4. Figure 3 shows electron and ion temperature versus altitude for the three power levels. The effect of 100 kW on the electrons is not quite double the effect of 50 kW. The error in T_e is less than 20°K, and errors for T_i are about 40°K. The ions do appear to be heated, but no firm conclusions can be drawn since the apparent magnitude of heating is less than the expected errors. Also note that the T_i for 100 kW is the same as for 50 kW, and that the apparent ion heating is above the region of close thermal coupling to neutrals. Figure 4 presents T_e and T_i versus time, averaged in altitude from 294 to 348 km. The vertical bars indicate the heater power. The electron temperature tracks remarkably well with the HF power, and, when the power is off, the ambient temperature resumes faster than the time between samples, which is 6 min. Here again there is a hint that T_i might follow the HF power. In a preliminary calculation (Showen and Gomez, private communication) for this experiment, the expected change in T_i was predicted to be 1/8 the change in T_e. This small amount of ion-temperature increase could not be detected with the present errors, nor could the ambient ionospheric temperatures be expected to remain constant to within these tolerances.

The extent of the O-mode heating has been determined by making maps in the magnetic meridian where the O-mode radio wave deviates toward the north. The ambient temperature is first measured, and then the heater is turned on while the interrogating beam is swung from about 4° north to 10° north (angles directly overhead are blocked out by the heater antenna). Figure 5 shows such a map, with a heated region

centered 35 km to the north of the observatory at an altitude of 320 km. To determine possible heating out of the meridian plane, a measurement to the west was made, and little heating is indicated there. The run illustrated here is for the reflected case, but penetrating cases show similar results, if the heater frequency is well matched to f_oF_2. No heating has been observed when the heater frequency is more than 1 MHz above f_oF_2. The line labeled B is the magnetic field line that passes through the center of the heated volume. From thermal-conductivity considerations, the heated region is expected to be elongated along B.

The inherent variability of the ionosphere has precluded measuring induced changes in electron number density during most of the experiments. During one run the heater was cycled on and off at 10-minute intervals; the electron temperature increased by 23%, and at the same time the electron density decreased by 14%.

During the day the HF heating observations to date have not exceeded a 50°K change.

Time Constants

The electron thermal time constant in the F-region is of the order of tens of seconds, and can be calculated from the energy loss rates to ions and neutral particles. The necessary accuracy plus time resolution in the backscatter data can be achieved only by superposition of several on/off heating cycles. A representative example of such a run is given in Figure 6. At HF transmitter turn-on, the temperature rises abruptly, and both rise and fall times for this example are approximately 20 s. The time between the data points is initially 1.5 s, then changes to 4.5 s.

ANOMALOUS ABSORPTION

Plasma-Line Enhancements

When the ionospheric F region is illuminated with a strong O-mode HF radio wave, excitations of longitudinal plasma and acoustic waves are observed by radar scattering. HF enhanced plasma lines were first observed at the Arecibo Observatory in 1971.[4] A summary of the observations is given by Kantor.[5] The decay line, the growing mode, and image of the decay line are identified and associated with the components of parametric instabilities. The broad line has been recently interpreted by Kruer and Valeo,[8] and Kuo and Fejer.[9] Asymmetries between the upshifted and downshifted plasma lines are observed but no explanation has been found. The peak amplitude of the growing mode and the broad line is approximately proportional to the peak amplitude of the decay line. The thickness of the layer producing the observed plasma line is less than 300 m.

Enhancement rise times after HF turn-on have been found to be on the order of tens of milliseconds and show a ringing of the plasma. The period of the ringing was about 8 ms on two measurements made under the same conditions. This ringing may be the same found by Kruer and Valeo.[8]

Decay times of the plasma-line intensity after HF turnoff are about 0.3 to 1 ms, consistent with the linear theory for the frequency range studied. They are primarily due to wave damping by photoelectrons, and are shortest for those waves going in the direction of the largest flux. This has obvious application to photoelectron-flux studies. At night the decay rates are slower by a factor of roughly 2 to 10, again consistent with the linear theory, primarily due to electron-ion collisions. No significant nonlinear damping has been detected yet through decay rate measurements.

There are fluctuations of the enhanced plasma-line intensity over a wide range of time scales. On time scales of hours, the observed severe decrease of intensity near mid-day in the 5-to-6-MHz range of HF frequencies appears to be due to F_1 region absorption. On time scales of tens of minutes, one sunset run showed severe regular periodic fading of the plasma-line intensity, which can be explained[5] in terms of sliding through consecutive maxima and minima of the (Airy function) interference field strength near the reflection height. The rate of fading from one minimum to the next depends on the rate of change of the local density gradient as f_oF_2 approaches the heater frequency f_{HF}. The envelope of the maxima decreases as f_oF_2 approaches f_{HF} (within the last few percent). This is the first time the Airy function has been observed in the ionosphere.

The amplitude of the decay line is observed, at times, to fluctuate almost one order of magnitude above or below its mean value (Ref. 5, Section 6.2). The spectral analysis of the variation of the peak intensity shows sharp resonances. The period of oscillation from all available data sampled every 3 s ranges from 35 s to 3 min. The amplitude distribution of these fluctuations (Figures 7 and 8) gives evidence of saturation in the plasma-line amplitude.[10] Note that the higher SNR edge of the distribution at 80 kW is higher than at 50 kW for the downshifted decay line but it is almost coincident for the upshifted; and, significantly, for both upshifted and downshifted, the lower HF power distribution has a substantially higher low SNR tail. This suggests that the signal is due to plasma waves above threshold in a saturating level. One must first rule out the possibility of saturation (of the plasma-line amplitude) in the receiving system before considering implications of saturation in the ionosphere. Saturation at the receiver/computer interface digitizer is ruled out by examination of

the levels individually recorded in real time on magnetic tape. None of the digits achieved the maximum. Saturation in a stage of the receiving system is harder to detect. Figure 9 is a histogram of the numerical values sampled by the interface. On 1050:00 AST most of the sampling had larger values than at 1051:40 AST. Saturation in any part of the receiving system would flatten the distribution of the numerical value of the 1050:00 AST curve relative to the 1051:40 AST distribution. This exemplifies the conclusion that no saturation is found in the receiving system, indicating that the data shown in Figures 7 and 8 (Ref. 10) represent saturation of the amplitude of the decay line in the ionospheric plasma.

Further investigation of the fluctuation and saturation of the plasma line was done using Barker coded signals. Figure 10 shows an altitude profile with a 900 m resolution of the upshifted and downshifted plasma line and the ion enhancement (see Ion-Line Enhancement below). Again the plasma line showed strong oscillations, and the amplitude probability distribution (Figure 11) had a shape similar to that observed in Figures 7 and 8. The HF transmitted power was reduced and then raised again in 5-min steps between 46 kW and 15 kW. This allowed comparison of the distribution function at the same HF power level but at different times in the half cycle of power steps (roughly 45 kW to 15 kW to 45 kW). The distribution functions at like HF powers were found to differ substantially between the down- and up-half of the series, presumably due to ionospheric variations. This obviates any firm conclusions. The inconclusive high-power-versus-low-power comparison for this entire run is shown in Figure 11. However, during the rising HF power portion of the series, the saturation level and the SNR of the peak of the relative probability distribution of the plasma-line intensities were relatively stable. In this

"relatively stable" time interval, one comparison is available between a 25-kW and a 45-kW power-level run adjacent in time, and is shown in Figure 12. There the lower HF power distributions had a substantially higher low SNR tail, consistent with the earlier results of Figures 7 and 8.

Note that Figures 7 and 8 represent the peak amplitudes of the decay line as measured in a 1-kHz-resolution spectral analysis of the signal, and the HF power was 50 kW and 80 kW. However, Figure 11 gives the peak-power, Barker-decoded plasma-line profile, which is received through a 6-us matched filter, and this contains all the power in about a 170-kHz band centered on the plasma-line peak. The saturation level of 1000 in Figures 7 and 8 corresponds to a saturation level in Figures 11 and 12 of about 6, the ratio of the bandwidths 1 kHz and 170 kHz.

Ion-Line Enhancement

Figure 10 shows an ion enhancement using the Barker coded pulse. Figure 13 shows a plot of the peak power of the ion-enhancement versus the peak power of the upshifted plasma-line, both measured with a height resolution of 900 m. The dashed line represents a square-law dependence

$$\text{Ion enhancement} = 0.04\ (\text{plasma line})^2 .$$

Data seem to follow the square law closely, suggestive of being above threshold.

The ion component shows a highly variable amount of enhancement. On two occasions measurement of the autocorrelation function indicated enhanced correlation beyond the first autocorrelation zero crossing, which indicates

the presence of spikes in the frequency spectrum at the ion acoustic frequency, as is predicted by the parametric theory. The fact that the cross section increases shows that the effect is due to HF enhancement of the ion line and not only temperature increase. The ratio of the second maximum to first minimum in the autocorrelation function also indicates this. On the first occasion the enhancement factor above the background ionospheric echo was about two orders of magnitude (with 600-m resolution). These autocorrelation data, gathered with a relatively crude program are shown in Figure 14. Substantially higher-quality ion-component autocorrelation data have since been gathered showing enhancement factors of about 2 to 5 (with 2.7-km resolution), (C. Zamlutti and T. Hagfors, private communication*). These data are of sufficient quality to permit estimates of the width of the apparent spikes on the ion spectral wings.

Gyroline Enhancements

The purpose of this subsection is to summarize the observations of the enhanced electron cyclotron line, which was seen for the first time in the spectrum of the backscattered echo during the Arecibo heating experiment. Concommitantly with the plasma-line enhancements, a new parametric instability was detected near the electron gyrofrequency and possibly its second harmonic. Our observed-power-spectrum data show a noticeable peak near the second-harmonic gyrofrequency, consistently above the statistical fluctuations of the measurements. However, since the SNR is small, and its line-width extremely narrow, the quantitative measurement of its characteristics is not possible at the present time. These new lines plus their harmonics are interpreted in terms of their threshold conditions and growth rates.[7]

---

* T. Hagfors and C. Zamlutti, "Observations of Enhanced Ion Line Frequency Spectrum During Arecibo Ionospheric Modification Experiment," to appear in Proceedings of 19th Technical Meeting of the Electromagnetic Wave Propagation Panel of the Advisory Group for Aerospace Research and Development, NATO, Edinburgh, Scotland, November 12-16, 1973.

From the analysis of the upshifted backscattered signal, the following results are obtained: (1) A new instability (and the existence of its second harmonic) around the electron gyrofrequency, having a full width at half maximum point of about 1 kHz, is detected unambiguously during certain runs. (2) The center frequency of the observed lines is seen to change. Since this change in frequency is much larger than the corresponding line width, it can be concluded that the gyroline comes from a thin layer. This change can be attributed to (a) the ionosphere changing in that layer, (b) the earth's magnetic field changing, or (c) some parameters affecting this instability changing. Note that this gyroline is sampled simultaneously with the enhanced plasma line, and that both lines seem to come from the same height. These results are summarized in Figure 15.

Airglow Observations

Both red-line enhancements and suppressions have been observed. X-mode suppressions of roughly one percent (out of 120 rayleighs) have been obtained, consistent with the temperature dependence of the recombination rate. O-mode enhancements have been observed of about 1 to 10 rayleighs offering both HF-power and enhancement-altitude-dependence information. (Figure 16).

6300-Å airglow enhancements were observed at Arecibo in October, coincident with the HF excitation of the ionospheric plasma waves. These manifestations of the plasma waves produced by the anomalous HF heating help better confirm and define the damping mechanisms, particularly with coincident plasma-line-decay-rate data. The airglow enhancement is also another indication that the Arecibo facility can deliver above-threshold power densities (airglow enhancements were

seen at a factor of 4 below available Arecibo transmitted power levels), given that the stronger airglow enhancements were comparable with those seen at Boulder.

The airglow enhancements are attributed to impact excitation by energetic (order of several eV) electrons driven by enhanced plasma waves. The airglow enhancements were measured for various powers (power dependence) and over a range of altitudes (altitude dependence of enhancement efficiency and decay rates). Simultaneous plasma-line-intensity data (plasma wave temperature) were also gathered, providing further information on the energy and altitude dependence of these enhancements. Decay rates of these 6300-Å enhancements should help define quenching coefficients and molecular-nitrogen number densities in the upper atmosphere, a qualitatively new technique afforded by the heating experiment.

IONOGRAMS -- ARECIBO AND BOULDER

F Region

Utlaut and Cohen[11] list effects observed on ionograms due to HF-radio-wave modification of the ionosphere. The five effects in their tabulation are listed first in Table 2. They are pertinent to ionograms and particularly to the Boulder (geomagnetic 49°N, 316°E) facility. Table 2 is an expanded version of their tabulation and includes results from ionograms at Arecibo (geomagnetic 30°N, 2°E). The symbols are defined as follows:

+	Positive results
-	Negligible effect
O	Results to date not completely conclusive
U	Information not yet available
?	Not explicitly covered in publications.

Table 2

HF IONOSPHERE MODIFICATION AT BOULDER AND ARECIBO

Effect No.	Effects on Ionograms	O-Excitation				X-Excitation			
		Day		Night		Day		Night	
		B	A	B	A	B	A	B	A
1	Spread O-echo	+	+	+	+	+	+	+	+
2	Spread X-echo	+	+	+	+	+	+	+	+
3	Attenuation of O-echo	O	+	+	+	O	O	-	+
4	Attenuation of X-echo	O	O	-	-	O	O	-	+
5	Delayed broadband echo	O	O	+	+	O	O	+	O
6	Branched penetrating frequency--O	?	+	+	+	?	+	+	+
7	Branched penetrating frequency--X	?	U	+	+	?	+	+	+
8	Frequency gap or attenuation of 1st or 2nd multiple	?	+	+	+	?	+	+	+
9	Possible E-region effects	+	+	+	+	?	U	?	U

Legend:

B Boulder
A Arecibo

\+ Positive results
\- Negligible effect

O Results to date not completely conclusive
U Information not yet available
? Not explicitly covered in publications

Effects 6 through 8 are listed because of the detailed description of their occurrence at Boulder by Utlaut and Violette,[12] who also observed short-lived sporadic-E echoes, possibly connected with HF heating.

Both HF transmitters radiate either O-mode or X-mode waves to the ionosphere, which are deflected from vertical due to the effects of the magnetic field. An ionosonde located at the same site as the transmitter and sounding vertically at the heating frequency, should obtain echoes from about the same area of the ionosphere that the heater is illuminating. This is the case at Arecibo, but at Boulder the heater and ionosonde are separated by about 26 km. (This distance is well within the radius of the area heated, but several Fresnel zones removed from the center of the heating beam.) Effects seen on the ionograms from the two locations differ in detail because of the different ionosonde and antenna equipment in use, and possibly because of the different magnetic dip-angles, the different characteristics of the HF transmitters, and the distance between the ionosonde and transmitter at Boulder.

The first two effects listed in Table 2 -- spread O and spread X echo -- are observed on ionograms at both locations, both day and night, and with O-mode or X-mode HF excitation. There appears to be little difference in the observations made at the two locations for these effects.

In the case of attenuation, however, there may be some real difference between O-mode and X-mode excitations and between Boulder and Arecibo observations. For Arecibo, daytime attenuation of the ordinary mode above the heating frequency is well observed for O excitation; for Boulder, the results are inconclusive. Consistent daytime attenuation of the O-echo due to X-mode excitation has not been seen at either location. At Boulder, nighttime O-echo

attenuation due to the X-mode excitation is reported to be negligible; at Arecibo, it is more pronounced. The observations of X-echo attenuation are more consistent (i.e., inconclusive or negligible) for both locations, the exception being that X-echo attenuation at night with X-mode excitation appears to be more pronounced at Arecibo than at Boulder.

It is not clear from published material whether branched O-echoes or X-echoes near penetrating frequencies have been observed at Boulder for daytime O-mode or X-mode excitation, but at Arecibo there is an observation of both effects with X-mode excitation, and an observation of a split trace near the O critical frequency with O-mode excitation. The effect is observed at both locations at night for both modes of excitation.

The frequency gap in, or attenuation of, the first multiple reported by Utlaut and Violette is also observed at Arecibo, where the greater virtual-height range of the ionograms (0 to 1000 km) displays the second multiple return, which often shows complementary effects. Daytime observations are reduced at either location due to D-region absorption.

Possible E-region effects of HF heating include a short-lived enhancement of the top frequency of E_s layers seen at both locations, attenuation of E-region echoes, and on one occasion at Arecibo what appeared to be production of "range-type spread" in an intense natural sporadic E layer (see next subsection).

The agreement between observations at Boulder and Arecibo indicates that there is little qualitative difference in the response of the ionosphere to HF heating.

The interpretation of the ionograms as modified by the heating transmitter is tentatively as follows:

(1) Effects 1 and 2 in Table 2 are thought of as an enhancement in the fluctuations of electron density generated at the height associated with the plasma line and propagated both upward and downward in height. The increased fluctuations produce a scattering of the HF signals, giving a spread appearance to the ionogram trace.

(2) Effects 3 and 4 of Table 2, the attenuation of the ionosonde echo at frequencies above the heater frequency, are thought of as a layer of anomalous absorption at the height where the plasma line is excited. The HF signal passing through this layer (the signals at frequencies above the heater frequency) suffer an extra attenuation.

(3) Effects 6, 7 and 8 of Table 2 are thought of as produced by a bubble in the electron density contours introduced at the height where the plasma is heated and conducted to other heights. The ionosonde observes one profile through the bubble and a second in the ambient ionosphere simultaneously, leading to pairs of traces on the ionograms.

Sporadic E Layers

Utlaut and Violette (1972) reported short-lived E-region echoes on ionograms from frequencies above f_oF_2 in connection with RF ionosphere modification experiments at Boulder. The returns appeared to be from sporadic E layers that blanket (obscure) the F region only below the E-region critical frequency (2 to 4 MHz). It was stated that due to the normal variability of the E region, particularly sporadic-E occurrence, the high-frequency returns could not definitely be associated with the ionosphere modification experiment.

Similar sporadic E echoes have been observed at Arecibo, in association with the ionosphere modification program there, but the effects, as at Boulder, are not reproducible to the extent that they can definitely be related to the heating experiment. On two occasions during ionosphere modification experiments an intense, blanketing natural sporadic E layer developed. On one of these occasions, HF-enhanced plasma line echoes at 5 MHz were observed in one patch (but not in other patches) of a sporadic E layer, requiring the plasma to have an electron density corresponding to 5 MHz. The blanketing frequency at the time was nearly 10 MHz. Failure to observe the plasma line continuously suggests that the blanketing may be associated with causes other than reflection of the HF waves.

A brief survey of all data within the time period covered by four series of heating experiments suggests that at Arecibo natural range-type spread frequency in a sporadic E layer is fairly common (for this sample) and is generally observed when the blanketing frequency is less than about eight-tenths of the maximum frequency in the sporadic E layers.

REFERENCES

1. Showen, R. L., Artificial Heating of the Lower Ionosphere, Journal of Geophysical Research, 77, 1923-1933, 1972.

2. Kantor, I. J., Artificial Heating Paradox of the Lower Ionosphere, M.S. Dissertation, Rice University, Houston, Texas, 1971.

3. Gordon, W. E., H. C. Carlson and R. L. Showen, Ionospheric Heating at Arecibo: First Tests, Journal of Geophysical Research, 76, 7808-7813, 1971.

4. Carlson, H. C., W. E. Gordon and R. L. Showen, High Frequency Induced Enhancements of the Incoherent Scatter Spectrum at Arecibo, Journal of Geophysical Research, 77, 1242-1250, 1972.

5. Kantor, I. J., Enhanced Plasma Lines Excited by HF Waves, Ph.D. Dissertation, Rice University, Houston, Texas, 1972.

6. Dias, L. A. and W. E. Gordon, The Observation of Electron Cyclotron Lines Enhanced by HF Radio Waves, Journal of Geophysical Research, 78, 1730-1732, 1973.

7. Dias, L. A., D. M. Kim and W. E. Gordon, HF-Enhanced Line Arising from Second Harmonic Electron Density Fluctuations in the Ionosphere, to be submitted for publication to Journal of Geophysical Research, 1974.

8. Kruer, W. L. and E. J. Valeo, Nonlinear Evolution of the Decay Instability in a Plasma with Comparable Electron and Ion Temperatures, Report MATT-919, Plasma Physics Laboratory, Princeton University, Princeton, N.J., 1972; Physics of Fluids, 16, 675, 1973.

9. Kuo, Y. and J. A. Fejer, Spectral Line Structures of Saturated Parametric Instabilities, Physics Review of Letters, 29, 1667-1670, 1972.

10. Gordon, W. E. and H. C. Carlson, Ionospheric Heating Analysis, RADC-TR-73-82 Interim Technical Report, Contract F30602-72-C-0278, Rice University, Houston, Texas, 1972.

11. Utlaut, W. F. and R. Cohen, Modifying the Ionosphere with Intense Radio Waves, Science, 174, 245, 1971.

11. Utlaut, W. F. and E. J. Violette, Further Ionosonde Observations of Ionospheric Modification by a High Powered Ground-Based Transmitter, Journal of Geophysical Research, 77, 6804, 1972.

BIBLIOGRAPHY

Behnke, Richard A., Vector measurements of the ion transport velocity with applications to F-region dynamics, Ph.D. Dissertation, Rice University, 1970.

Carlson, H. C., W. E. Gordon and R. L. Showen, High frequency induced enhancements of the incoherent scatter spectrum at Arecibo, Journal of Geophysical Research, 77, 1242-1250, 1972.

Dias, Luiz A.V., High frequency radio heating of the ionosphere, M.S. Dissertation, Rice University, 1971.

Dias, L. A. and W. E. Gordon, The observation of electron cyclotron lines enhanced by HF radio waves, Journal of Geophysical Research, 78, 1730-1732, 1973.

Dias, L. A., D. M. Kim and W. E. Gordon, HF-enhanced line arising from second harmonic electron density fluctuations in the ionosphere, to be submitted for publication to Journal of Geophysical Research, 1974.

Gordon, W. E., R. L. Showen and H. C. Carlson, Ionospheric heating at Arecibo: First tests, Journal of Geophysical Research, 76, 7808-7813, 1971.

Gordon, W. E., H. C. Carlson and R. L. Showen, Ionospheric heating analysis - HF plasma line enhancements at Arecibo, Interim Technical Report, Contract F30602-71-C-0155, June 1971, RADC-TR-71-190, DDC Nr. AD-732-884.

Gordon, W. E., H. C. Carlson and R. L. Showen, Ionospheric heating analysis - HF plasma line enhancements at Arecibo, Final Technical Report, Contract F30602-71-C-0155, February 1972, RADC-TR-72-120.

Gordon, W. E. and H. C. Carlson, Ionospheric heating analysis, Interim Technical Report, Contract F30602-72-C-0278, July, 1972, RADC-TR-72-208.

Gordon, W. E. and H. C. Carlson, Ionospheric heating analysis, Technical Report, Contract F30602-72-C-0278, December, 1972, RADC-TR-73-82.

Harper, Robert M., Dynamics of the neutral atmosphere in the 200-500 km height region at low latitudes, Ph.D. Dissertation, Rice University, 1971.

Harper, R. M., Observation of a large nighttime gravity wave at Arecibo, Journal of Geophysical Research, 77, 1311-1315, 1972.

Harper, R. M., Nighttime meridional neutral winds near 350 km at low to mid-latitudes, Journal of Atmospheric and Terrestrial Physics, 35, 2023-2034, 1973.

Kantor, Ivan J., Artificial heating paradox of the lower ionosphere, M.S. Dissertation, Rice University, 1971.

Kantor, Ivan J., Enhanced plasma lines excited by HF waves, Ph.D. Dissertation, Rice University, 1972.

Kantor, Ivan J., High frequency induced enhancements of the incoherent scatter spectrum at Arecibo, 2, Journal of Geophysical Research, 79, 199-208, 1974.

Laird, A. R., Arecibo ionogram effects due to modification of the ionosphere by HF radio waves, submitted to Journal of Geophysical Research for publication, 1974.

Showen, R. L., Artificial heating of the lower ionosphere, Journal of Geophysical Research, 77, 1923-1933, 1972.

Wickwar, Vincent B., Photoelectrons from the magnetic conjugate point studied by means of the 6300 predawn enhancement and the plasma line enhancement, Ph.D. Dissertation, Rice University, 1971.

FIGURE CAPTIONS

Figure 1 Electron-temperature contours from incoherent-backscatter data. The temperatures are elevated at and below the HF reflection altitude. After the HF is turned off, the temperature relaxes to ambient conditions.

Figure 2 Changes in electron temperature for penetrating and reflecting O-mode propagation. The two electron-temperature profiles on the right-hand faces of the cubes are averages of heated and unheated samples.

Figure 3 Electron and ion temperature vs. altitude for zero-, half-, and full-power heater operation. The electron-temperature change is clear, while a possible ion-temperature change is uncertain.

Figure 4 Electron and ion temperature vs. time for zero-, half, and full-power heater operation. This is the same experiment as the previous figure. The electron temperature tracks remarkably well with the vertical bars, which represent transmitted power. The possible ion-temperature correlation with transmitted power is smaller than the estimated error, which is slightly less than 50°K.

Figure 5 Contour map of change in electron temperature. The vertical scale is altitude in km, and the horizontal scale is distance to the north and to the west of the Observatory. The O-mode ray was reflected at 340 km, and the center of the heated region was deviated 35 km toward the north.

Figure 6 Change in electron temperature with fine time resolution. This is a superposition of 10 on-off cycles of HF transmitter power. The fall time seems reasonably smooth, but there seems to be unexplained structure immediately following turn-on.

Figure 7 Amplitude probability distribution for the downshifted decay line. The relative probability scale is linear and starts at zero. Note that the peak SNR is logarithmic. The probability distribution is given for two transmitted powers.

Figure 8 Amplitude probability distribution for the upshifted decay line. The relative probability scale is linear and starts at zero. Note that the peak SNR is logarithmic. The probability distribution is given for two transmitted powers.

Figure 9 Histogram of the numbers sampled by the interface of the computer. Curves are given for two occasions, over 10 s of sampling data.

Figure 10 Barker-code profile for upshifted and downshifted plasma line and ion enhancement. Individual points are separated by 900 m. HF power was 25 kW.

Figure 11 Peak-power probability distribution of the upshifted plasma line from Barker decoder data. Solid-line curve adds all data where HF power was between 30 kW and 46 kW. Dashed line adds data between 15 kW and 25 kW.

Figure 12 Peak-power probability distribution of the upshifted plasma line from Barker decoder data. For the solid-line curve the HF power is 45 kW, and for the dashed line it is 25 kW. These are 5-minute averages, adjacent in time.

Figure 13 Peak power of the ion enhancement vs. upshifted-plasma-line peak, from Barker decoder. Dashed line represents quadratic power dependence.

Figure 14 HF-enhanced ion-component autocorrelation functions, showing enhanced minima and maxima beyond the first zero crossing, as theory predicts.

Figure 15 Diagram showing simultaneously the plasma line and gyroline power spectra. The frequency scale denotes the frequency separation from the operating backscatter frequency (430 MHz). In the lower diagrams the HF transmitter was off while in the upper diagram it is on.

Figure 16 6300-Å airglow intensity and average HF enhanced plasma line intensity vs. time. The HF transmitter is cycled on and off in 4 minutes. The difference between the dashed (background) and solid curves is the O-mode, HF induced impact excitation. The time constant is a measure of the N_2 number concentration times the quenching coefficient.

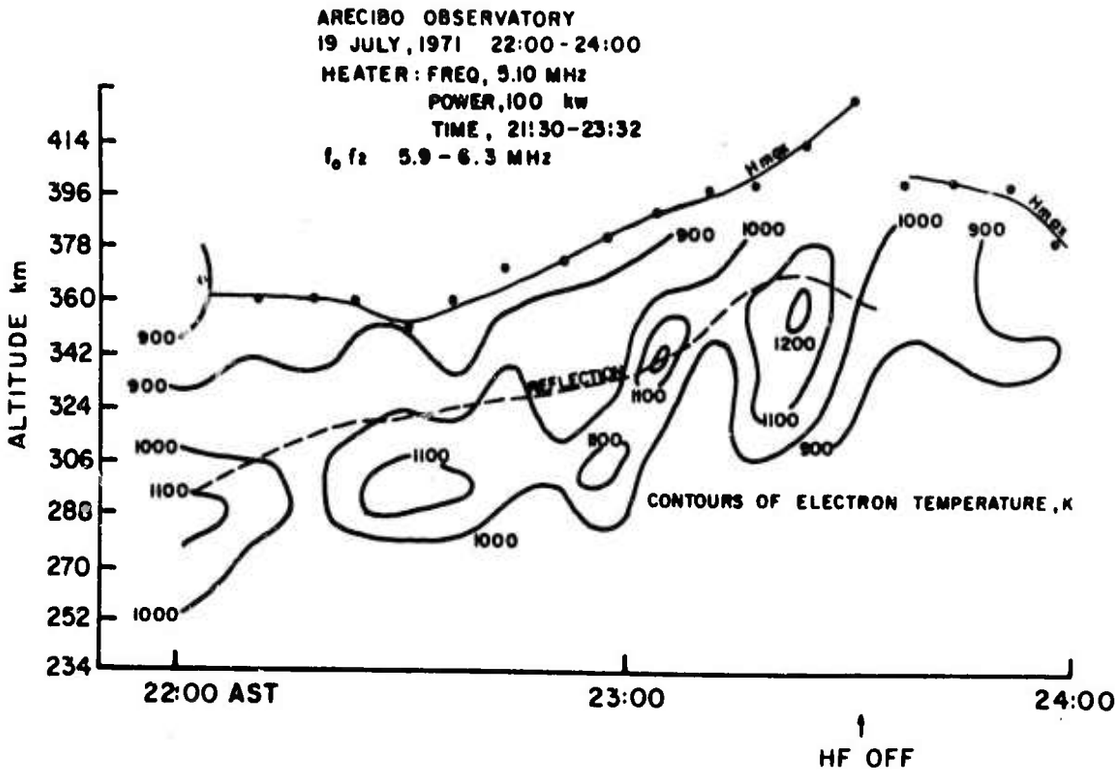
ARECIBO OBSERVATORY
19 JULY, 1971 22:00 - 24:00
HEATER: FREQ, 5.10 MHz
POWER, 100 kw
TIME, 21:30-23:32
f_o fz 5.9 - 6.3 MHz
ALTITUDE km
414
396
378
360
342
324
306
288
270
252
234
22:00 AST
23:00
24:00
HF OFF
CONTOURS OF ELECTRON TEMPERATURE, K
REFLECTION
Hmax
Hmax
900
1000
1100
1200
800

FIGURE 1

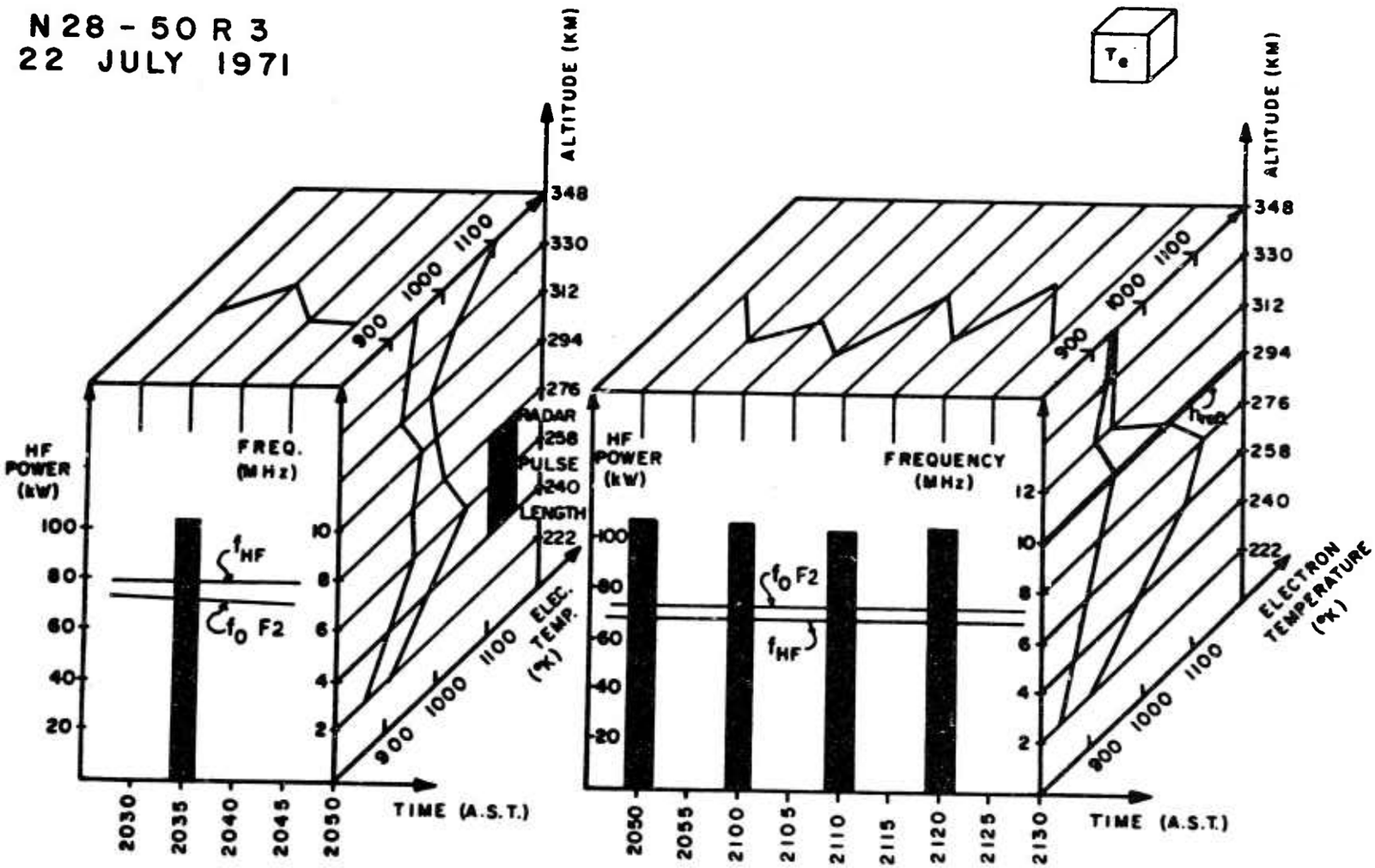
N28 - 50 R 3
22 JULY 1971
ALTITUDE (KM)
348
330
312
294
276
RADAR
PULSE
LENGTH
258
240
222
900
1000
1100
HF
POWER
(kW)
FREQ.
(MHz)
100
80
60
40
20
f_{HF}
f_0 F2
10
8
6
4
2
ELEC.
TEMP.
(°K)
TIME (A.S.T.)
2030
2035
2040
2045
2050
T_e
HF
POWER
(kW)
FREQUENCY
(MHz)
f_0 F2
f_{HF}
12
2050
2055
2100
2105
2110
2115
2120
2125
2130
ELECTRON
TEMPERATURE
(°K)

FIGURE 2

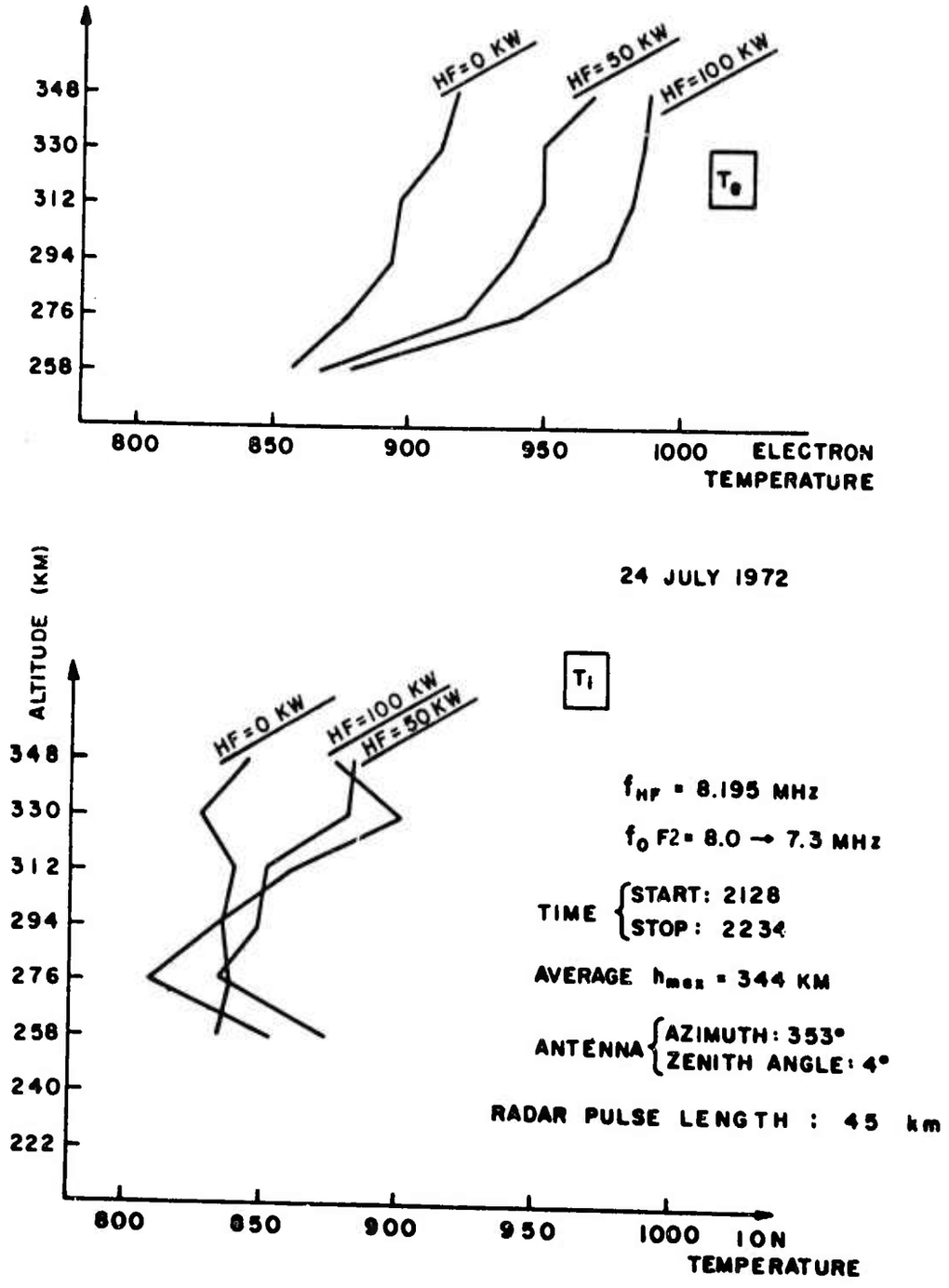
HF=0 KW
HF=50 KW
HF=100 KW
T_e
348
330
312
294
276
258
800
850
900
950
1000
ELECTRON TEMPERATURE
24 JULY 1972
ALTITUDE (KM)
T_i
HF=0 KW
HF=100 KW
HF=50 KW
f_{HF} = 8.195 MHz
f_0 F2 = 8.0 → 7.3 MHz
TIME {START: 2128
STOP: 2234
AVERAGE h_{max} = 344 KM
ANTENNA {AZIMUTH: 353°
ZENITH ANGLE: 4°
RADAR PULSE LENGTH : 45 km
348
330
312
294
276
258
240
222
800
850
900
950
1000
ION TEMPERATURE

FIGURE 3

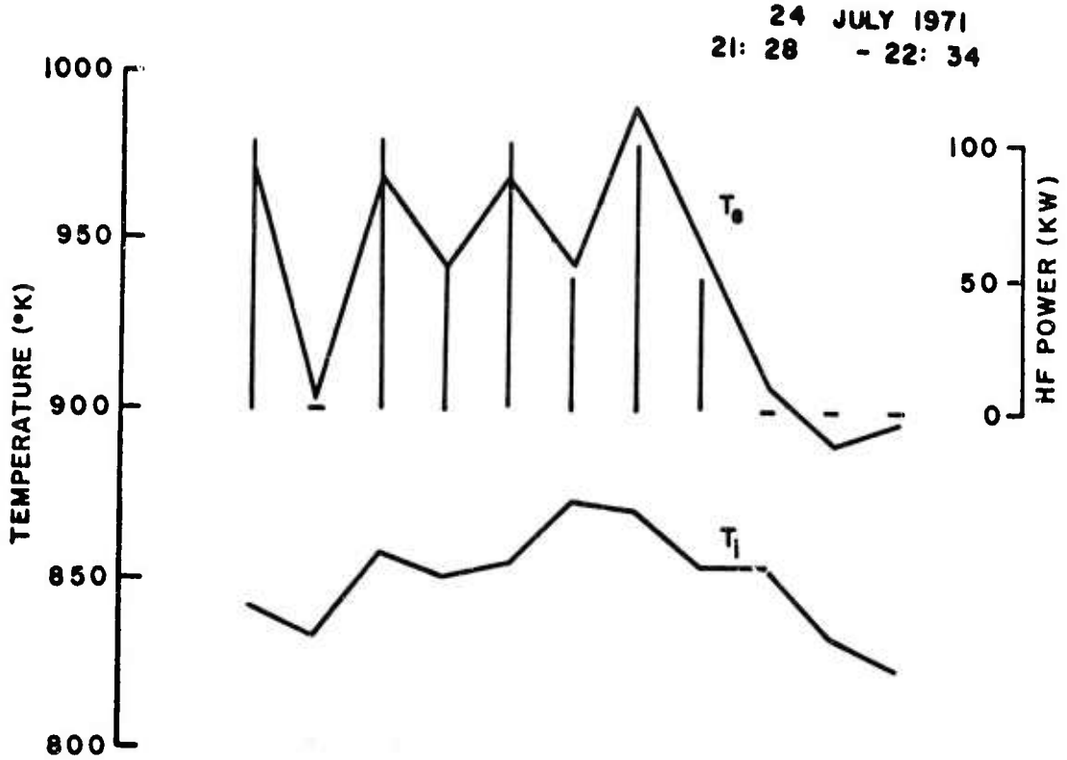
24 JULY 1971
21: 28 - 22: 34
1000
950
900
850
800
TEMPERATURE (°K)
100
50
0
HF POWER (KW)
T_e
T_i

FIGURE 4

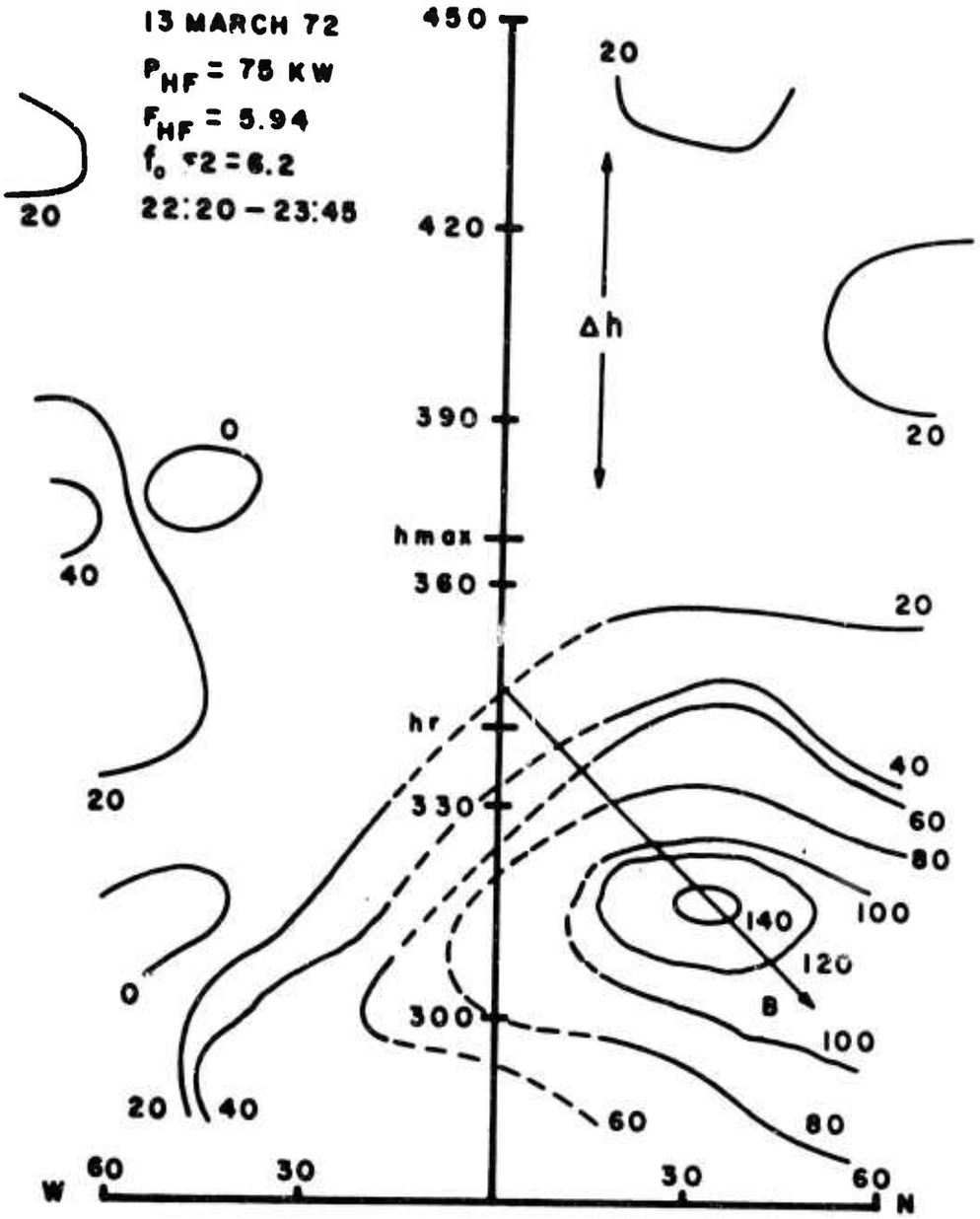
13 MARCH 72
P_{HF} = 75 KW
F_{HF} = 5.94
f_o F2 = 6.2
22:20 – 23:45
450
420
390
hmax
360
hr
330
300
Δh
20
0
40
60
80
100
120
140
B
W
N
60
30
30
60

FIGURE 5

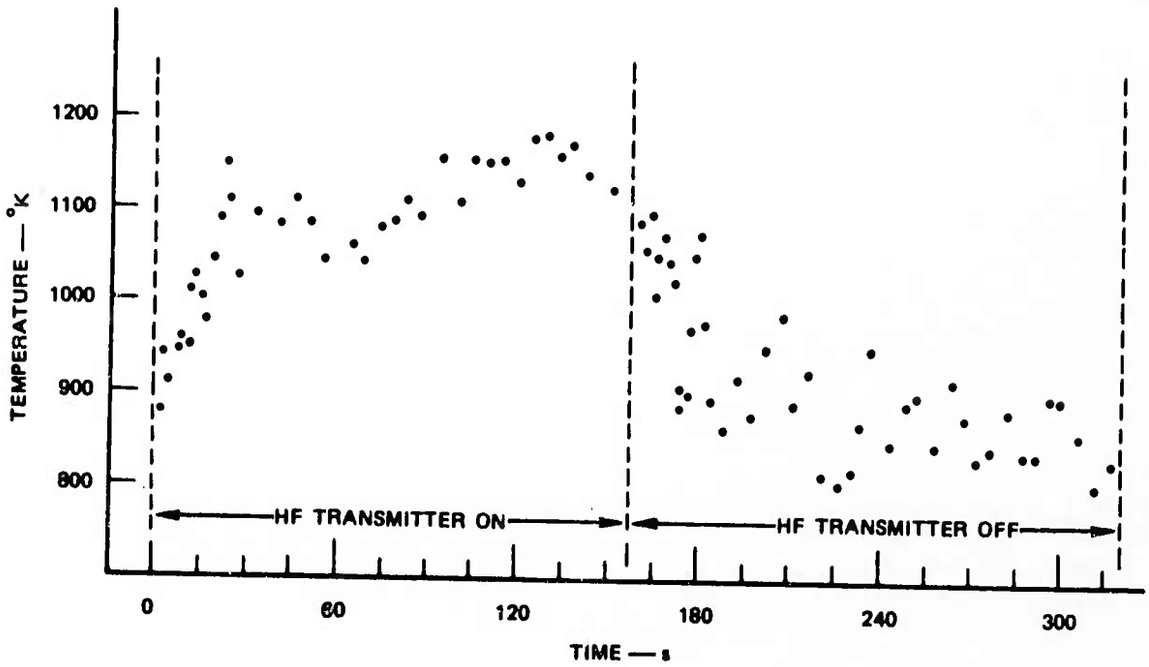
TEMPERATURE — °K
1200
1100
1000
900
800
HF TRANSMITTER ON
HF TRANSMITTER OFF
0
60
120
180
240
300
TIME — s

FIGURE 6

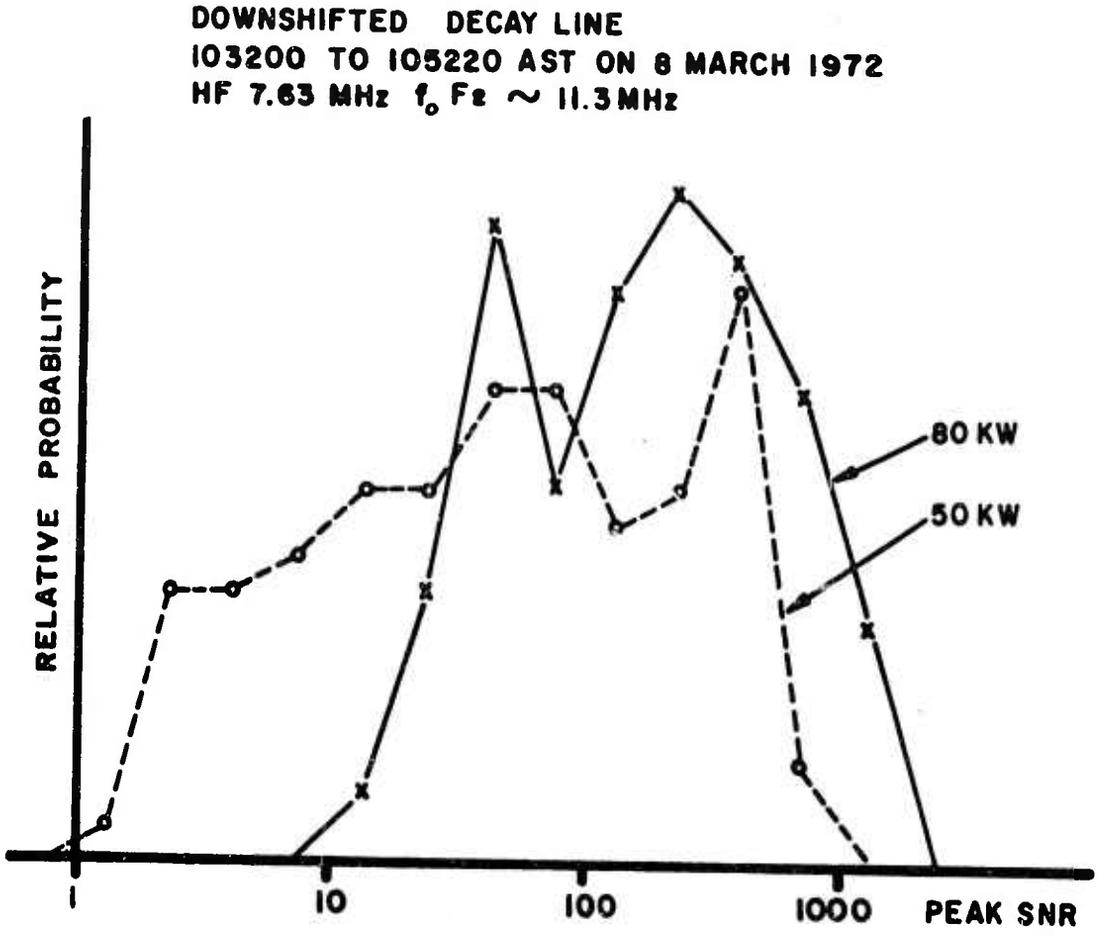
DOWNSHIFTED DECAY LINE
103200 TO 105220 AST ON 8 MARCH 1972
HF 7.63 MHz f_o Fz ~ 11.3 MHz
RELATIVE PROBABILITY
80 KW
50 KW
1
10
100
1000
PEAK SNR

FIGURE 7

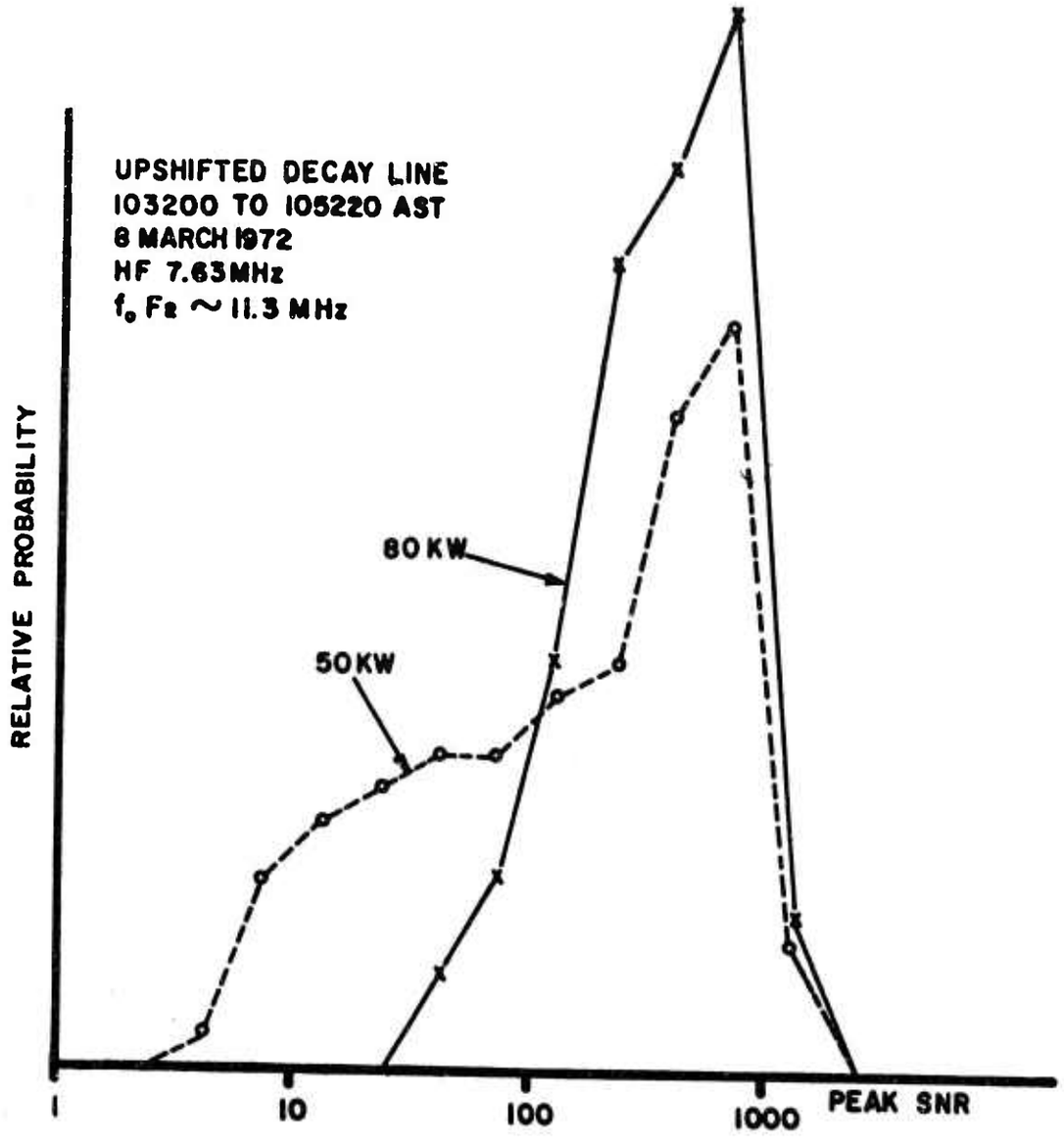
UPSHIFTED DECAY LINE
103200 TO 105220 AST
8 MARCH 1972
HF 7.63MHz
f_o F2 ~ 11.3 MHz
RELATIVE PROBABILITY
80 KW
50 KW
1
10
100
1000
PEAK SNR

FIGURE 8

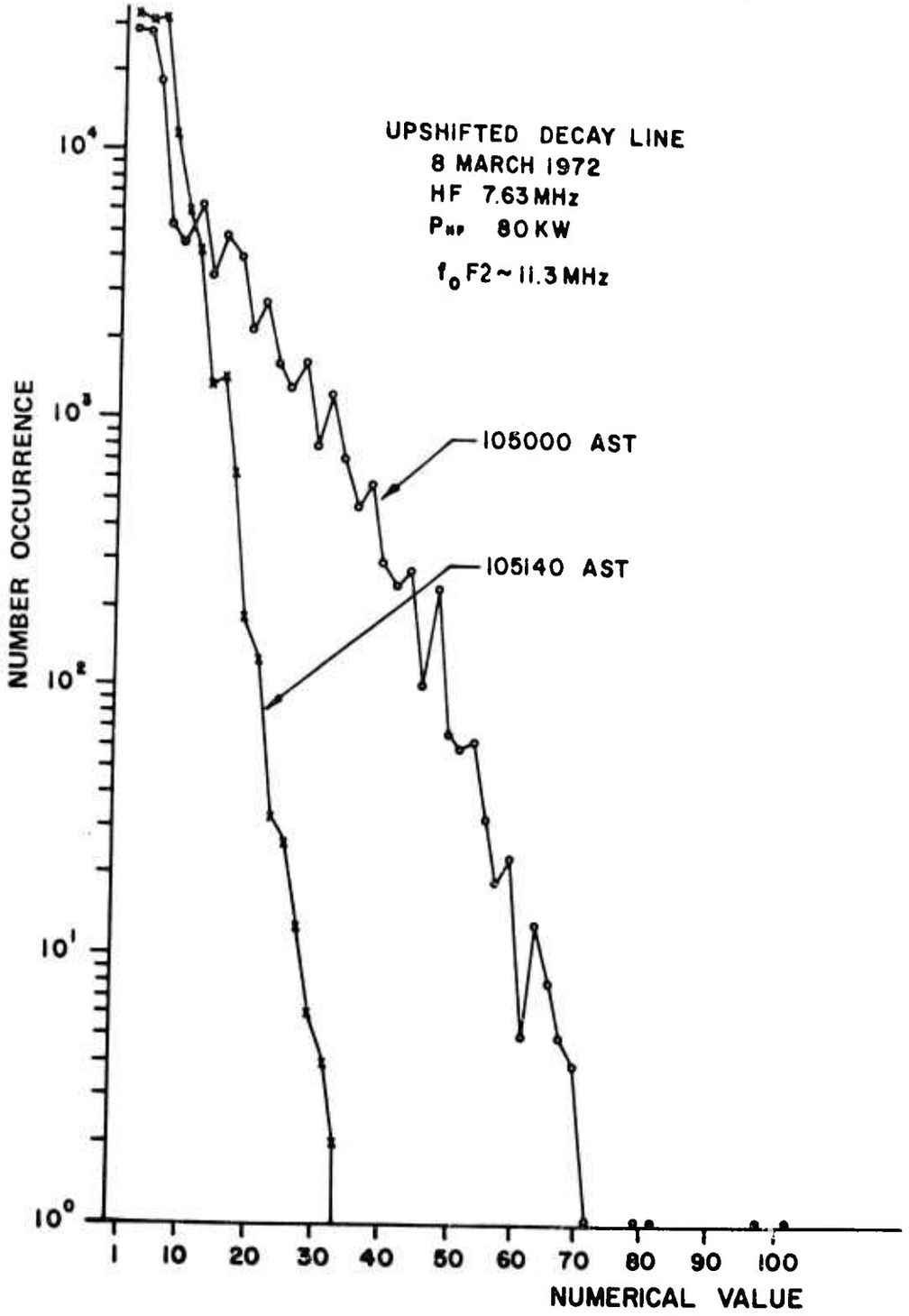
UPSHIFTED DECAY LINE
8 MARCH 1972
HF 7.63 MHz
P_{HP} 80 KW
$f_0F2 \sim 11.3$ MHz
105000 AST
105140 AST
NUMBER OCCURRENCE
10^4
10^3
10^2
10^1
10^0
1
10
20
30
40
50
60
70
80
90
100
NUMERICAL VALUE

FIGURE 9

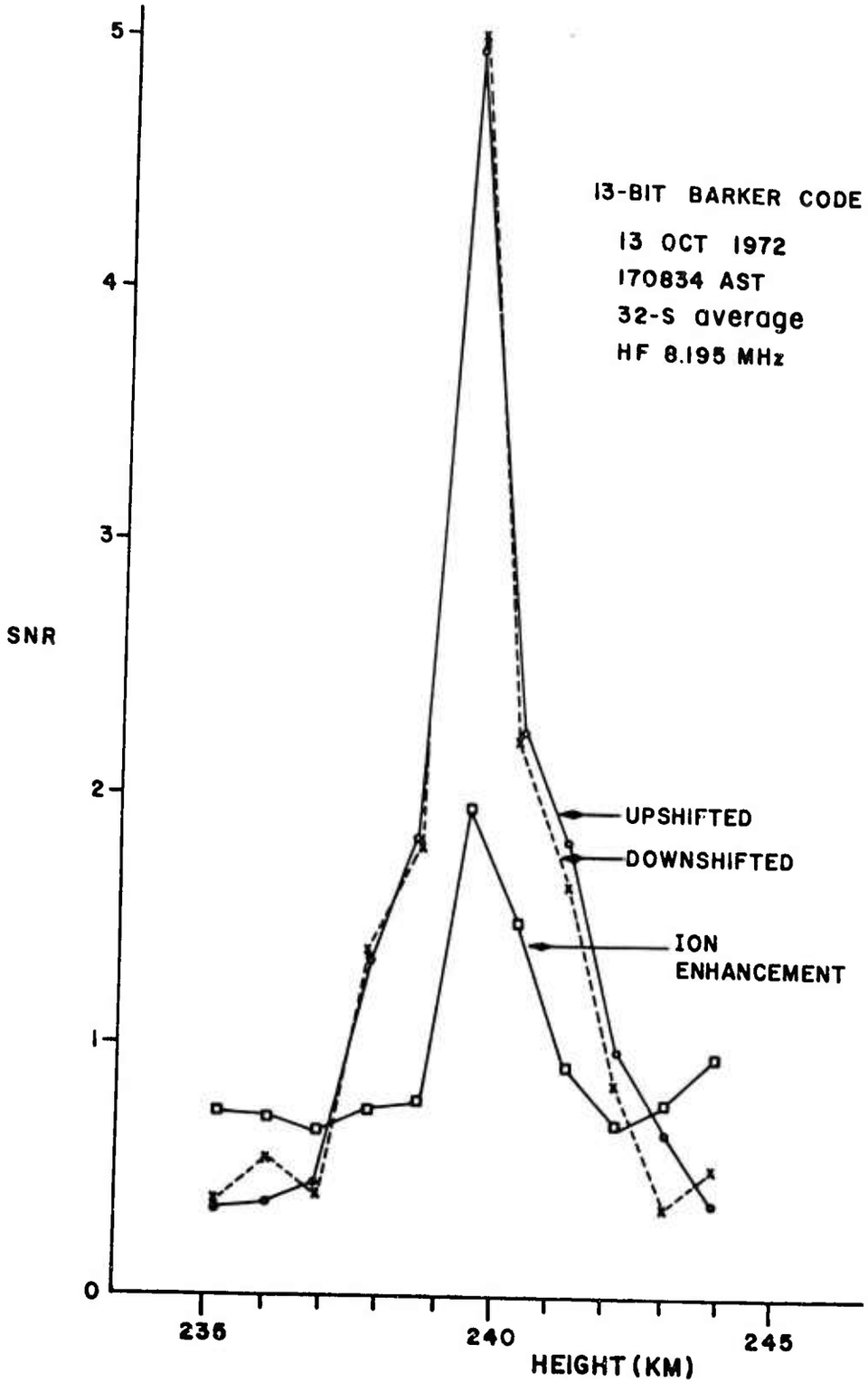
13-BIT BARKER CODE
13 OCT 1972
170834 AST
32-S average
HF 8.195 MHz
SNR
5
4
3
2
1
0
UPSHIFTED
DOWNSHIFTED
ION
ENHANCEMENT
235
240
245
HEIGHT (KM)

FIGURE 10

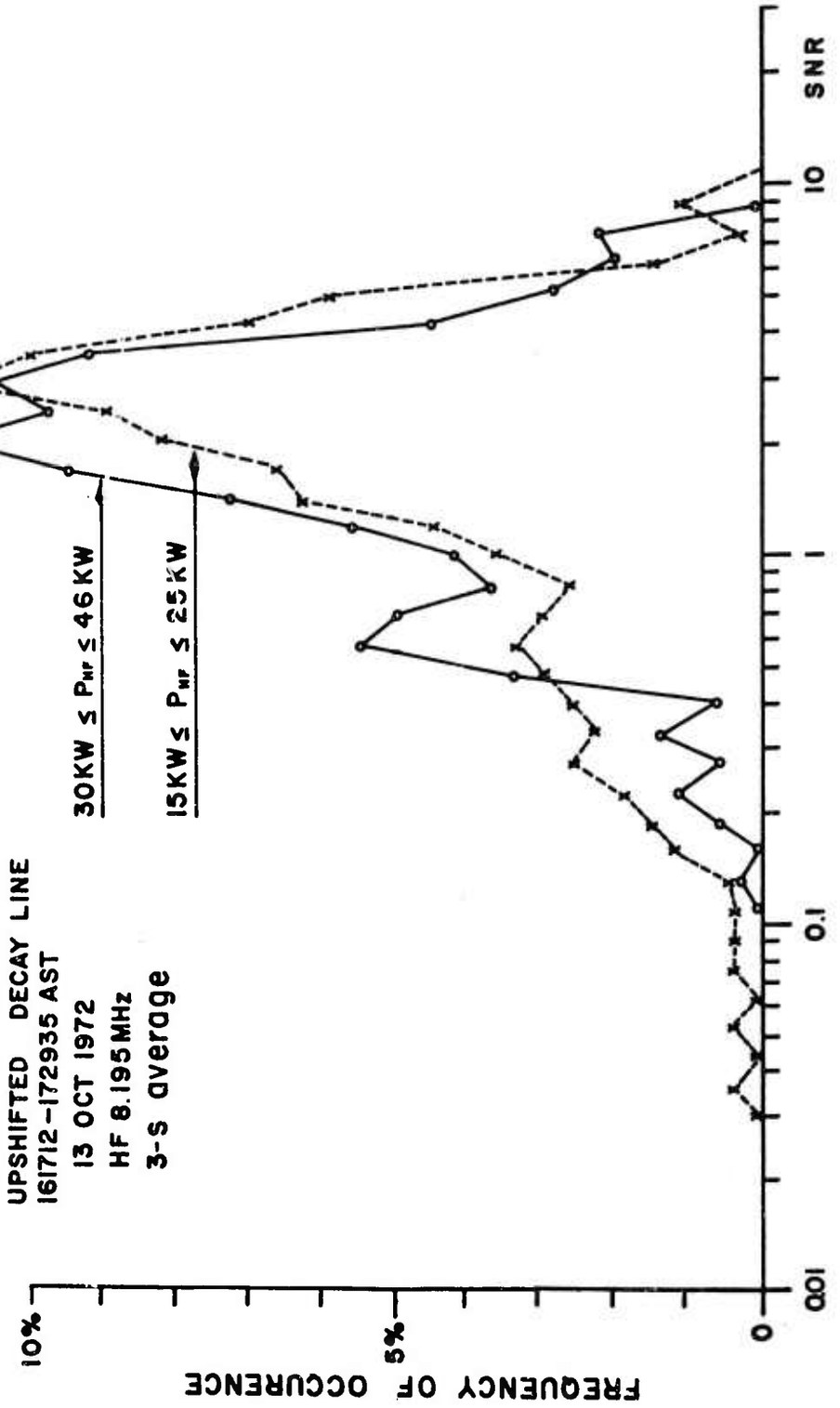
UPSHIFTED DECAY LINE
161712-172935 AST
13 OCT 1972
HF 8.195 MHz
3-S average
30KW ≤ P_HF ≤ 46 KW
15KW ≤ P_HF ≤ 25 KW
FREQUENCY OF OCCURENCE
10%
5%
0
.001
.01
.1
1
10
SNR

FIGURE 11

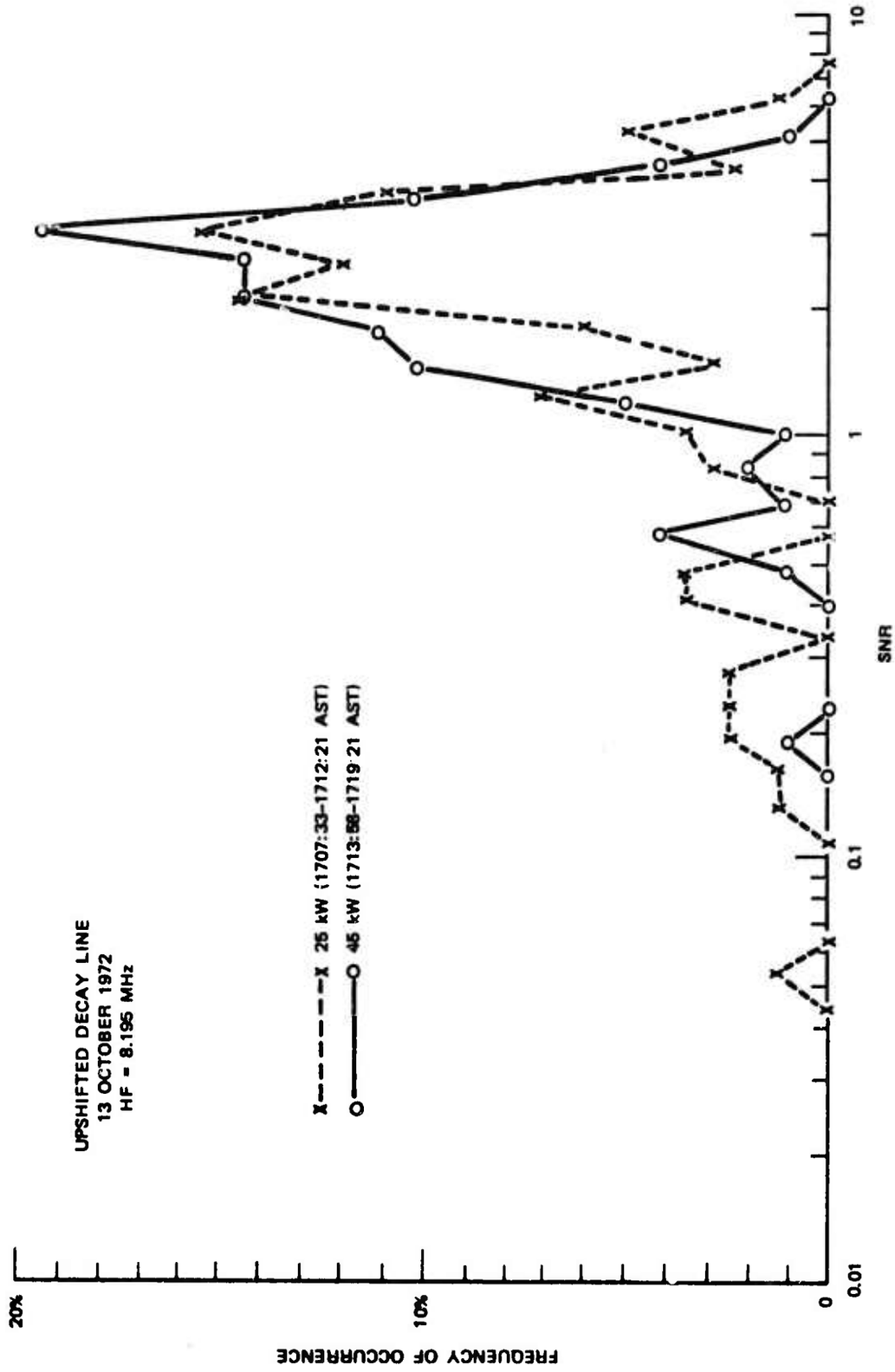
UPSHIFTED DECAY LINE
13 OCTOBER 1972
HF = 8.195 MHz
X- - - - - -X 25 kW (1707:33-1712:21 AST)
O——O 45 kW (1713:58-1719:21 AST)
FREQUENCY OF OCCURRENCE
20%
10%
0
0.01
0.1
1
10
SNR

FIGURE 12

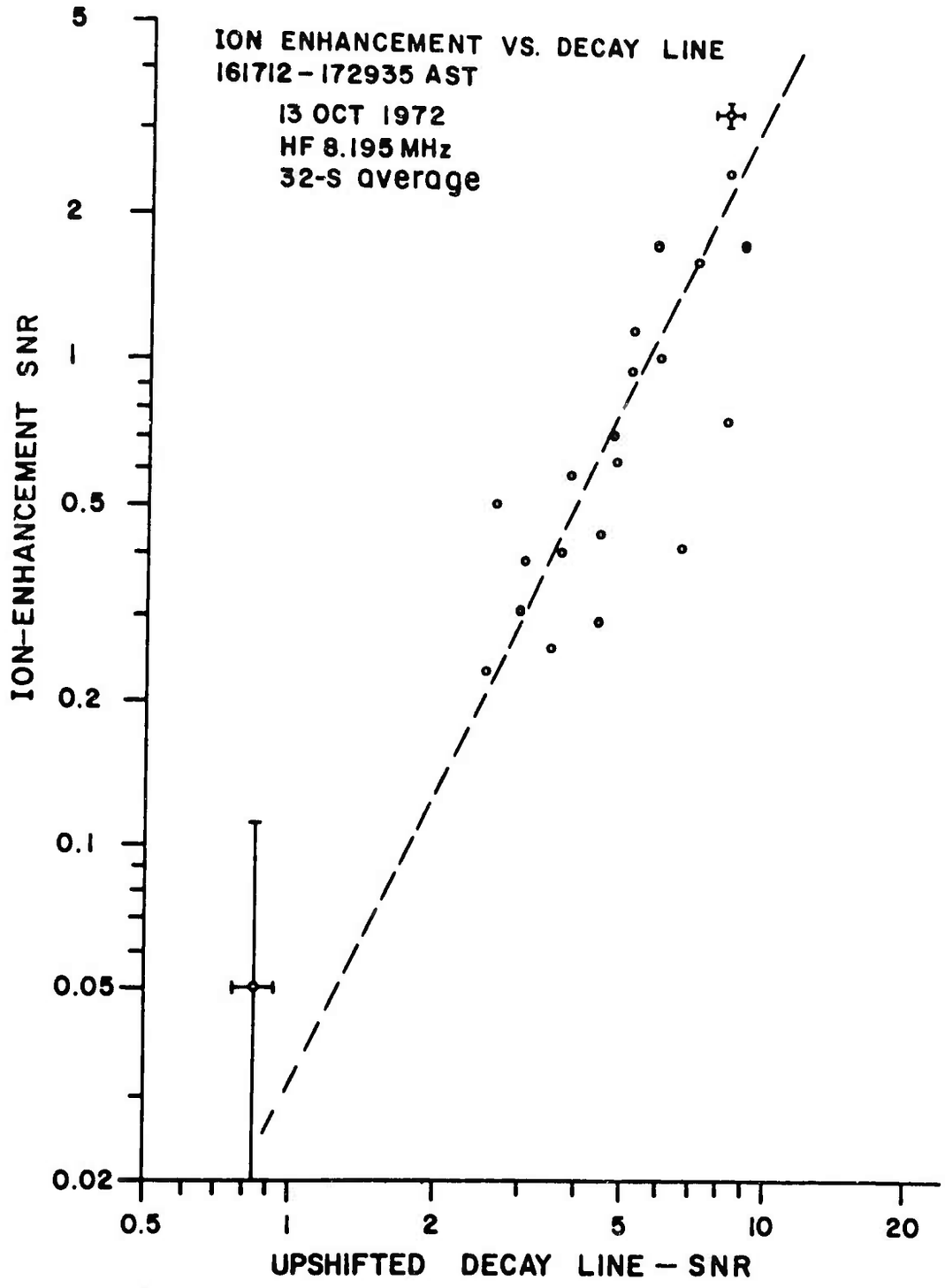
ION ENHANCEMENT VS. DECAY LINE
161712 - 172935 AST
13 OCT 1972
HF 8.195 MHz
32-S average
ION-ENHANCEMENT SNR
5
2
1
0.5
0.2
0.1
0.05
0.02
0.5
1
2
5
10
20
UPSHIFTED DECAY LINE — SNR

FIGURE 13

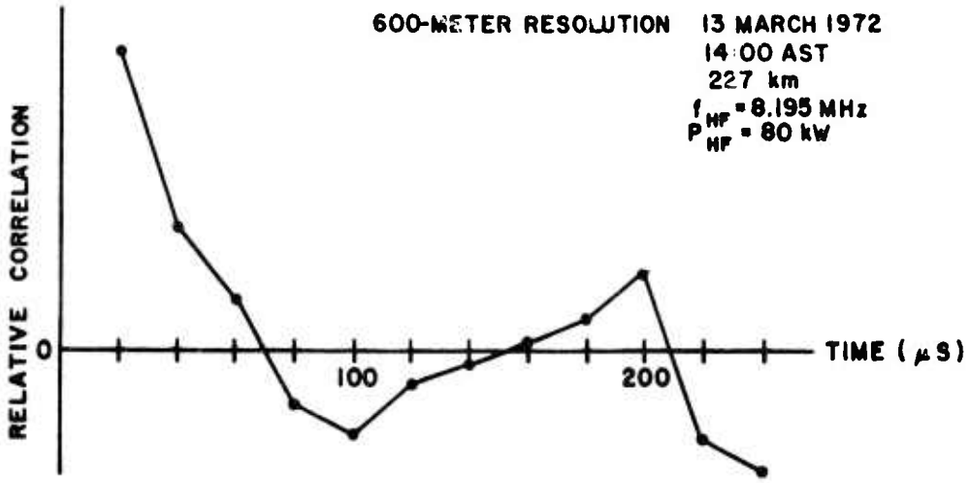
600-METER RESOLUTION
13 MARCH 1972
14:00 AST
227 km
f_{HF} = 8.195 MHz
P_{HF} = 80 kW
RELATIVE CORRELATION
0
100
200
TIME (μS)

FIGURE 14

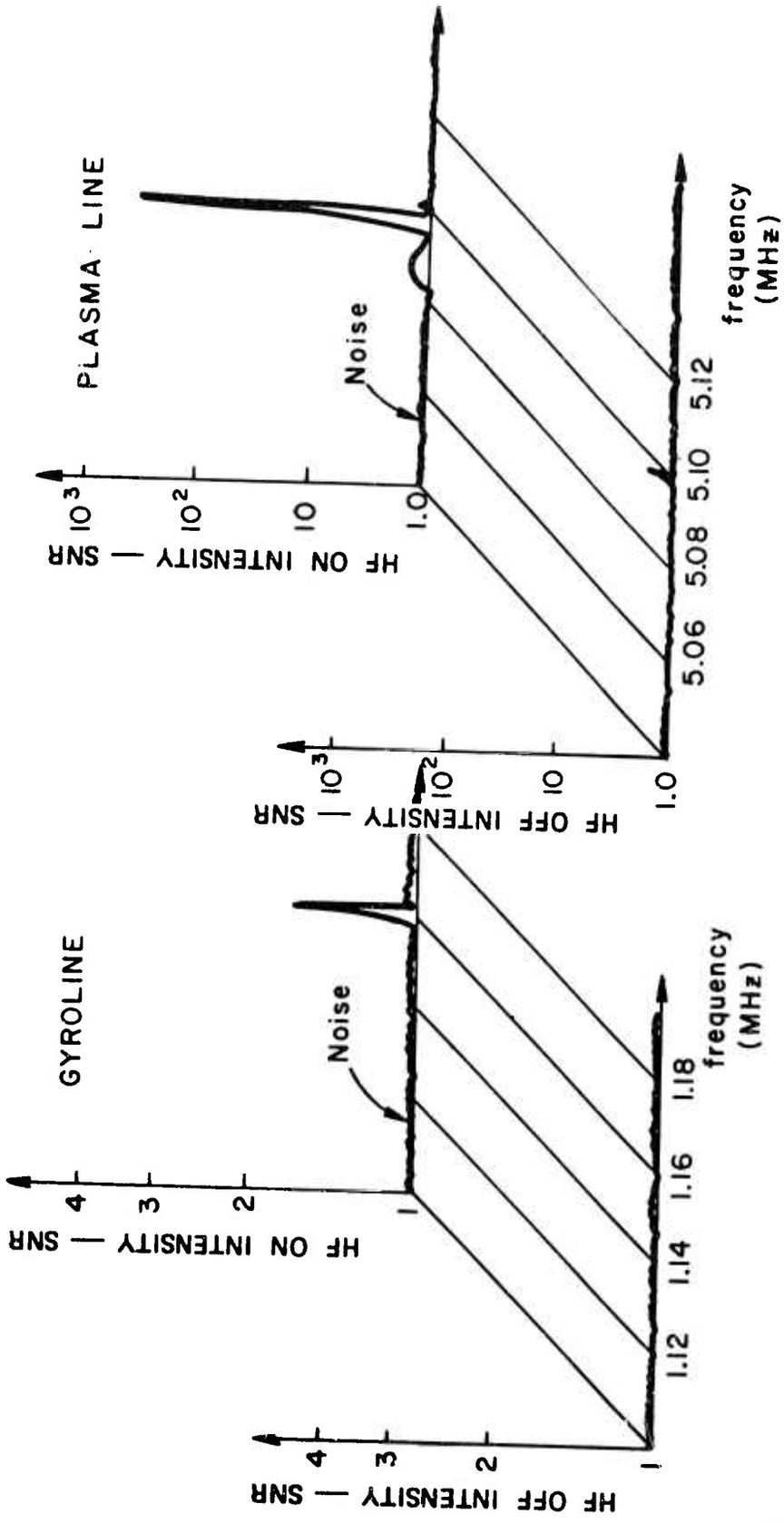
PLASMA LINE
Noise
HF ON INTENSITY — SNR
1.0
10
10^2
10^3
5.06
5.08
5.10
5.12
frequency (MHz)
HF OFF INTENSITY — SNR
GYROLINE
Noise
HF ON INTENSITY — SNR
1
2
3
4
1.12
1.14
1.16
1.18
frequency (MHz)
HF OFF INTENSITY — SNR

FIGURE 15

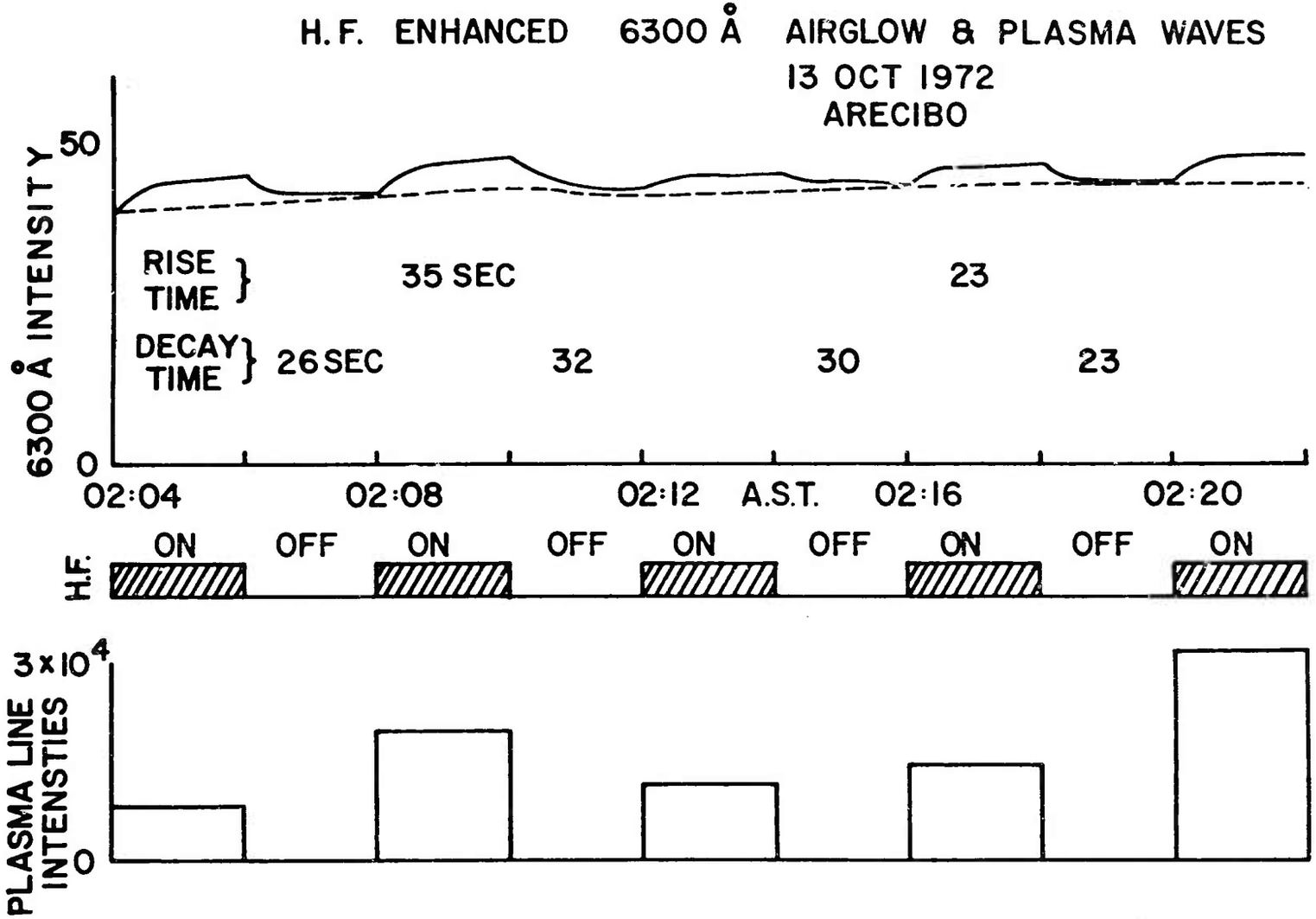
H.F. ENHANCED 6300 Å AIRGLOW & PLASMA WAVES
13 OCT 1972
ARECIBO
6300 Å INTENSITY
50
0
RISE TIME
DECAY TIME
35 SEC
23
26 SEC
32
30
23
02:04
02:08
02:12
A.S.T.
02:16
02:20
H.F.
ON
OFF
ON
OFF
ON
OFF
ON
OFF
ON
PLASMA LINE INTENSTIES
3 x 10^4
0

FIGURE 16

APPENDIX

Plasma Lines Enhanced by High Frequency Radio Waves

The observational feature that attracted the most attention is the power spectrum of the plasma lines enhanced by high frequency radio waves. The interpretation of the spectra was developed in the thesis by I. J. Kantor. Here we present series of spectra selected from the many observations recorded.

The general conditions for the experiment are briefly summarized in the following paragraphs. The particular conditions are listed in Table 1 and Table 2. The electron and ion temperatures as observed by the radar and the penetration frequencies (f_oF_2) from the ionosondes are given in Table 3 for times near the times of the spectral observations. Plots of the spectra follow. Each spectrum has a number that relates it to Table 1 and, therefore, to the other tables.

The spectra are observed using the incoherent scatter radar with a transmitted frequency centered at 430 MHz and a receiving window shifted upward or downward by a frequency equal to that of the HF transmitter. The radar beam is directed four degrees magnetic north of the zenith and has a half-power beam width of 0.2°. The HF radiation is directed vertically upward and has a half-power width of about ten degrees (the 1000 foot reflector fed by crossed dipoles serves as the antenna).

The spectra are plotted on frequency power coordinates. The frequency increases to the right and the unit marked on the abscissa is 5 kHz. The marker extending below the abscissa corresponds to the frequency of the HF transmitter

relative to the radar center frequency, 430 MHz. The power scale is linear in power and normalized. The maximum value for each spectrum is given in watts by the product of $(SNR)(RES)(kT_R)$ where SNR is the signal-to-noise ratio in Table 1, RES is the spectral resolution equal to 1.0 kHz for all of the spectra included, k is Boltzman's constant, 1.4×10^{-20} watts $(kHz)^{-1}(\text{degree K})^{-1}$, and T_R is the receiving system noise temperature given in Table 2. The units in the tables are those indicated in Boltzman's constant. The zero on the power scale is zero power in the spectrum, i.e., the receiver noise has been subtracted.

The column labels in Table 1 are:

START — The start of the observation in hours minutes and seconds (Atlantic Standard Time) hhmmss.

STOP — The end of the observation (time as in START).

DATE — Day month year DDMMYY

IPPS — Interpulse periods, the number of radar pulses used in the computation of the spectrum.

σ — The standard deviation of the power observation in percent.

SNR — The signal-to-noise ratio of the maximum point in the spectrum corrected for antenna and receiver gains and referenced to the system noise level at 430 MHz.

PHF — The power generated by the HF transmitter in kilowatts.

FHF — The frequency of the HF transmitter in kilohertz relative to the radar center frequency, 430 MHz, a + meaning the spectral window is above 430 MHz and a - meaning the spectral window is below 430 MHz.

H	The height in kilometers at which the observational data begin. Normally the enhanced region is a few tens of kilometers above this height.
BLK	The identifying number (label) of the spectrum.

TABLE 1

Times AST START	STOP	DATE	IPPS	σ	SNR	PHF	kHz FHF	H	BLK
194901	194909	230771	381	5.1	71.2	126	-8195	312	1
194911	194919	230771	381	5.1	29.1	126	+8195	312	2
194921	194929	230771	381	5.1	47.1	100	-8195	312	3
194931	194939	230771	381	5.1	26.5	100	+8195	312	4
194941	194949	230771	381	5.1	50.9	80	-8195	312	5
194951	194959	230771	381	5.1	29.1	80	+8195	312	6
195001	195009	230771	381	5.1	46.3	59	-8195	312	7
195011	195019	230771	381	5.1	25.8	59	+8195	312	8
195021	195029	230771	381	5.1	24.9	40	-8195	312	9
195031	195039	230771	381	5.1	12.6	40	+8195	312	10
195121	195129	230771	381	5.1	9.2	25	-8195	312	15
195131	195139	230771	374	5.1	4.0	25	+8195	312	16
195141	195149	230771	381	5.1	96.5	43	-8195	312	17
195151	195159	230771	381	5.1	6.0	43	+8195	312	18
195221	195229	230771	381	5.1	52.5	102	-8195	312	21
195231	195239	230771	381	5.1	23.8	102	+8195	312	22
195241	195249	230771	381	5.1	135.2	125	-8195	312	23
195251	195259	230771	381	5.1	42.4	125	+8195	312	24
195901	195909	230771	208	7.1	97.3	125	-8195	350	25
195911	195919	230771	211	7.1	65.5	125	+8195	350	26
195921	195929	230771	211	7.1	54.8	94	-8195	350	27
195931	195939	230771	211	7.1	33.8	94	+8195	350	28
195941	195949	230771	211	7.1	42.9	77	-8195	350	29
195951	195959	230771	211	7.1	19.9	77	+8195	350	30
200001	200009	230771	211	7.1	23.7	54	-8195	350	31
200011	200019	230771	211	7.1	11.2	54	+8195	350	32

Times AST START	STOP	DATE	IPPS	σ	SNR	PHF	kHz FHF	H	BLK
200021	200029	230771	211	7.1	14.9	33	-8195	350	33
200031	200039	230771	211	7.1	6.6	33	+8195	350	34
200121	200129	230771	211	7.1	11.5	24	-8195	350	39
200131	200139	230771	211	7.1	9.6	24	-8195	350	40
200141	200149	230771	211	7.1	29.1	50	-8195	350	41
200151	200159	230771	211	7.1	9.9	50	+8195	350	42
200201	200209	230771	211	7.1	52.5	70	-8195	350	43
200211	200219	230771	211	7.1	23.2	70	+8195	350	44
200221	200229	230771	211	7.1	53.2	90	-8195	350	45
200231	200239	230771	211	7.1	29.8	90	+8195	350	46
200241	200249	230771	211	7.1	79.7	105	-8195	350	47
200251	200259	230771	211	7.1	41.7	105	+8195	350	48
200301	200309	230771	211	7.1	86.6	126	-8195	350	49
200311	200319	230771	211	7.1	43.7	126	+8195	350	50
200321	200329	230771	211	7.1	44.0	104	-8195	350	51
200331	200339	230771	211	7.1	21.8	104	+8195	350	52
200341	200349	230771	211	7.1	24.9	77	-8195	350	53
200351	200359	230771	211	7.1	16.6	77	+8195	350	54
200401	200410	230771	211	7.1	21.8	53	-8195	350	55
200412	200420	230771	211	7.1	12.6	53	+8195	350	56
200422	200430	230771	211	7.1	5.7	30	-8195	350	57
200432	200440	230771	211	7.1	9.9	30	+8195	350	58
200502	200510	230771	211	7.1	17.2	31	-8195	350	61
200512	200520	230771	211	7.1	4.6	31	+8195	350	62
200522	200530	230771	211	7.1	40.6	52	-8195	350	63
200532	200540	230771	211	7.1	21.2	52	+8195	350	64
200542	200550	230771	211	7.1	68.2	76	-8195	350	65
200552	200600	230771	211	7.1	37.1	76	+8195	350	66
200602	200610	230771	211	7.1	68.6	102	-8195	350	67
200612	200620	230771	211	7.1	37.1	102	+8195	350	68
200622	200630	230771	211	7.1	55.5	107	-8195	350	69

Times AST START	STOP	DATE	IPPS	σ	SNR	PHF	kHz FHF	H	BLK
162331	162339	240771	381	5.1	255.0	80	+8195	267	70
162341	162349	240771	381	5.1	213.7	80	-8195	267	71
162351	162349	240771	381	5.1	220.0	80	+8195	267	72
162401	162409	240771	381	5.1	388.0	80	-8195	267	73
162411	162419	240771	381	5.1	559.0	80	+8195	267	74
162421	162429	240771	381	5.1	643.0	80	-8195	267	75
162431	162439	240771	381	5.1	762.0	80	+8195	267	76
162441	162449	240771	381	5.1	140.9	80	-8195	267	77
162451	162459	240771	381	5.1	198.0	80	+8195	267	78
162501	162509	240771	381	5.1	154.3	80	-8195	267	79
162511	162519	240771	381	5.1	181.4	80	+8195	267	80
162521	162529	240771	381	5.1	191.5	80	-8195	267	81
162531	162539	240771	381	5.1	274.0	80	+8195	267	82
162541	162549	240771	381	5.1	468.0	80	-8195	267	83
162551	162559	240771	381	5.1	335.0	80	+8195	267	84
162601	162609	240771	381	5.1	359.0	80	-8195	267	85
162611	162619	240771	381	5.1	465.0	80	+8195	267	86
162621	162629	240771	381	5.1	538.0	80	-8195	267	87
162631	162639	240771	381	5.1	578.0	80	+8195	267	88
162641	162649	240771	381	5.1	933.0	80	-8195	267	89
162651	162659	240771	381	5.1	916.0	80	+8195	267	90
162701	162709	240771	381	5.1	1165.0	80	-8195	267	91
162711	162719	240771	381	5.1	941.0	80	+8195	267	92
162721	162729	240771	381	5.1	897.0	80	-8195	267	93
162731	162739	240771	381	5.1	852.0	80	+8195	267	94
162741	162749	240771	381	5.1	642.0	80	-8195	267	95
162751	162759	240771	381	5.1	851.0	80	+8195	267	96
162801	162809	240771	381	5.1	956.0	80	-8195	267	97

Times AST START	STOP	DATE	IPPS	σ	SNR	PHF	kHz FHF	H	BLK
162811	162819	240771	381	5.1	385.0	80	+8195	267	98
162821	162829	240771	381	5.1	164.3	80	-8195	267	99
162831	162839	240771	381	5.1	352.0	80	+8195	267	100
162841	162849	240771	381	5.1	311.0	80	-8195	267	101
162851	162859	240771	381	5.1	657.0	80	+8195	267	102
164611	164619	240771	374	5.2	741.0	80	-8195	267	103
164601	164609	240771	381	5.1	596.0	80	+8195	267	104
164641	164649	240771	381	5.1	118.7	43	-8195	267	105
164631	164639	240771	381	5.1	165.5	62	+8195	267	106
164651	164659	240771	381	5.1	232.0	43	+8195	267	107
164711	164719	240771	381	5.1	6.6	22	+8195	267	108
164801	164809	240771	381	5.1	130.2	45	-8195	267	109
164811	164819	240771	381	5.1	103.3	45	+8195	267	110
164821	164829	240771	381	5.1	298.0	71	-8195	267	111
164831	164839	240771	381	5.1	722.0	71	+8195	267	112
164841	164849	240771	381	5.1	1622.0	83	-8195	267	113
164851	164859	240771	381	5.1	1037.0	83	+8195	267	114
164901	164909	240771	381	5.1	1128.0	100	-8195	267	115
164911	164919	240771	381	5.1	1019.0	100	+8195	267	116
164921	164929	240771	381	5.1	660.0	80	-8195	267	117
164931	164939	240771	381	5.1	968.0	80	+8195	267	118
164941	164949	240771	381	5.1	543.0	60	-8195	267	119
164951	164959	240771	381	5.1	634.0	60	+8195	267	120
165001	165009	240771	381	5.1	161.6	36	-8195	267	121
165011	165019	240771	381	5.1	220.0	36	+8195	267	122
165031	165039	240771	381	5.1	10.6	16	+8195	267	123

Times AST START	STOP	DATE	IPPS	σ	SNR	PHF	kHz FHF	H	BLK
101401	101409	250771	381	5.1	6.8	96	+6790	267	124
101421	101429	250771	381	5.1	10.7	57	+6790	267	125
101621	101629	250771	381	5.1	18.5	82	+6790	267	126
101641	101649	250771	381	5.1	10.2	95	+6790	267	127
101701	101709	250771	381	5.1	70.6	50	+6790	267	128
101721	101729	250771	381	5.1	3.0	26	+6790	267	129
101941	101949	250771	381	5.1	19.4	106	+6790	267	130
102001	102009	250771	381	5.1	2.2	65	+6790	267	131
102021	102029	250771	381	5.1	1.4	45	+6790	267	132
073911	073919	280771	381	5.1	60.8	101	-5425	225	133
073901	073909	280771	381	5.1	2.9	101	+5425	225	134
074151	074159	280771	381	5.1	207.4	100	-5425	225	135
074141	074149	280771	381	5.1	50.8	100	+5425	225	136
110043	110107	80372	572	4.2	119.1	40	-7630	249	137
110043	110107	80372	572	4.2	689.0	40	+7630	249	138
110109	110119	80372	239	6.5	1579.0	90	-7630	249	139
110109	110119	80372	239	6.5	7594.0	90	+7630	249	140
110121	110139	80372	429	5.2	1622.0	100	-7630	249	141
110121	110139	80372	429	5.2	4885.0	100	+7630	249	142
110141	110159	80372	429	5.2	1022.0	86	-7630	249	143
110141	110159	80372	429	5.2	3660.0	86	+7630	249	144
110201	110219	80372	430	5.2	2662.0	80	-7630	249	145
110201	110219	80372	430	5.2	5571.0	80	+7630	249	146
110221	110239	80372	430	5.2	1949.0	80	-7630	249	147
110221	110239	80372	430	5.2	4395.0	80	+7630	249	148
110241	110259	80372	430	5.2	1122.0	50	-7630	249	149
110241	110259	80372	430	5.2	2353.0	50	+7630	249	150

TABLE 2

Receiving System Noise Temperature

Date	T_R
23-28 July 1971	350°K
8 March 1972	275°K

TABLE 3a

Ion and Electron Temperatures Measured by the Radar

23 July 1971 2020-2025 AST
HF Transmitter on at 8.195 MHz at 115 kw

Altitude (km)	Temperatures T_e (°K)	T_i (°K)
302	885	954
344	944	916
386	972	872
428	993	928
470	991	1085
512	1126	1062
554	1120	1036

24 July 1971 1554-1608 AST
HF Transmitter on at 8.198 MHz at 78 kw

Altitude (km)	Temperatures T_e (°K)	T_i (°K)
222	1722	940
240	1854	1066
258		
276	1743	1086
294	1634	1031
312	1469	1082
330	1450	1062
348	1402	1166

24 July 1971 1723-1735 AST
HF Transmitter on at 8.198 MHz at 100 kw

Altitude (km)	Temperatures T_e (°K)	T_i (°K)
222	1765	1000
240	1860	1146
258		
276	1662	1176
294	1546	1085
312	1496	1071
330	1402	1098
348	1397	1101

24 July 1971 1735-1746 AST
HF Transmitter off

Altitude (km)	Temperatures T_e (°K)	T_i (°K)
222	1751	976
240	1879	977
258	1870	942
276	1764	985
294	1567	1069
312	1477	1084
330	1373	1107
348	1405	1086

25 July 1971 0936-0949 AST
HF Transmitter on at 5.425 MHz at 100 kw

Altitude (km)	Temperatures T_e (°K)	T_i (°K)
222	1742	898
240	1962	941
258	1891	958
276	1945	935
294	1853	985
312	1807	1023
330	1749	1021
348	1733	1108

25 July 1971 1025-1036 AST
HF Transmitter on at 6.79 MHz at 100kw

Altitude (km)	Temperatures T_e (°K)	T_i (°K)
222	1744	764
240	1937	762
258	1830	817
276	1839	829
294	1709	836
312	1597	951
330	1647	999
348	1546	969

28 July 1971 0715-0724 AST
HF Transmitter on at 5.425 MHz at 91 kw

Altitude (km)	Temperatures T_e (°K)	T_i (°K)
218	1879	751
260	2311	796
302	2540	835
344	2702	895
386	2611	886
428	2746	807
470	2822	774

28 July 1971 0746-0756 AST
HF Transmitter on at 5.425 MHz at 100 kw

Altitude (km)	Temperatures T_e (°K)	T_i (°K)
218	1845	786
260	2154	835
302	2427	861
344	2417	989
386	2571	967
428	2643	1108

8 March 1972 1133-1137 AST
HF Transmitter off

Altitude (km)	Temperatures T_e (°K)	T_i (°K)
218	1627	1021
260	1449	963
302	1123	1132
344	1197	1069
386	1224	1096
428	1339	1136
470	1307	1238
512	1637	1363
554	1915	1346
596	1984	1742

8 March 1972 1137-1141 AST
HF Transmitter on at 7.63 MHz at 100 kw

Altitude (km)	Temperatures T_e (°K)	T_i (°K)
218	1690	806
260	1389	991
302	1217	1040
344	1209	1108
386	1125	1181
428	1211	1256
470	1500	1137
512	1673	1402
554	1952	1636
596	2046	1801

TABLE 3b

Penetration Frequencies From the Ionosonde

23 July 1971

Time (AST)	Frequencies f_oF_2 (MHz)
1924	9.0
1939	8.7
1945	> 8.0 E
1954	8.5 E
2009	> 8.0 E,M
2024	7.8 M
2039	7.5 M

M = multiple reflection
E = sporadic E

24 July 1971

Time (AST)	Frequencies f_oF_2 (MHz)
1520	9.5 F
1530	9.5/10 F
1540	9.7 F
1550	9.7 F
1600	9.8 F
1610	9.8 F
1620	9.9 F
1630	9.5/10 F
1640	9.8 F
1650	9.8 F
1700	9.4 F
1710	9.3 F
1720	9.1 F
1730	9.0 F
1740	8.9 F
1750	8.6 F
1800	8.8 F

F = thick traces

25 July 1971

Time (AST)	Frequencies f_oF_2 (MHz)
0900	6.8
0905	6.9
0910	7.0
0915	7.0
0920	7.1
0925	7.2
0935	7.4
0940	7.5
0945	7.5
0950	7.6
0955	8.0
1000	8.0 F
1005	8.1 F
1010	8.1 F
1015	8.1
1020	8.1
1025	8.1
1030	8.1
1035	8.1
1040	8.0
1045	8.1
1050	8.1
1055	8.1
1100	8.1
1105	8.2

F = thick traces

28 July 1971

Time (AST)	Frequencies f_oF_2 (MHz)
0630	4.7
0635	4.7
0640	4.8
0645	4.9
0650	4.5/5.5
0655	4.5/5.5
0700	4.8
0705	4.8
0720	5.5
0750	6.1
0857	6.5
0900	6.5
0910	6.4
0940	7.1

8 March 1972

Time (AST)	Frequencies f_oF_2 (MHz)
0200	5.1
0302	5.0
0401	4.0
0510	3.3
0600	3.2
0703	6.0
0750	7.5
0815	7.9
0855	8.8
0930	9.7
1030	11.2
1140	13.0
1240	12.5
1340	12.8
1430	13.0
1515	13.0
1605	13.3
1710	13.2
1815	12.0
1905	9.4
1920	8.7
2005	7.2
2049	7.4

SPECTRA

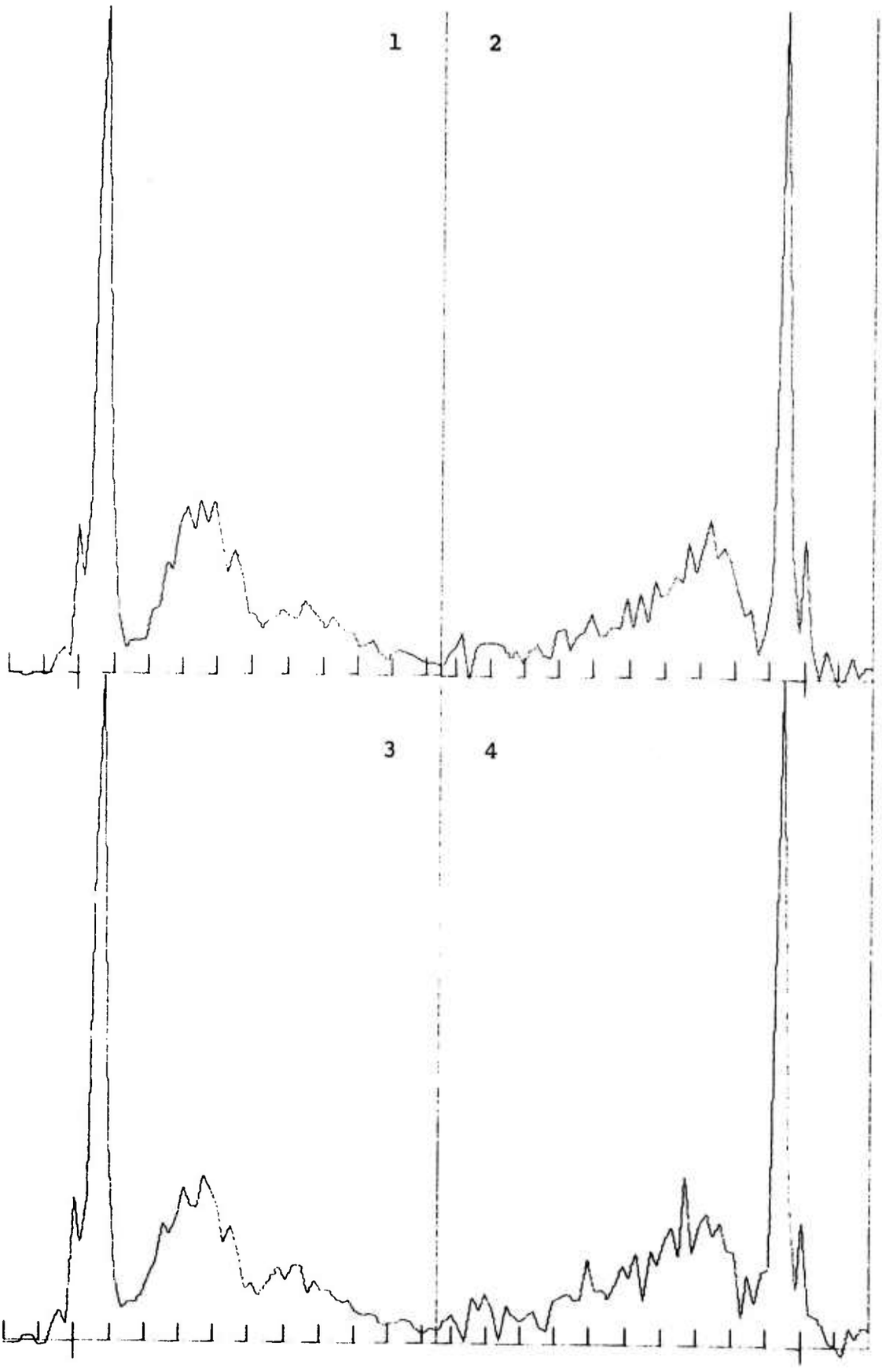
1
2
3
4

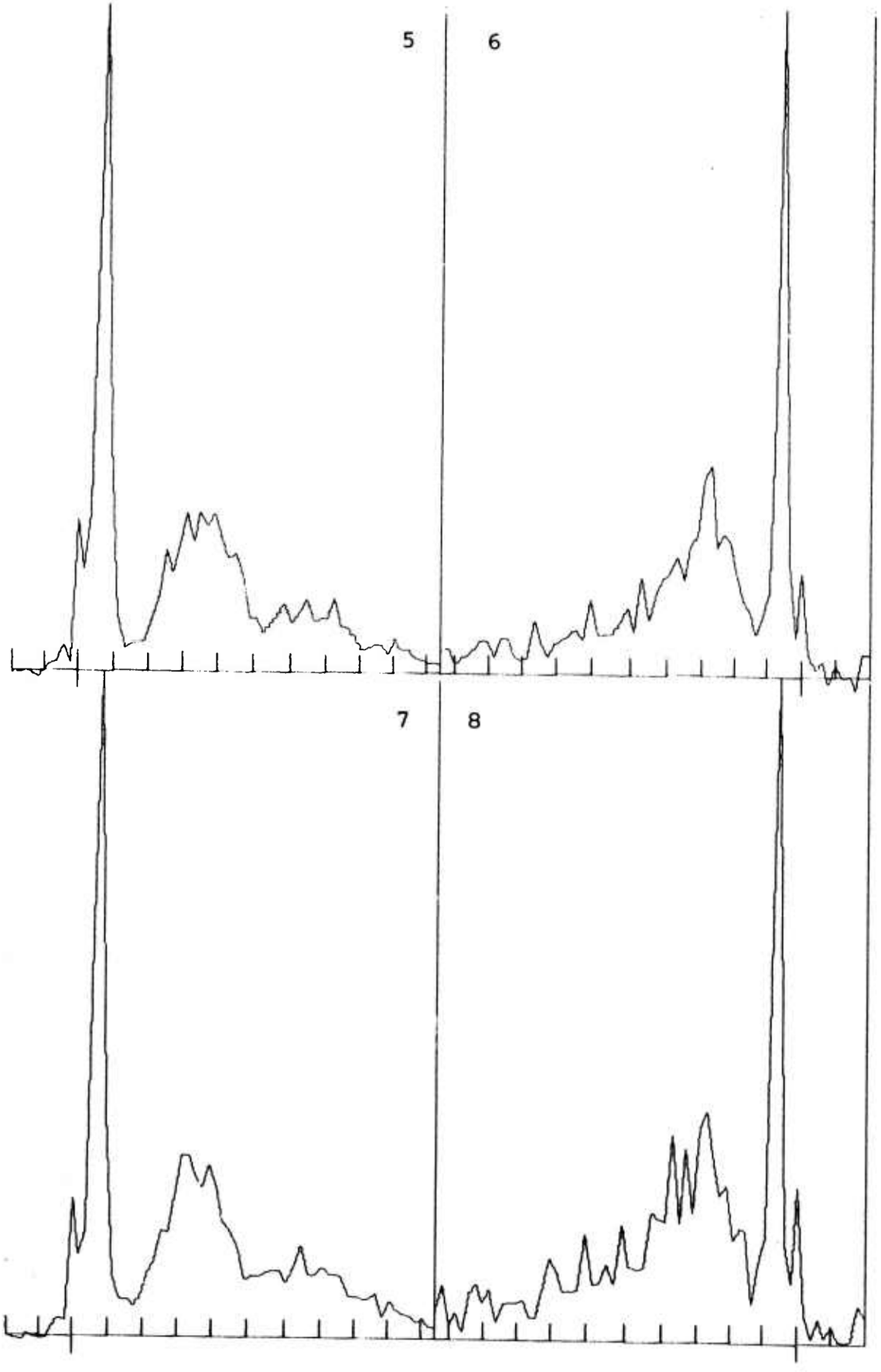
5
6
7
8

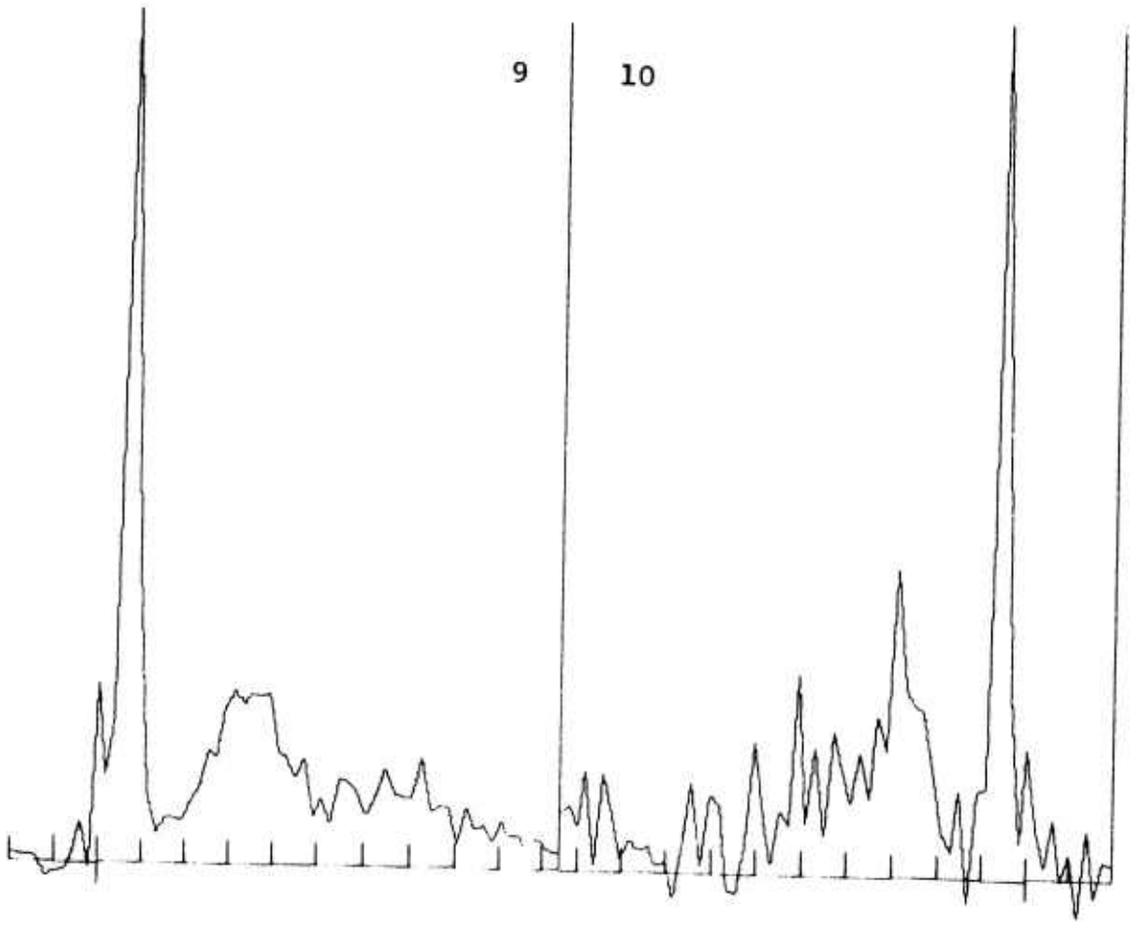
9
10

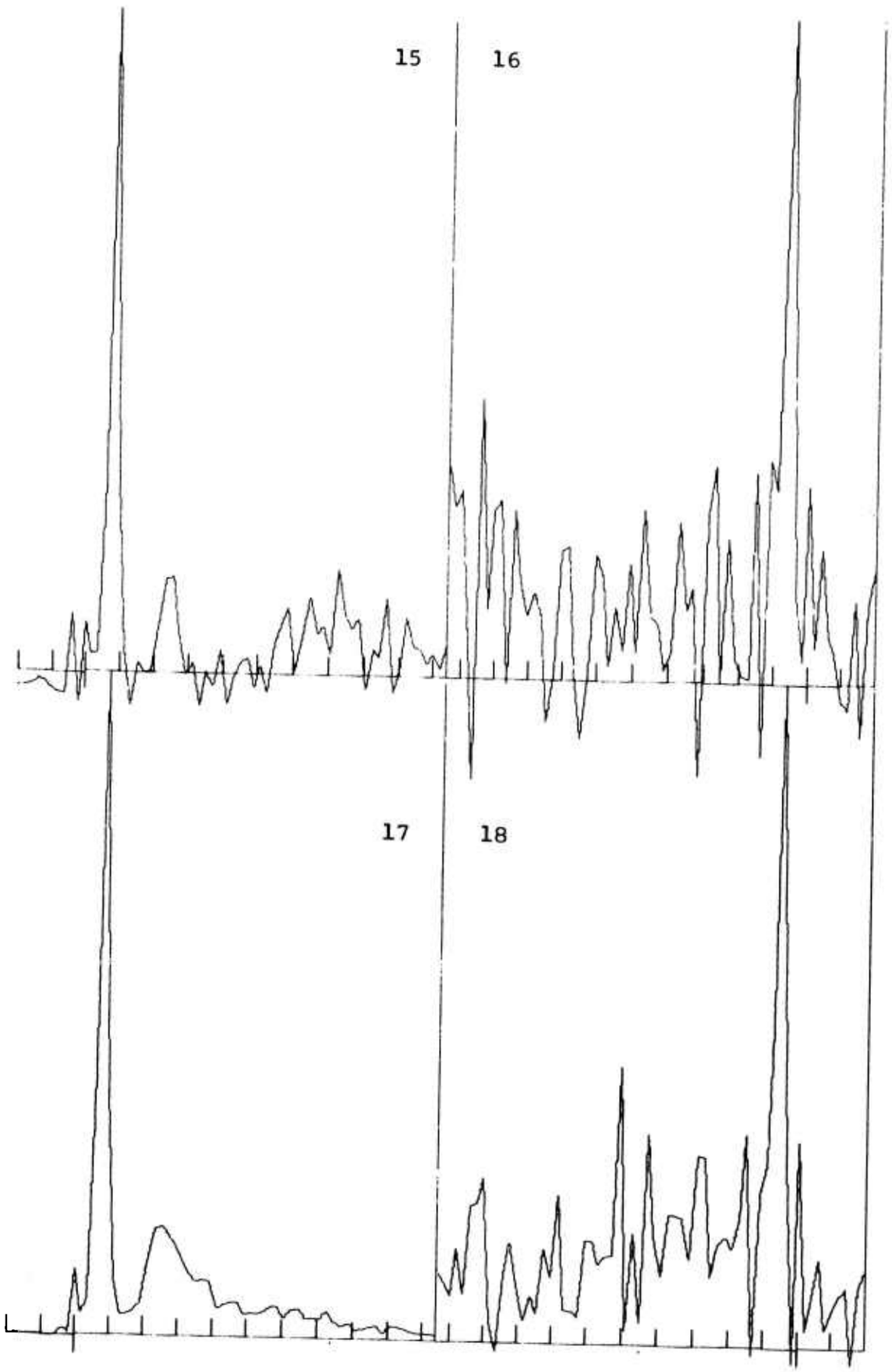
15
16
17
18

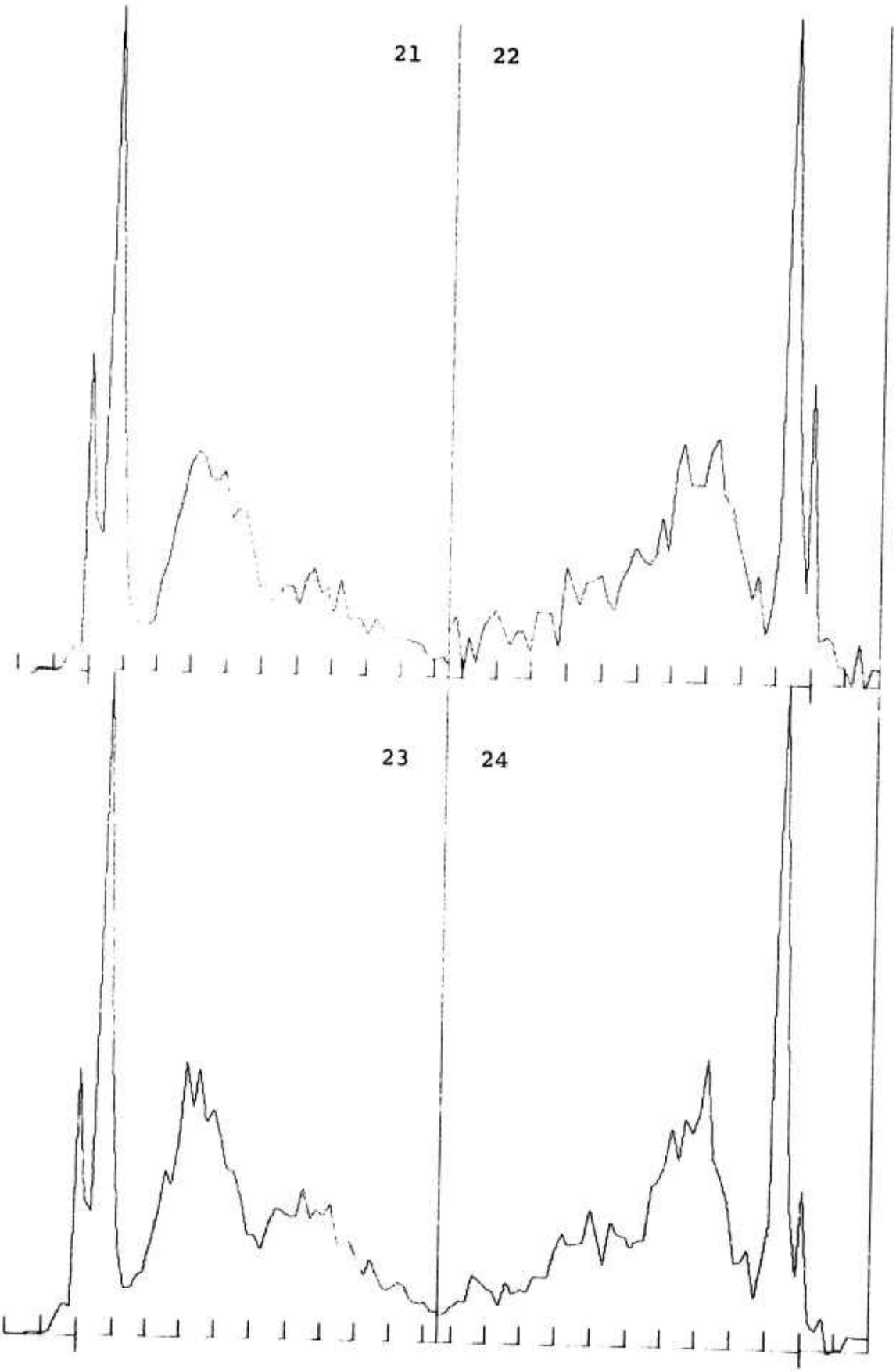
21
22
23
24

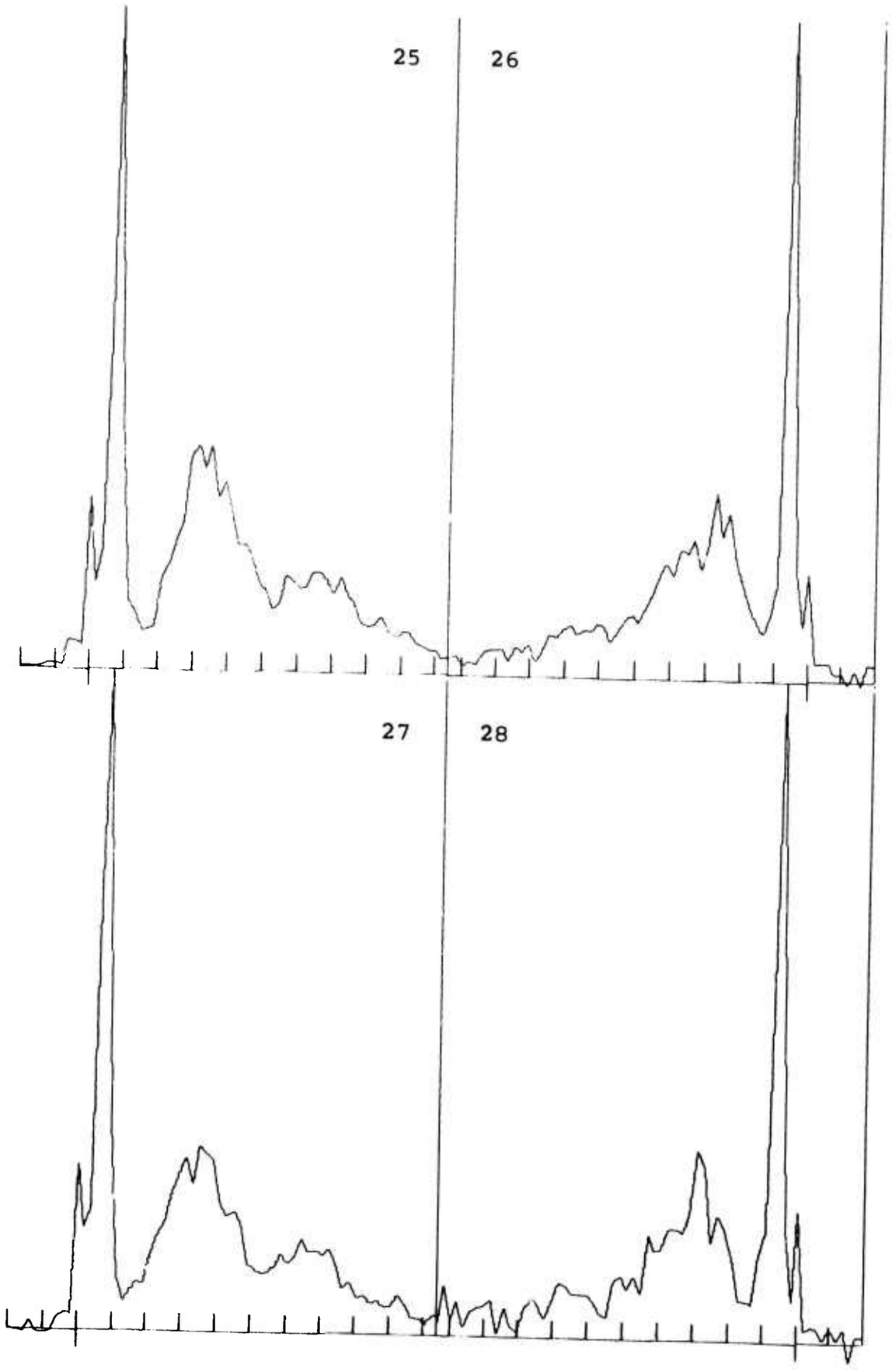
25
26
27
28

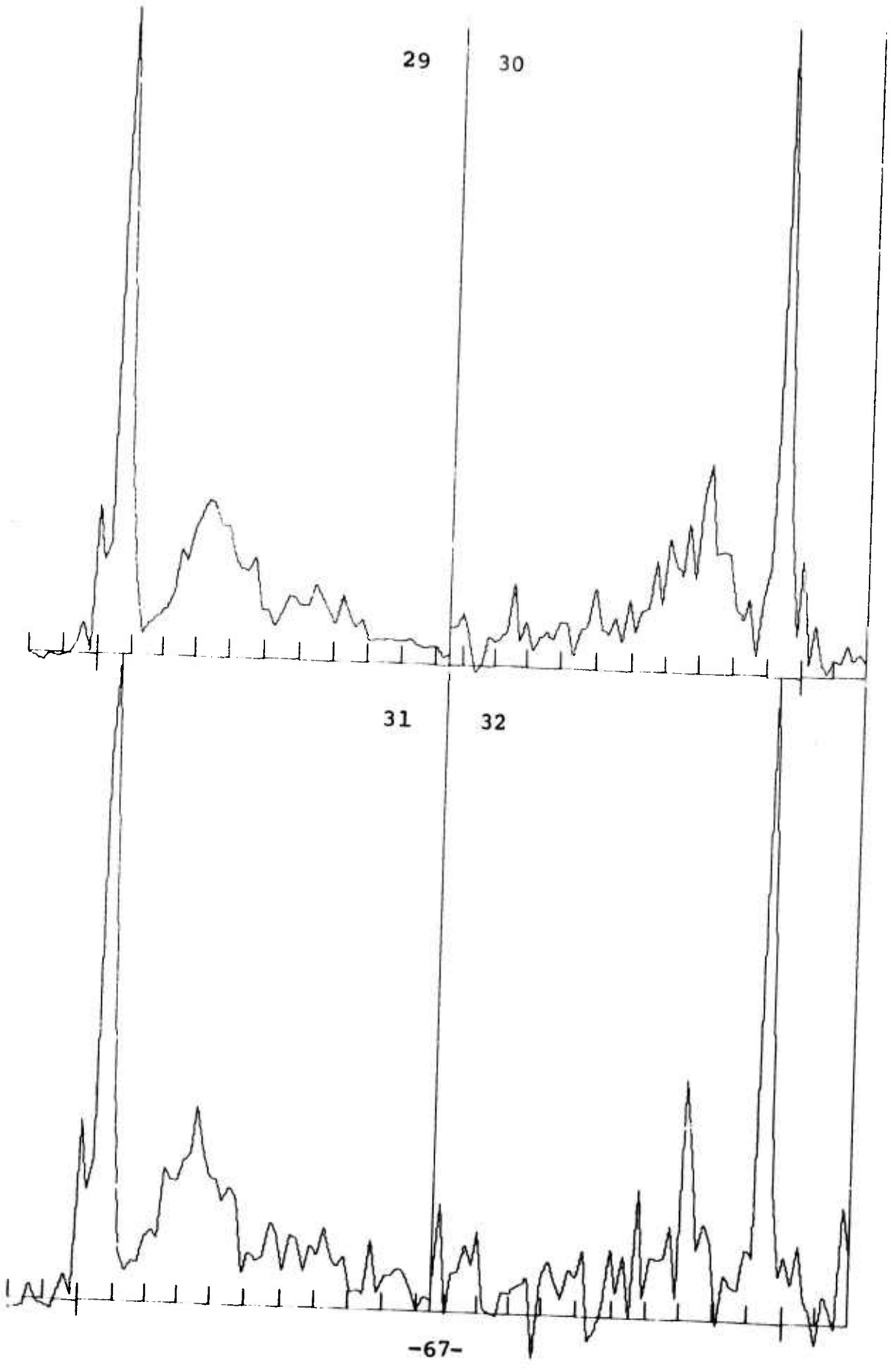
29
30
31
32

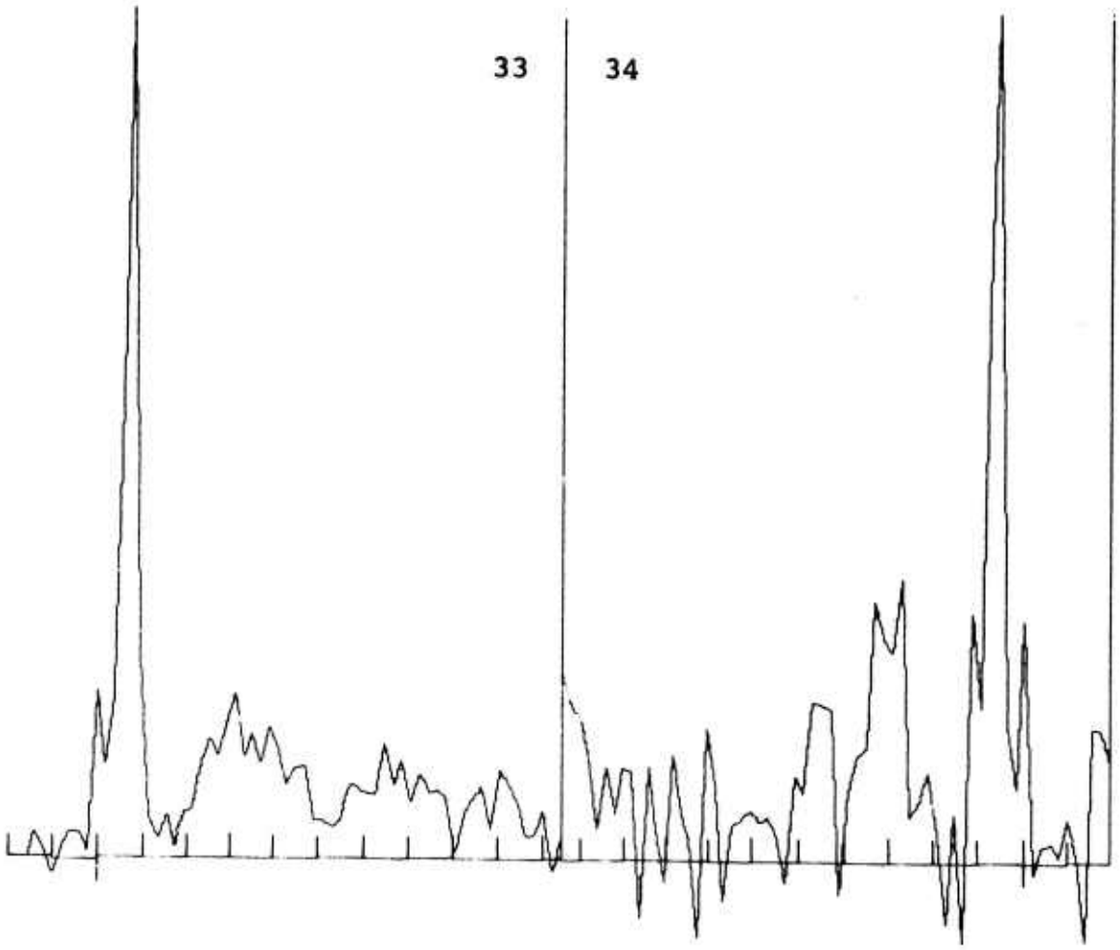
33
34

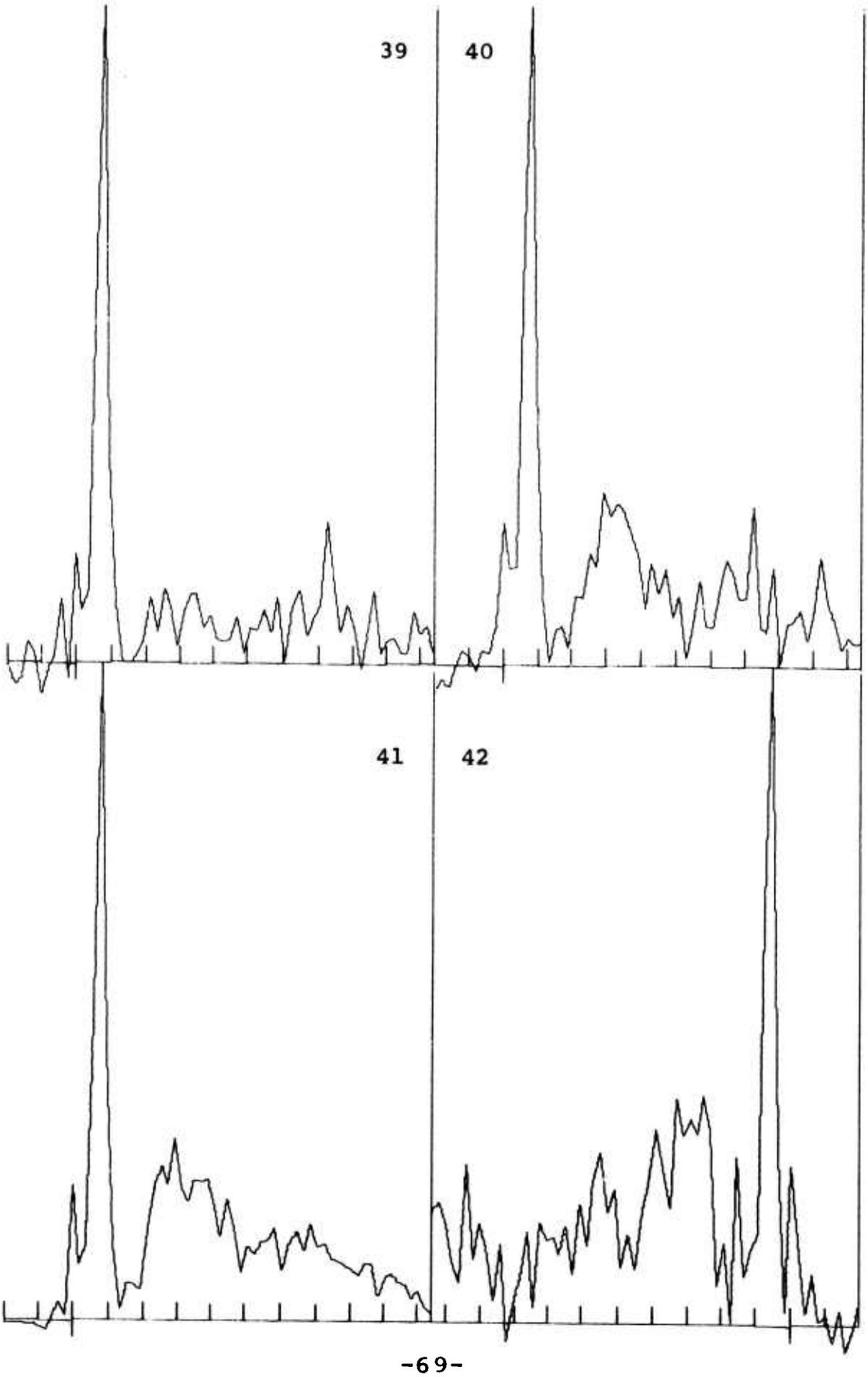
39
40
41
42

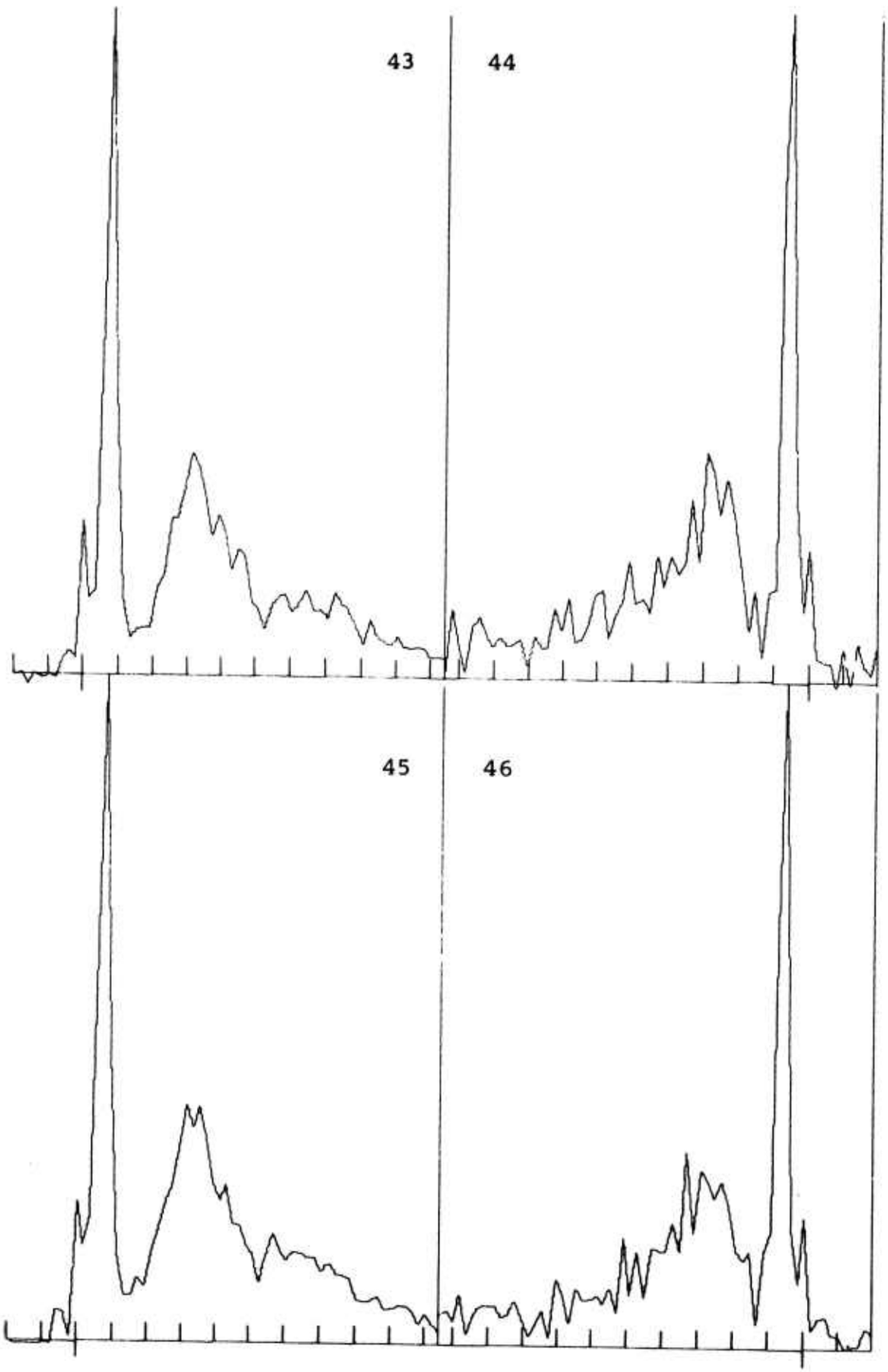
43
44
45
46

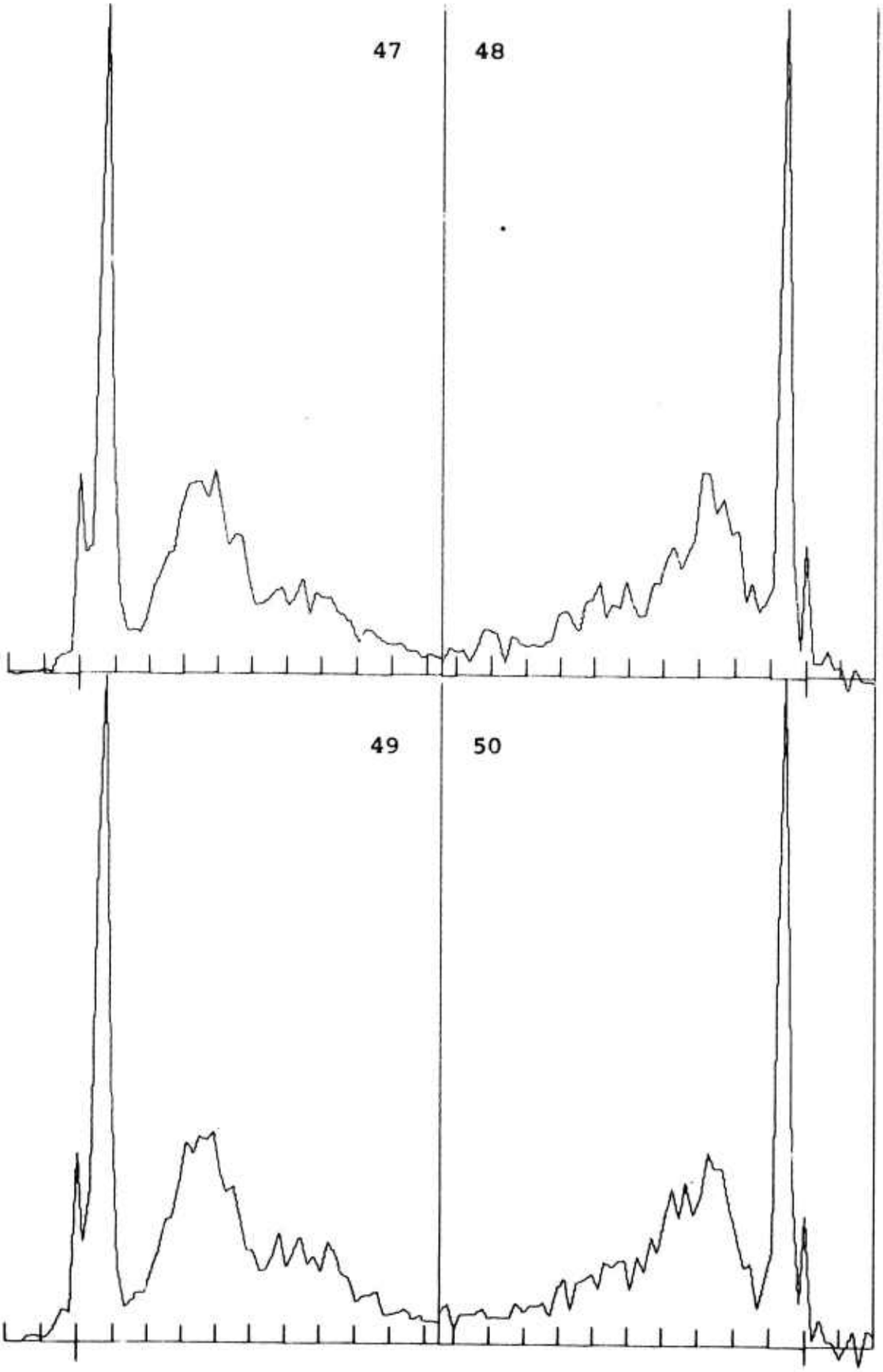
47
48
49
50

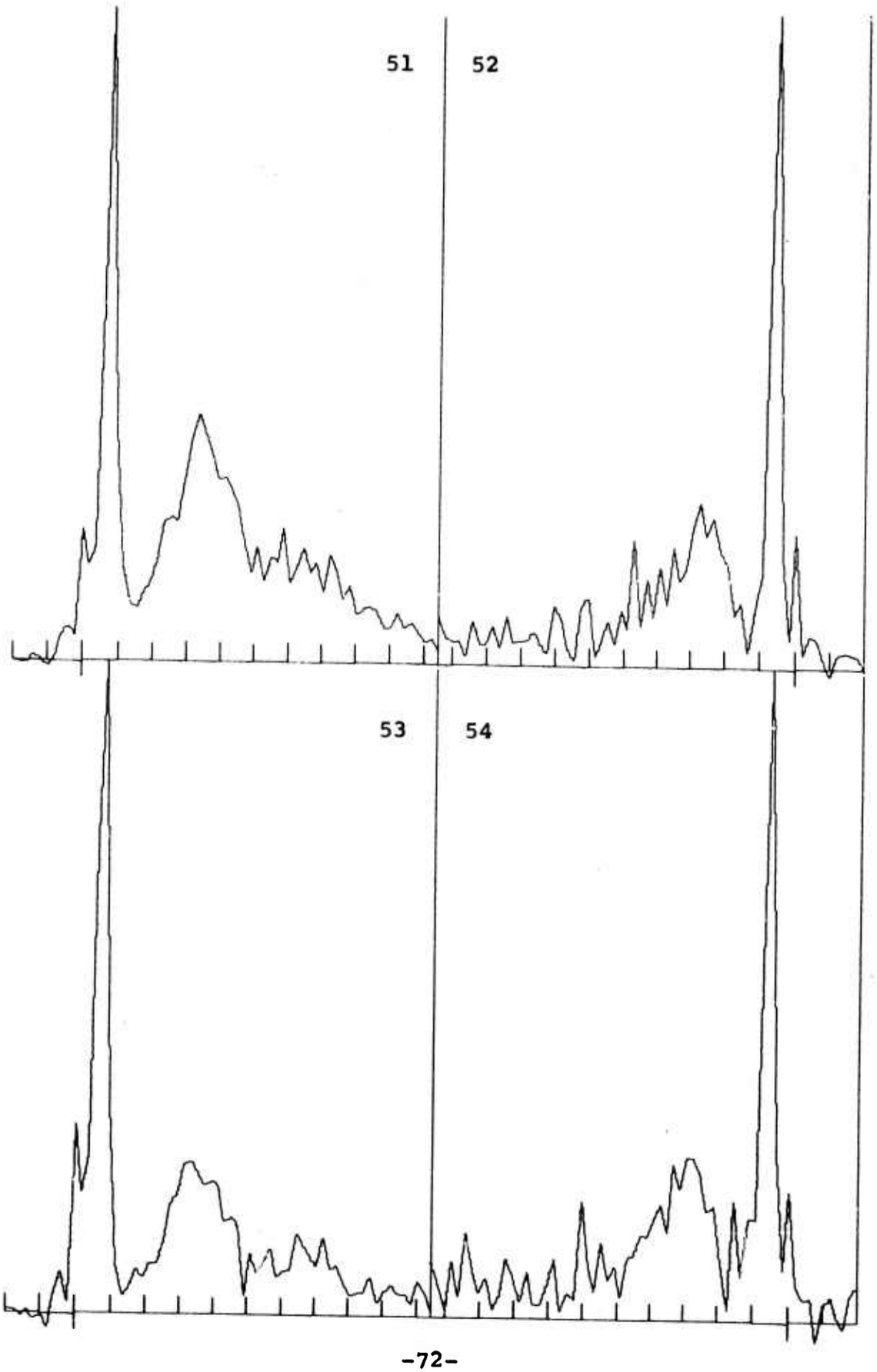
51
52
53
54

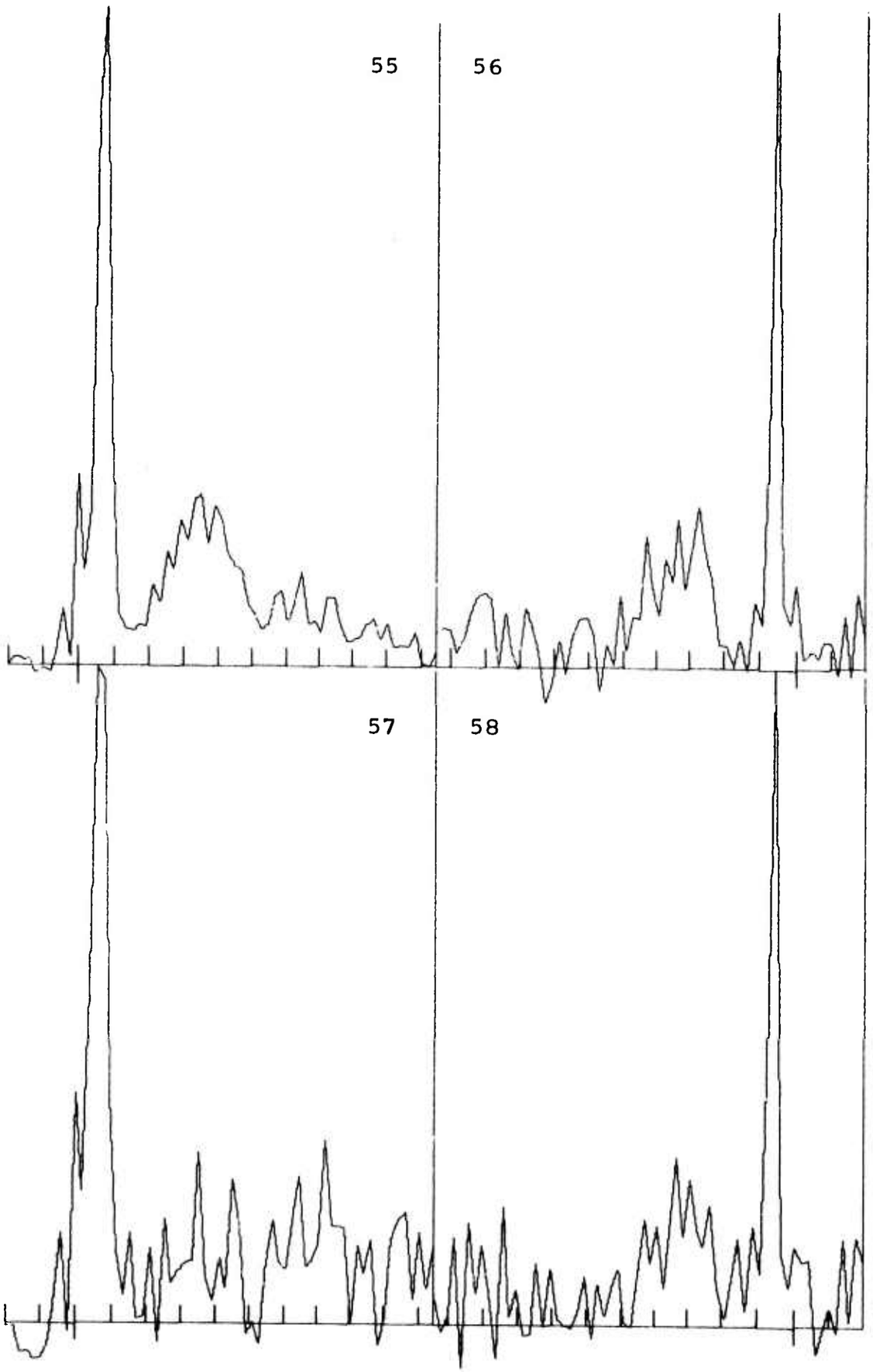
55
56
57
58

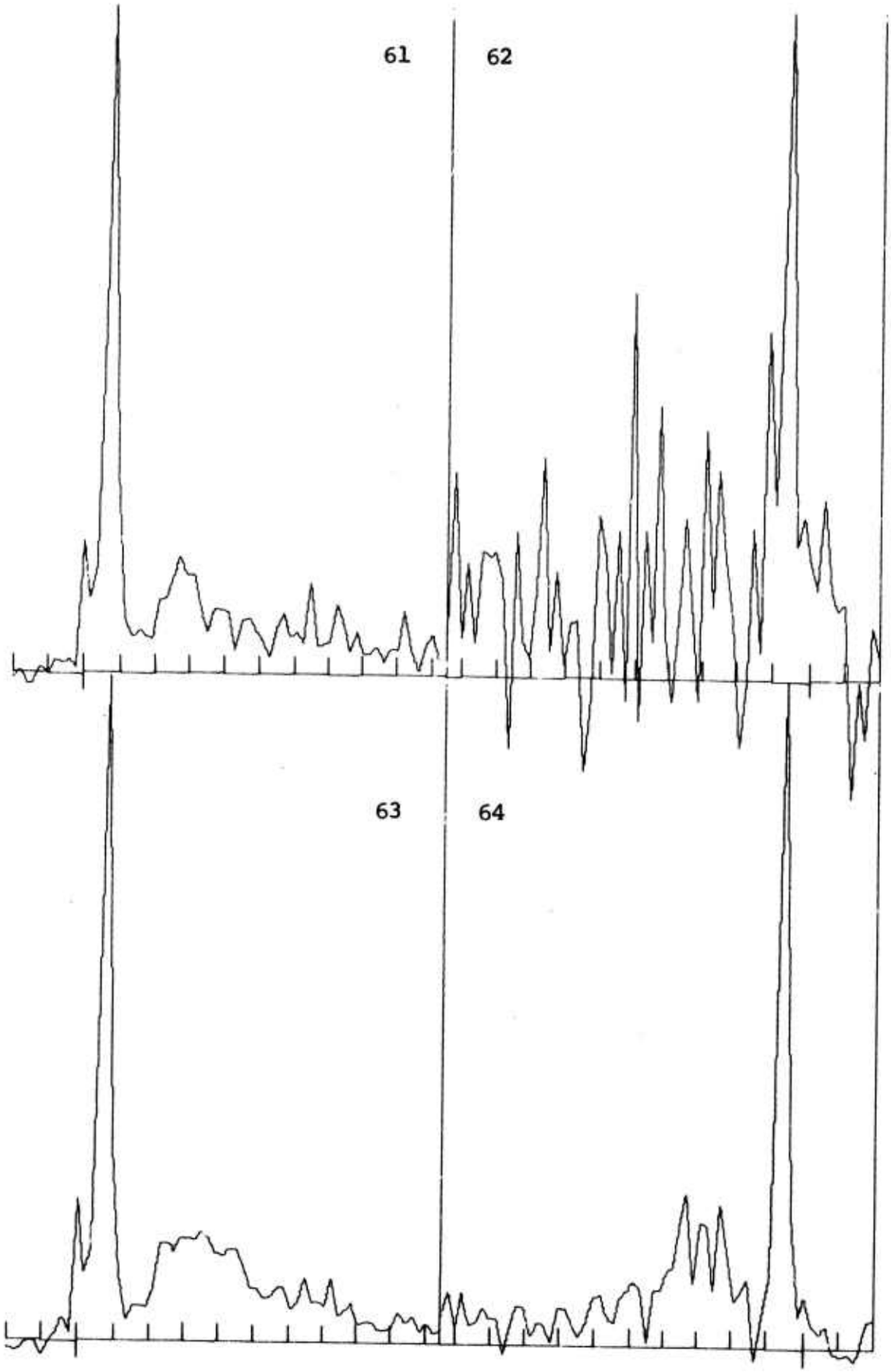
61
62
63
64

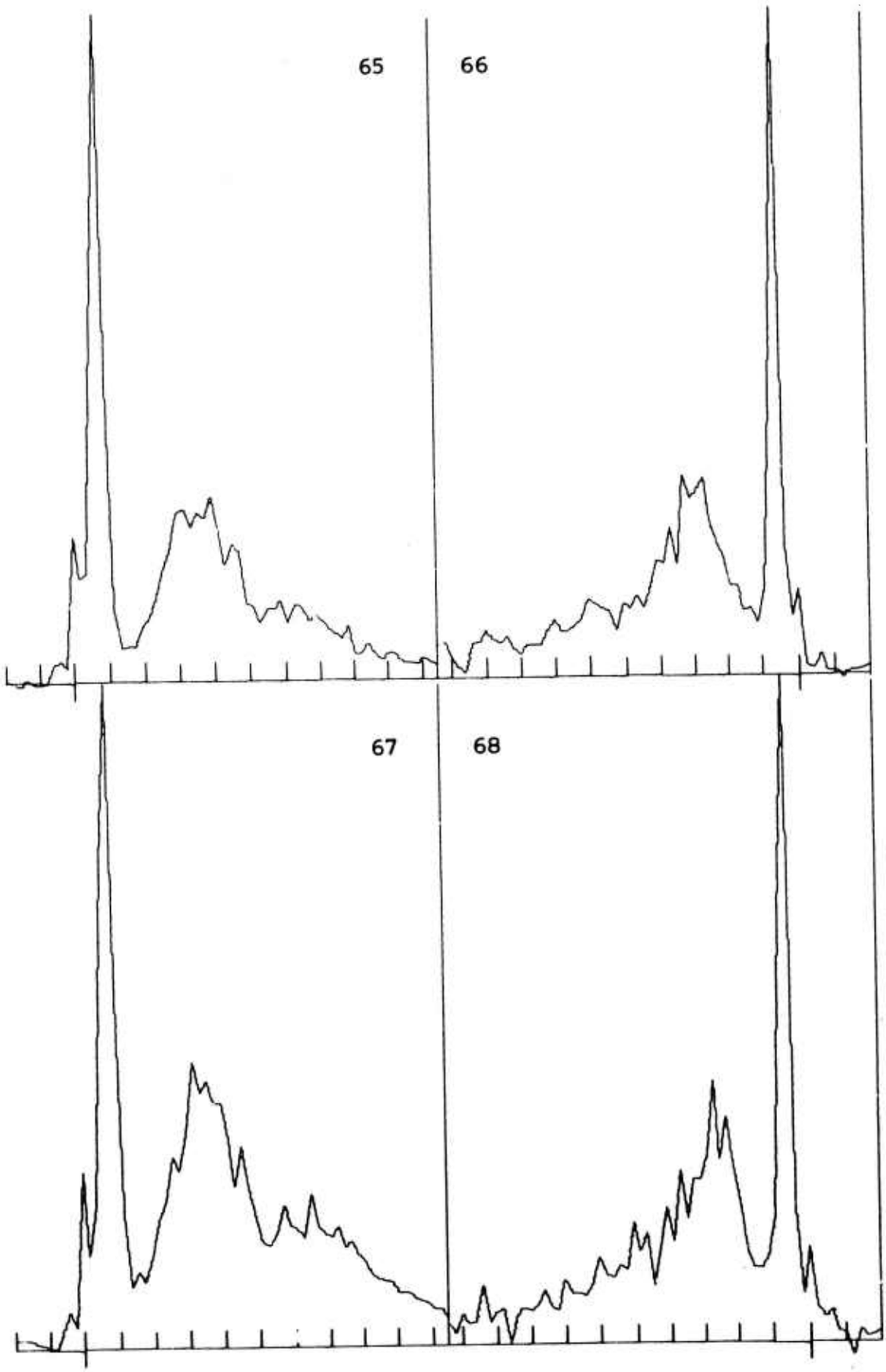
65
66
67
68

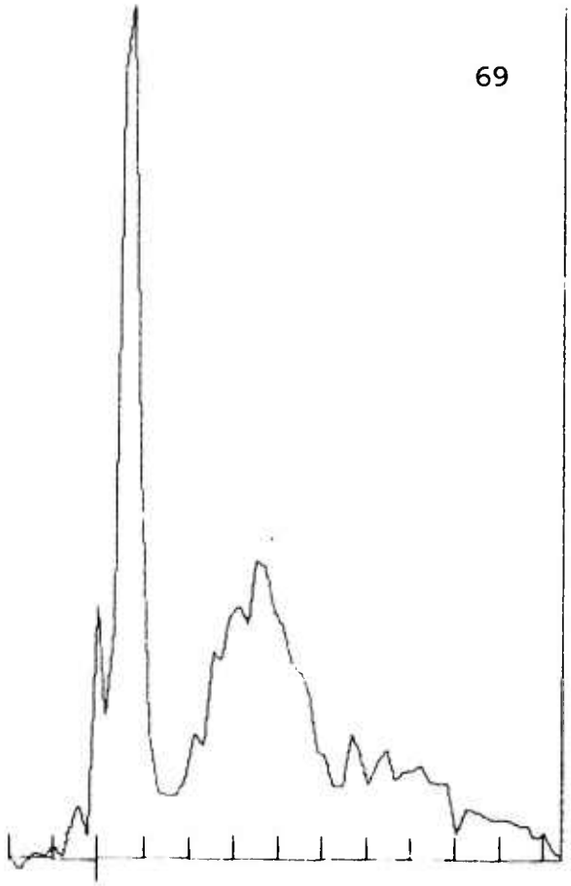
69

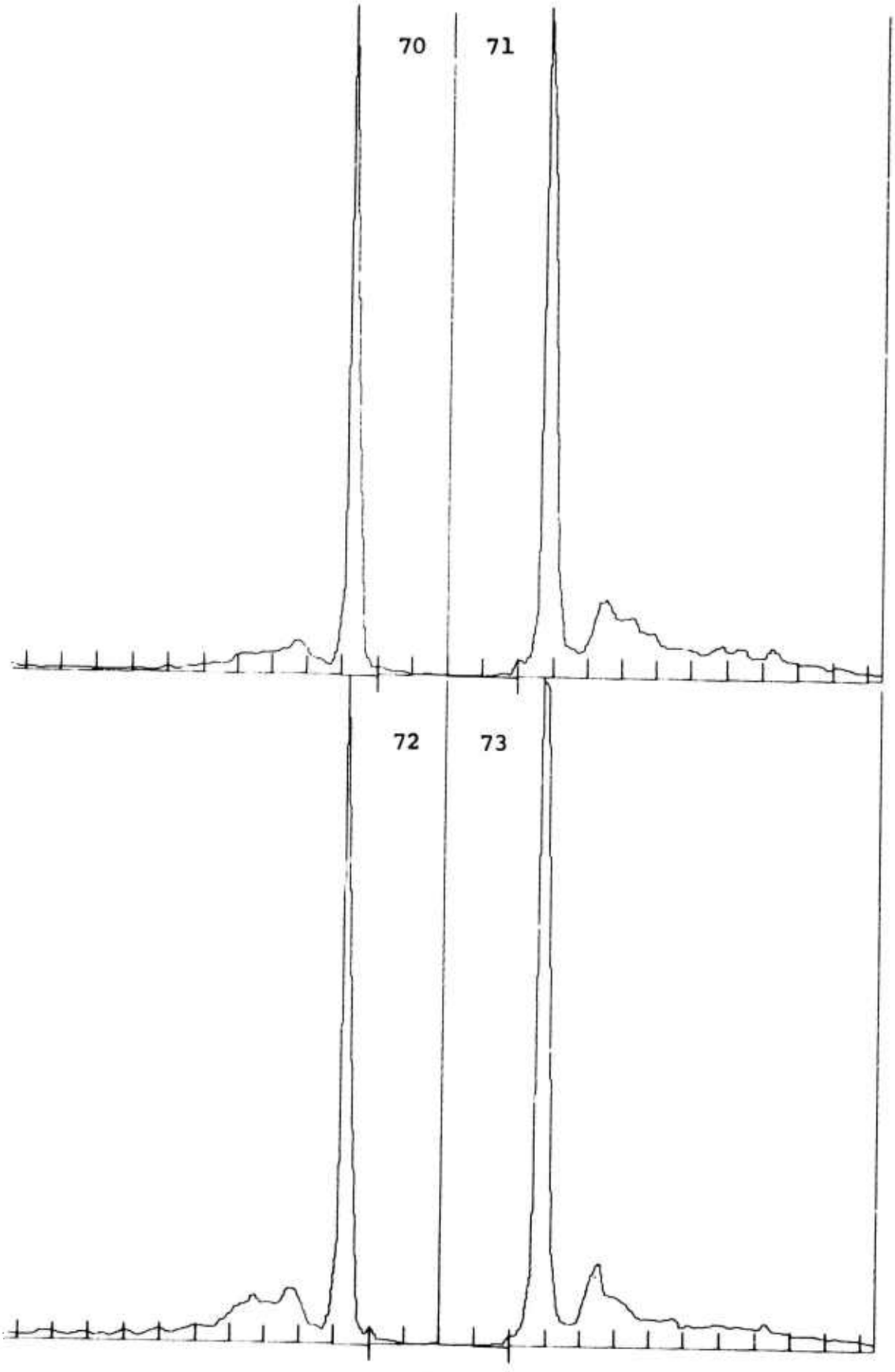
70
71
72
73

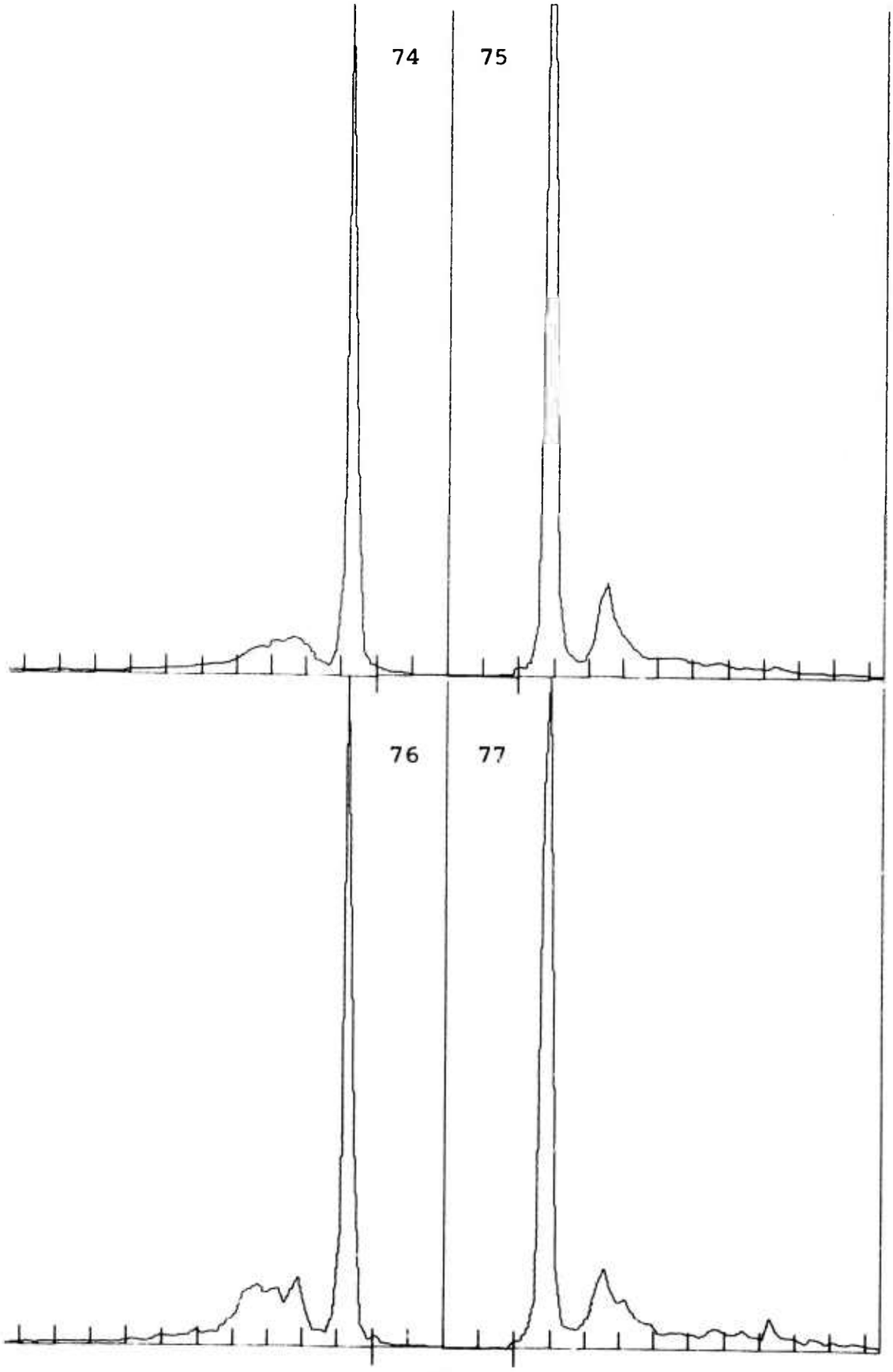
74
75
76
77

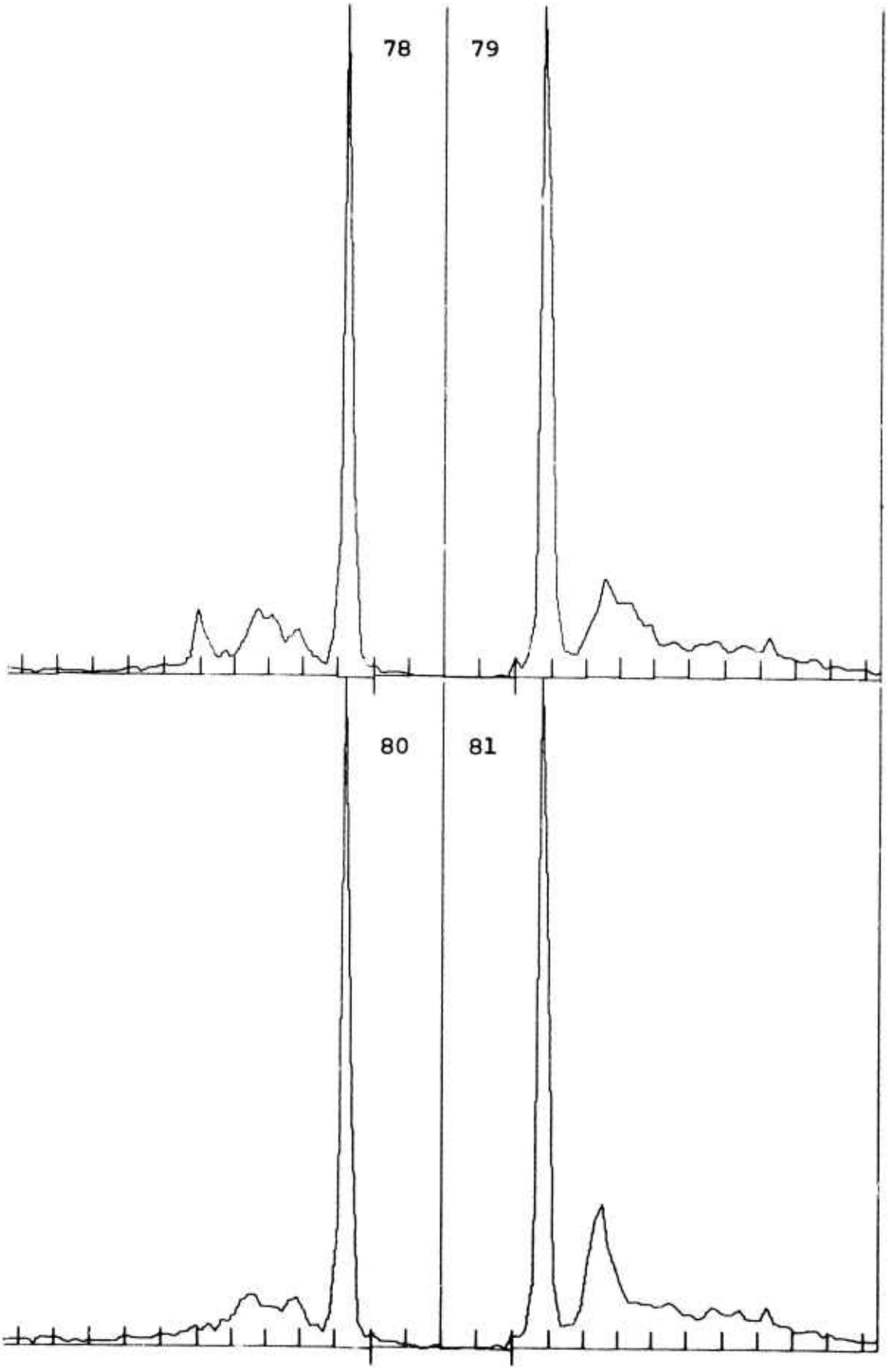
78
79
80
81

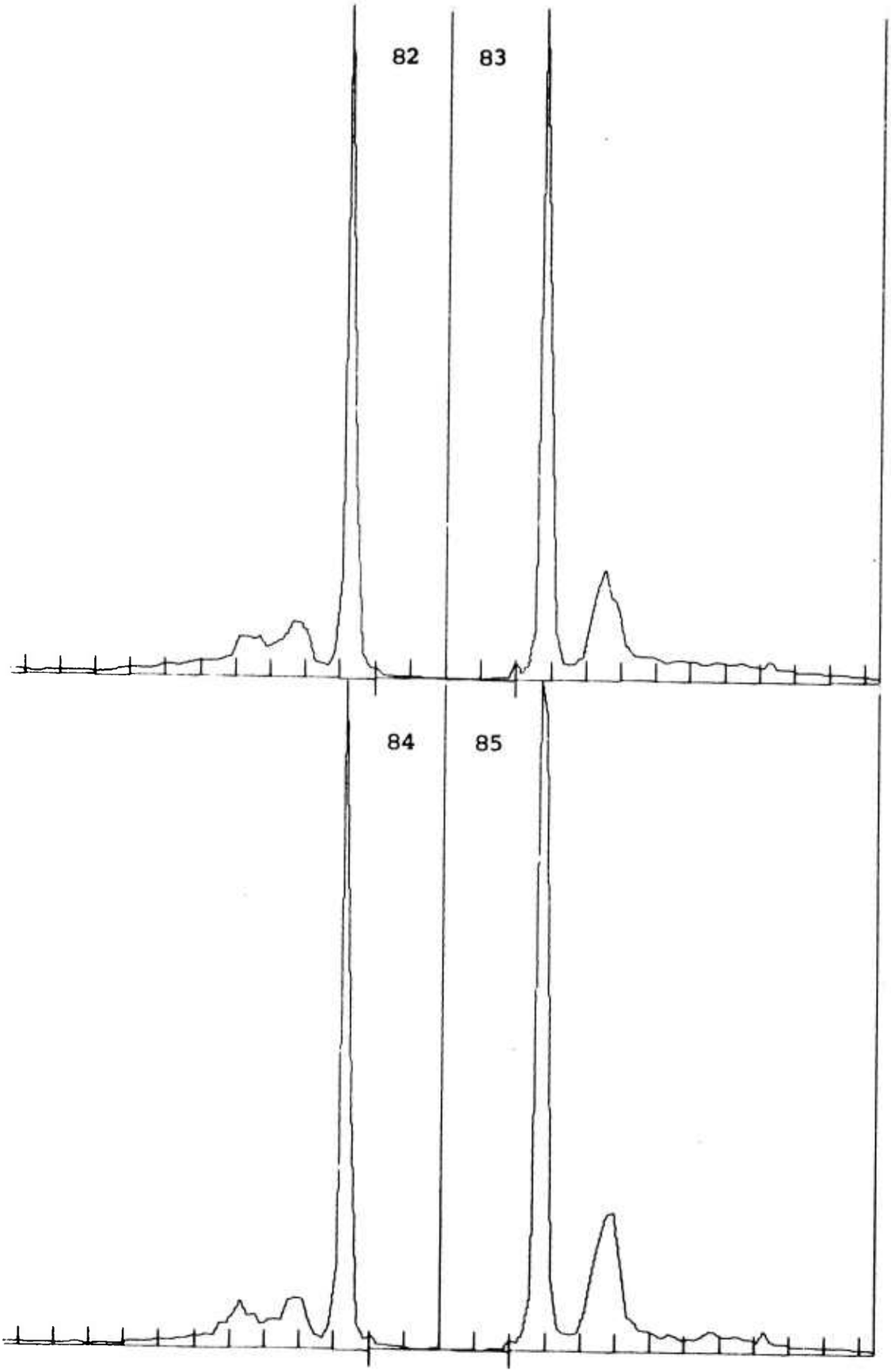
82
83
84
85

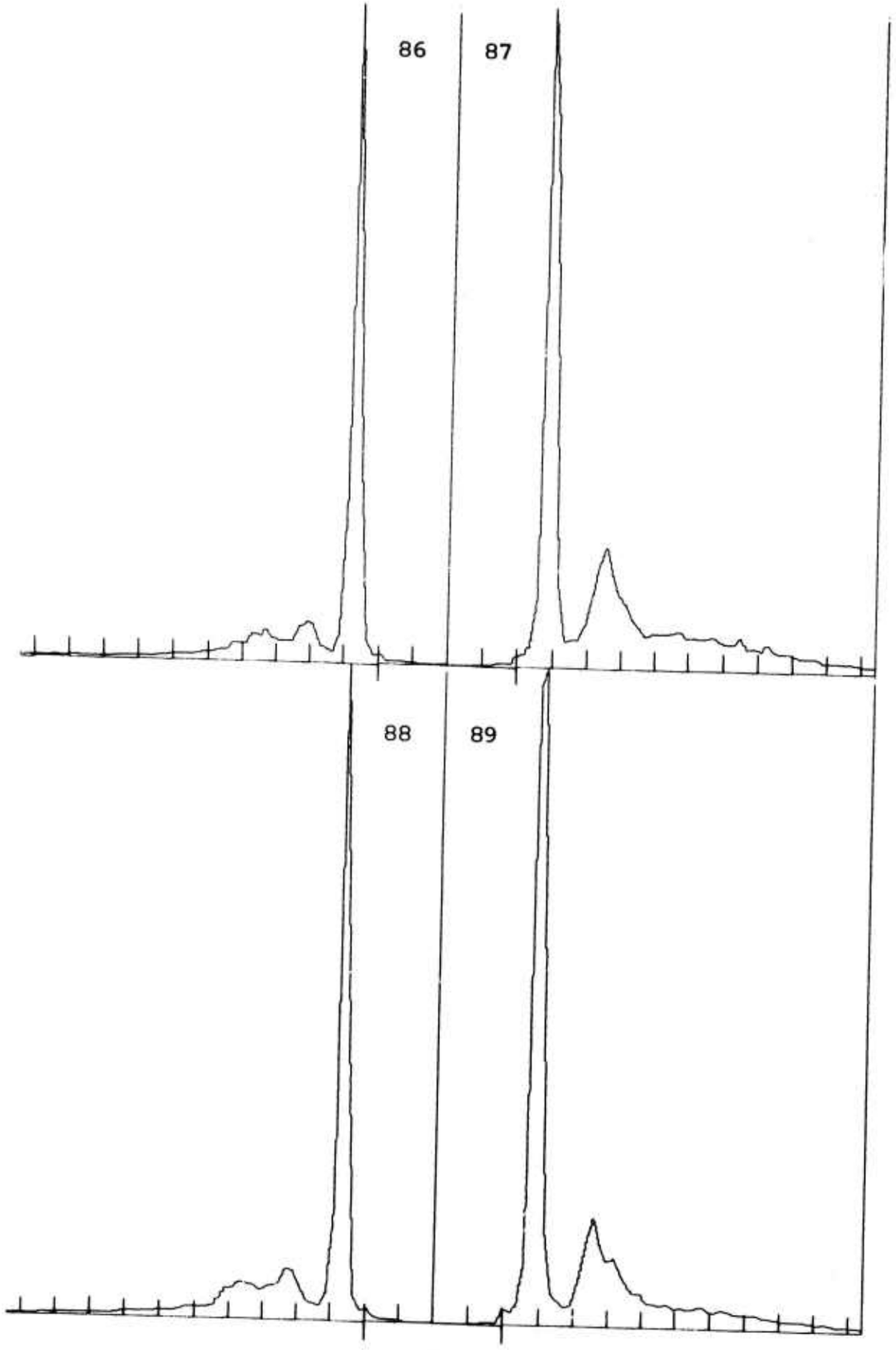
86
87
88
89

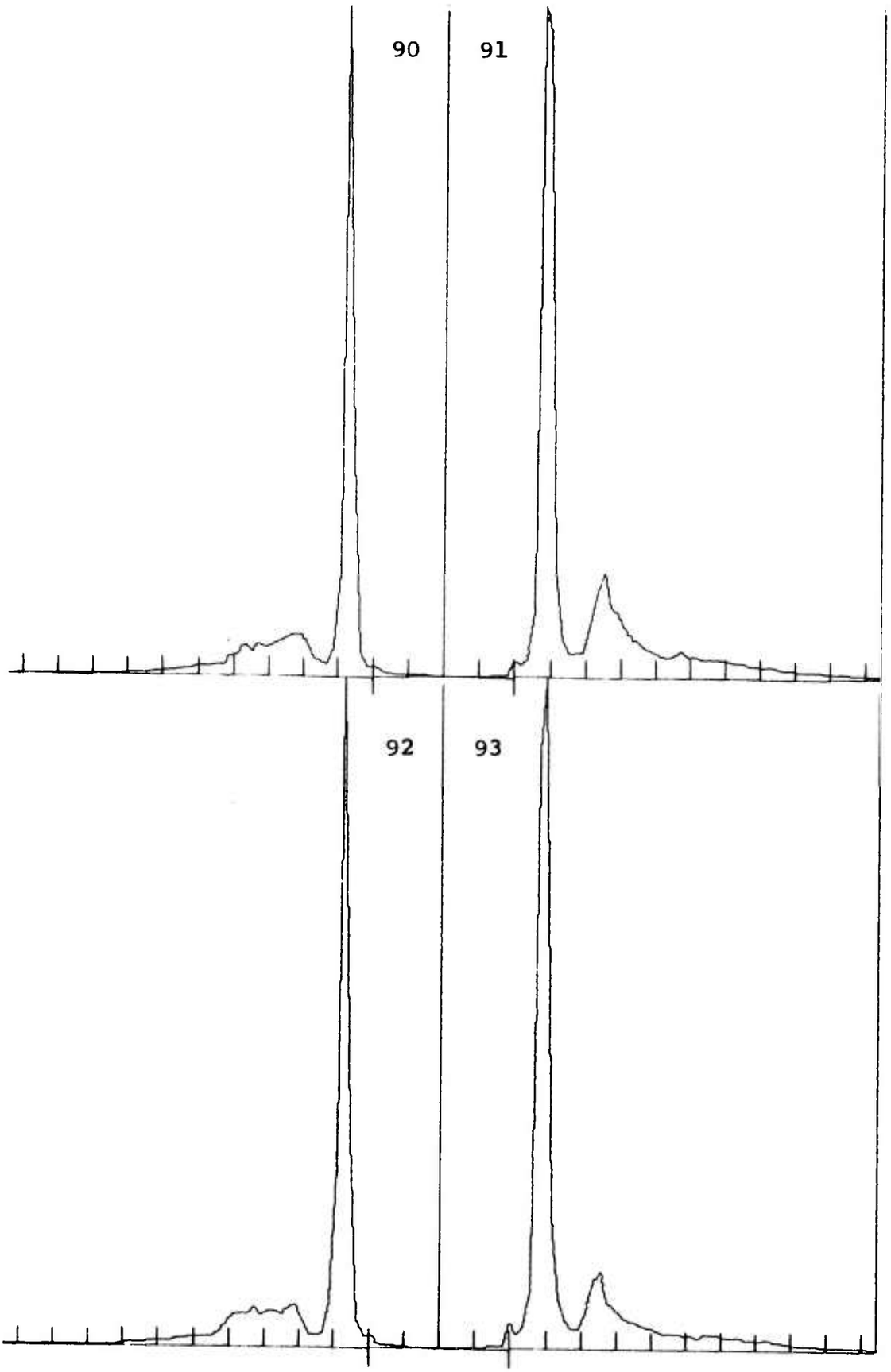
90
91
92
93

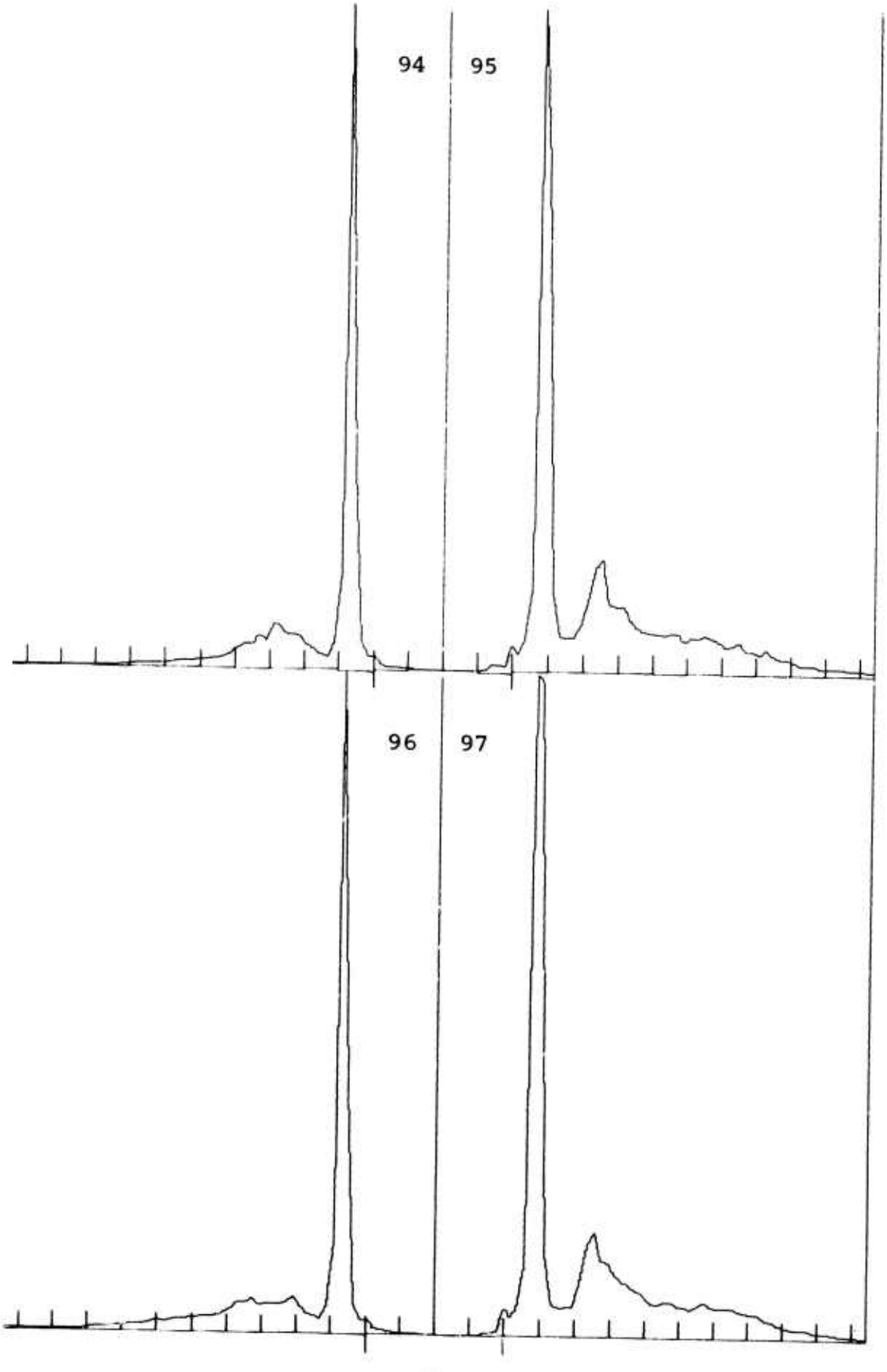
94
95
96
97

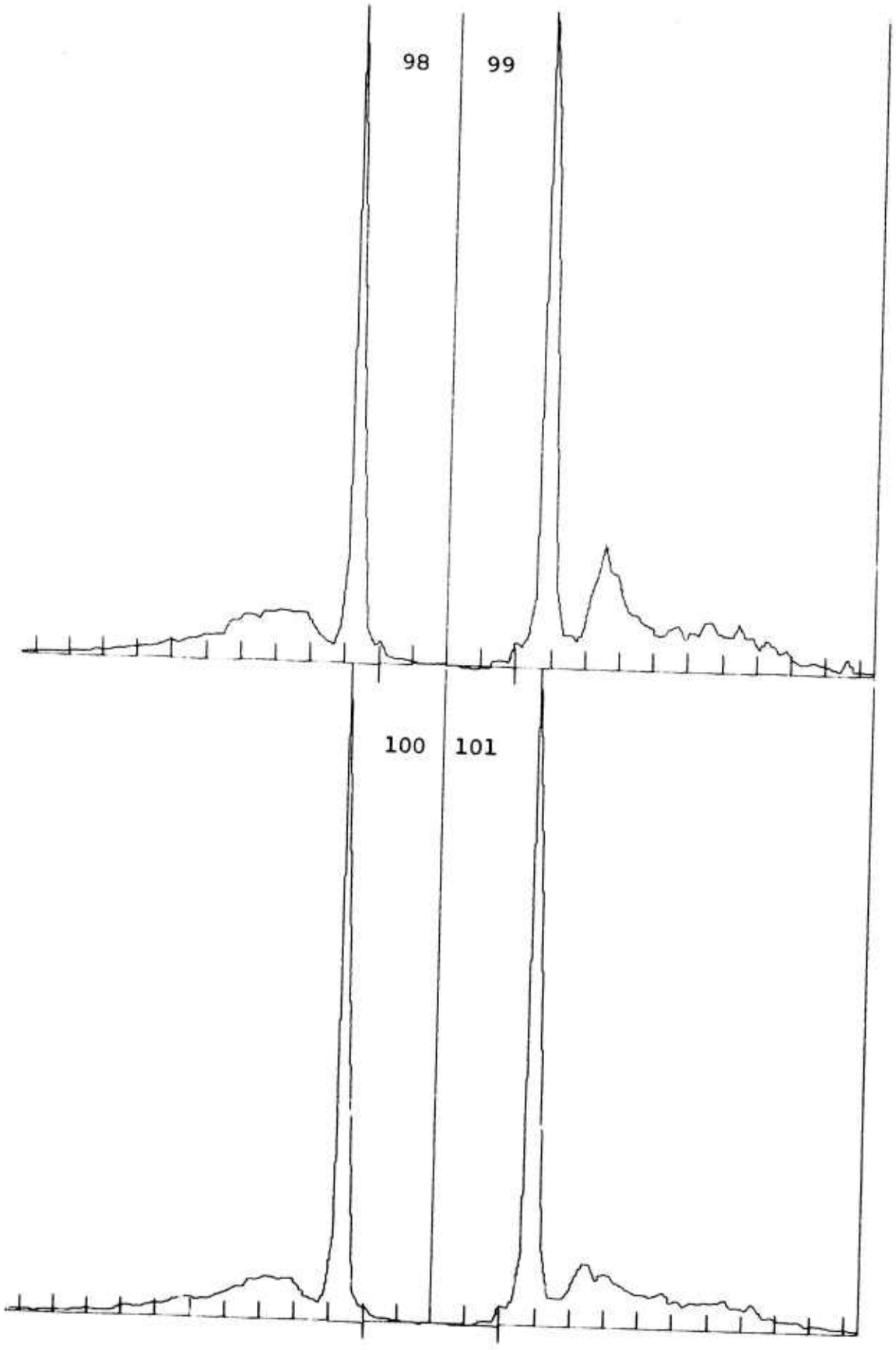
98
99
100
101

102

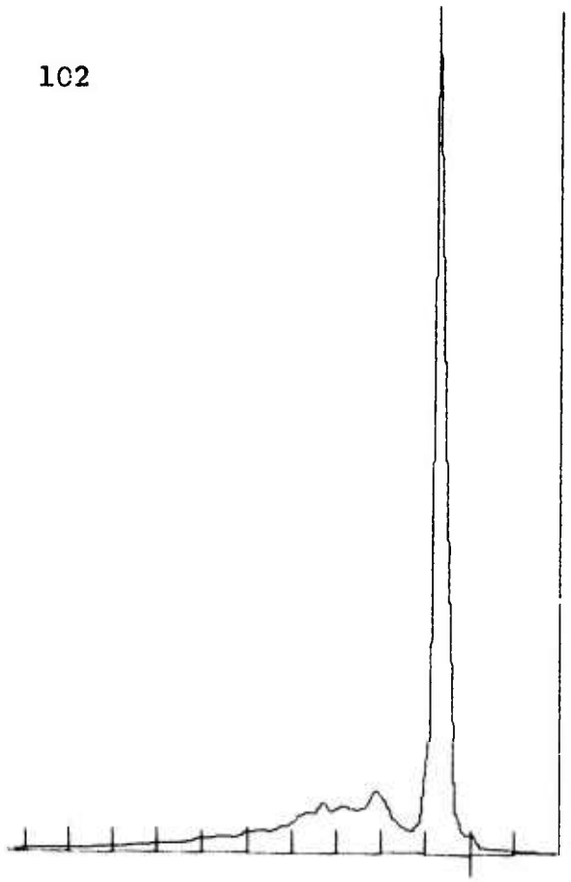

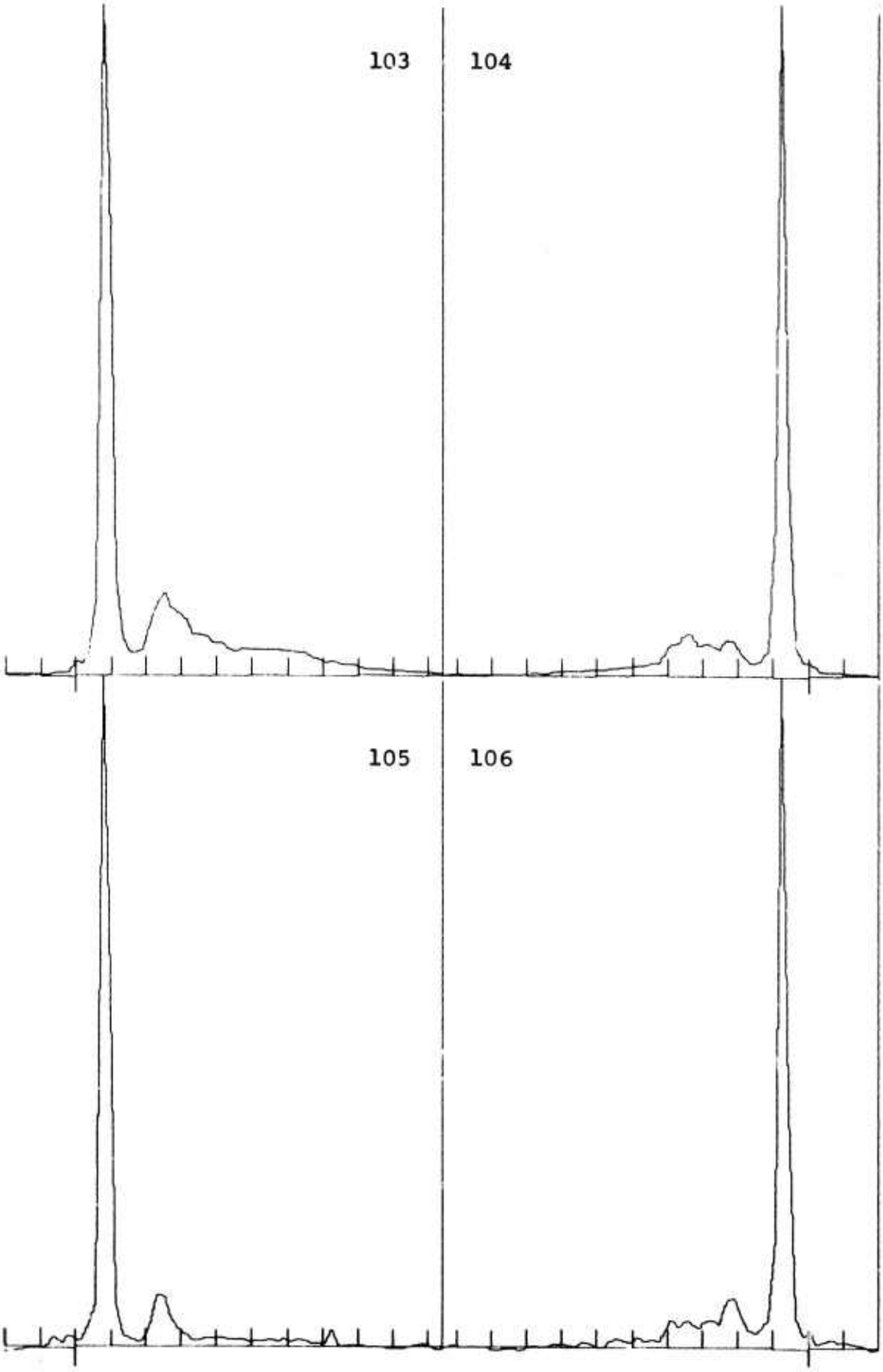
103
104
105
106

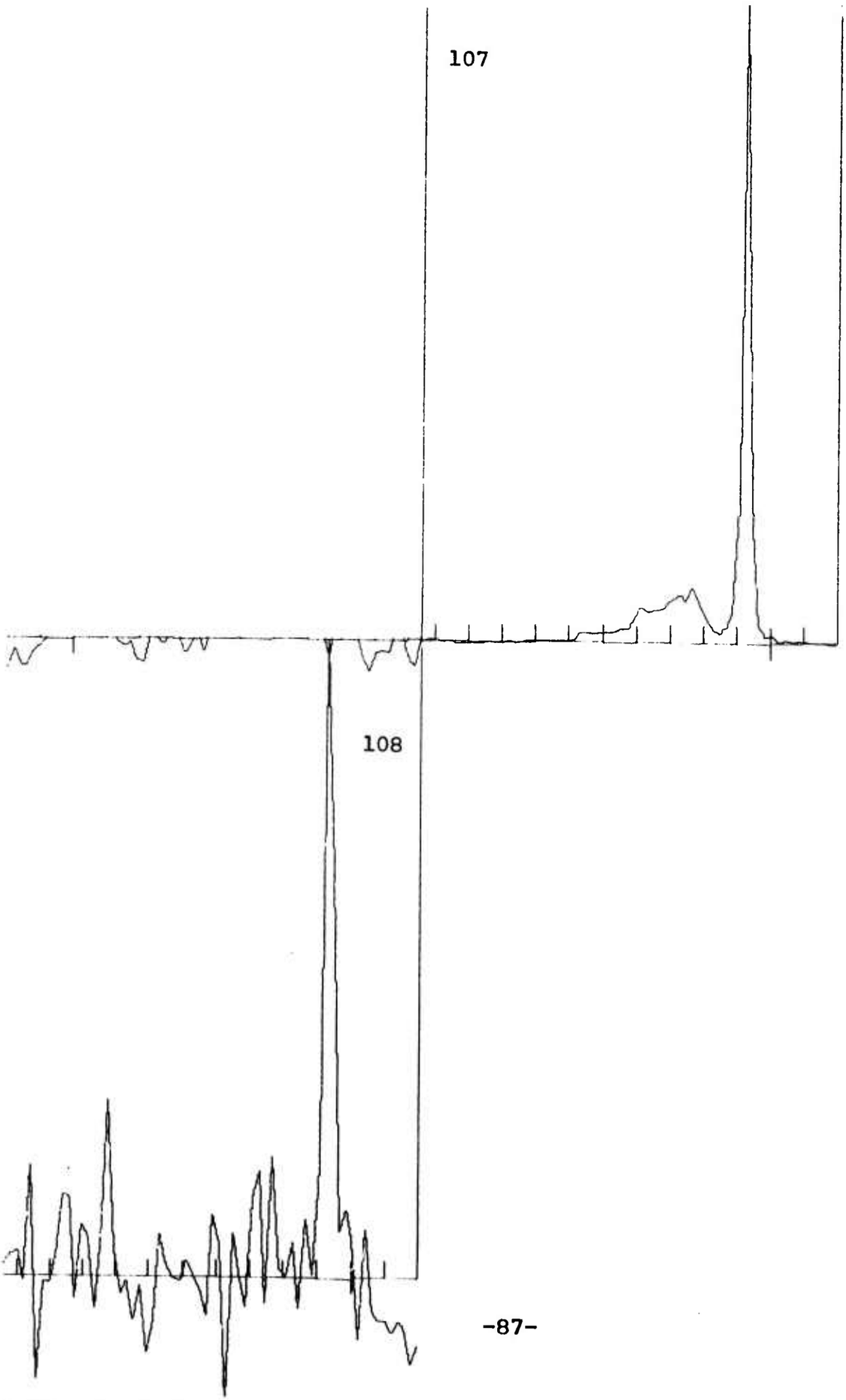
107
108

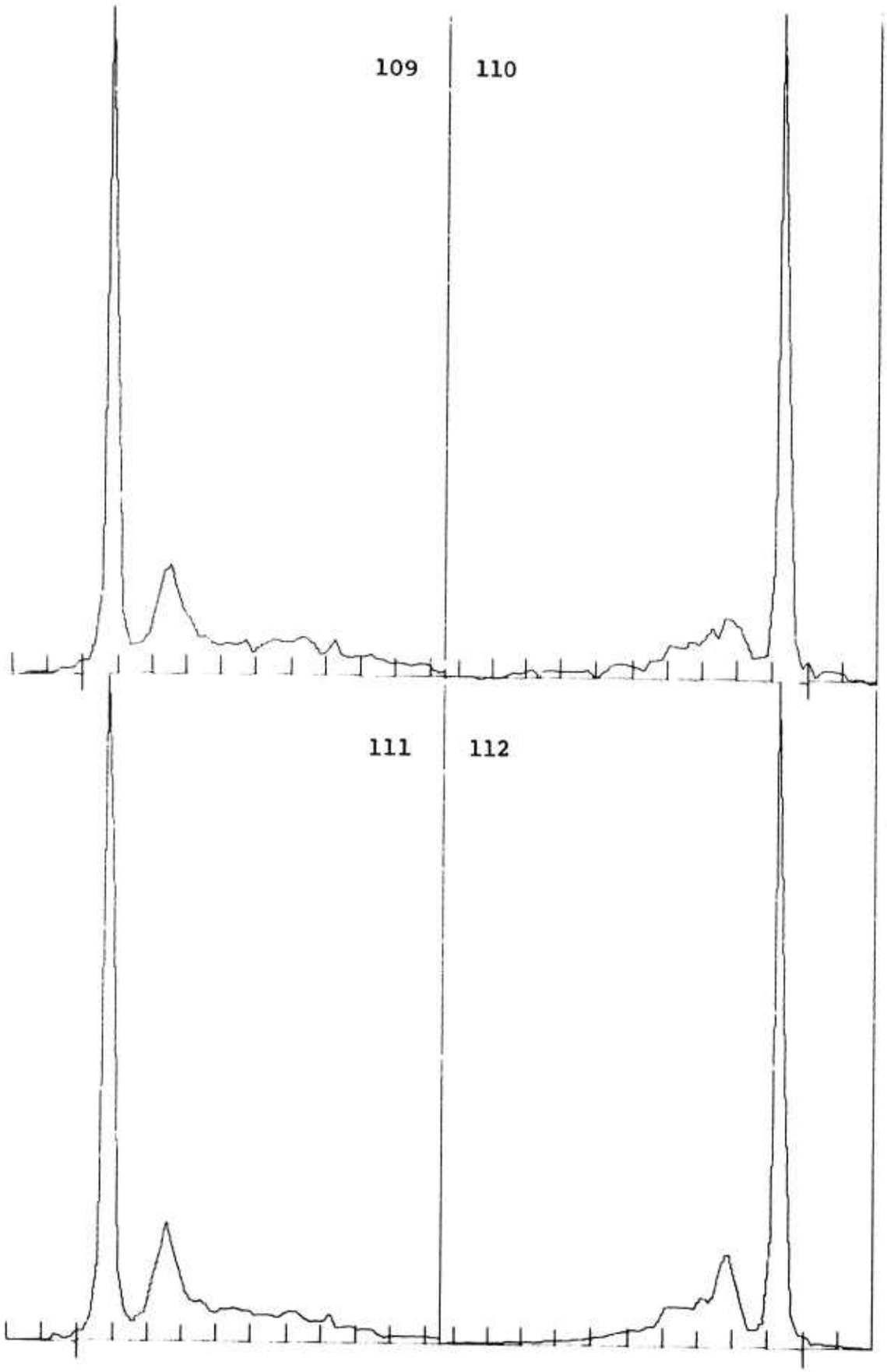
109
110
111
112

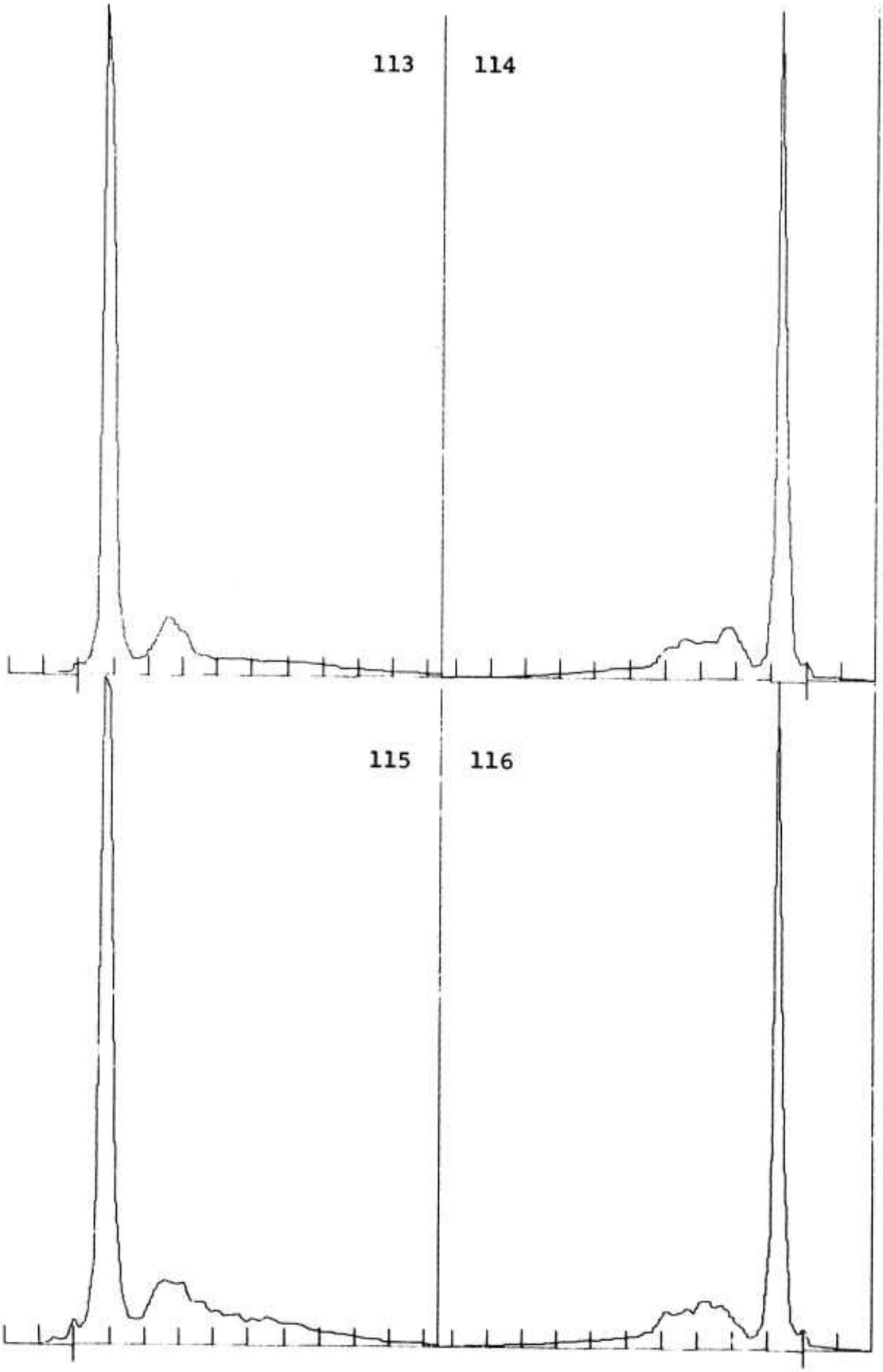
113
114
115
116

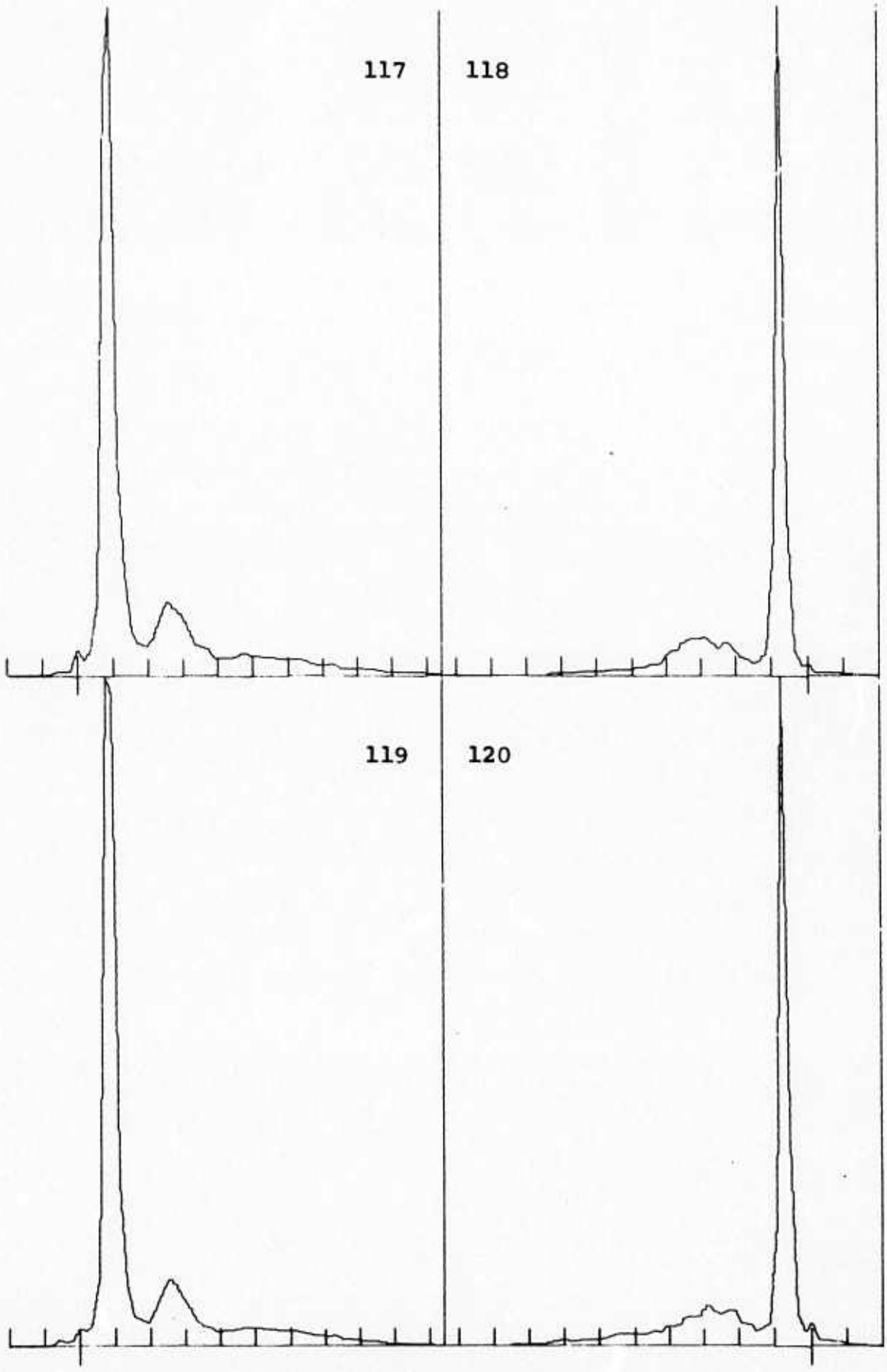
117
118
119
120

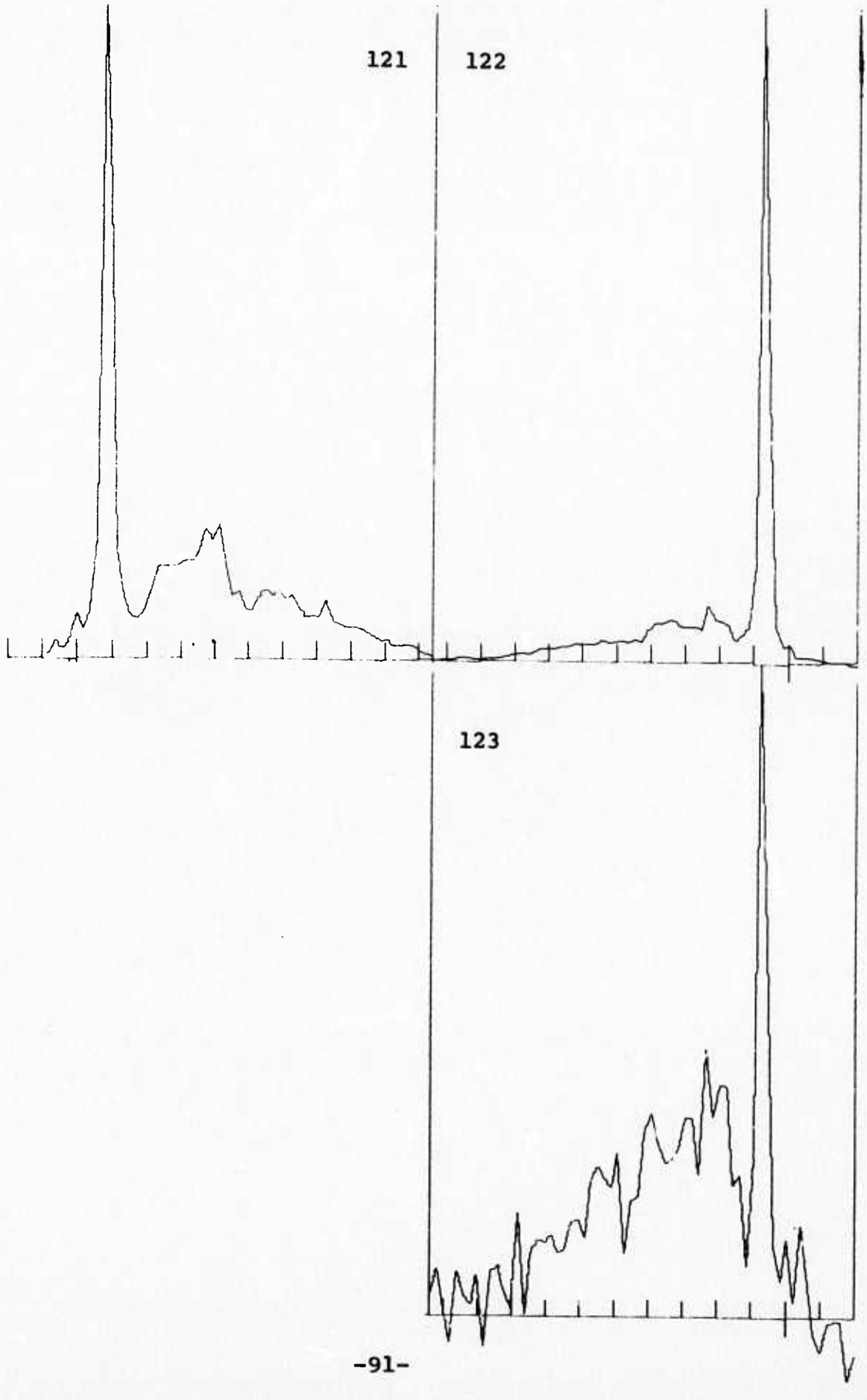
121
122
123

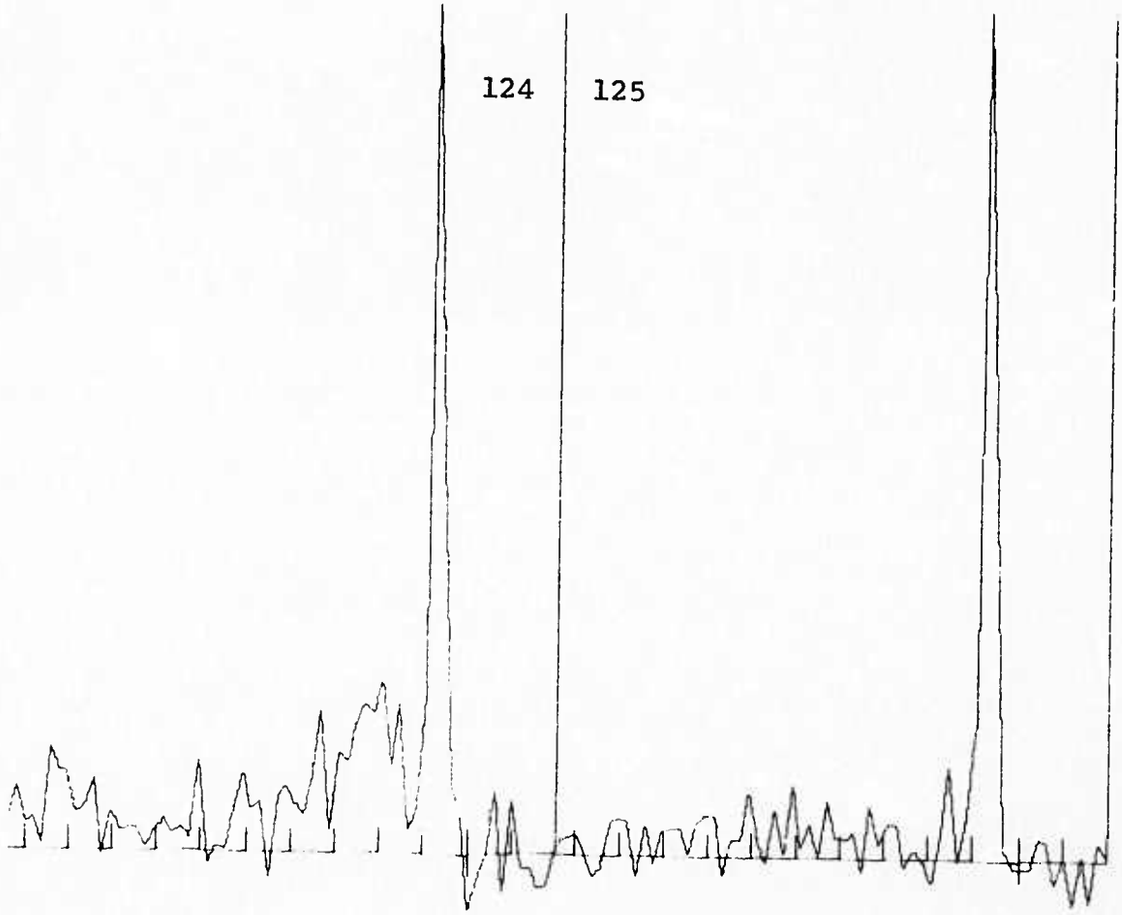
124
125

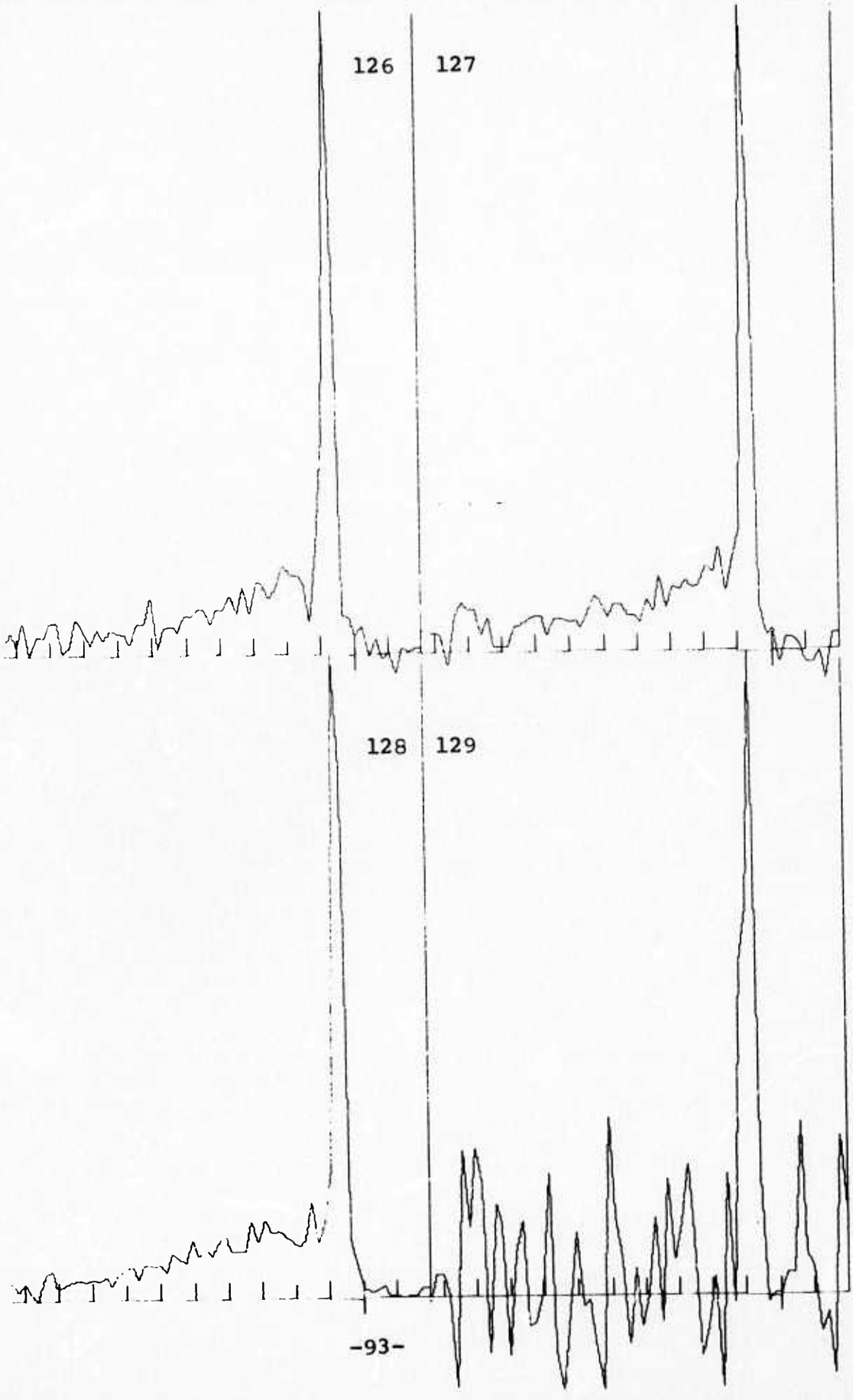
126
127
128
129

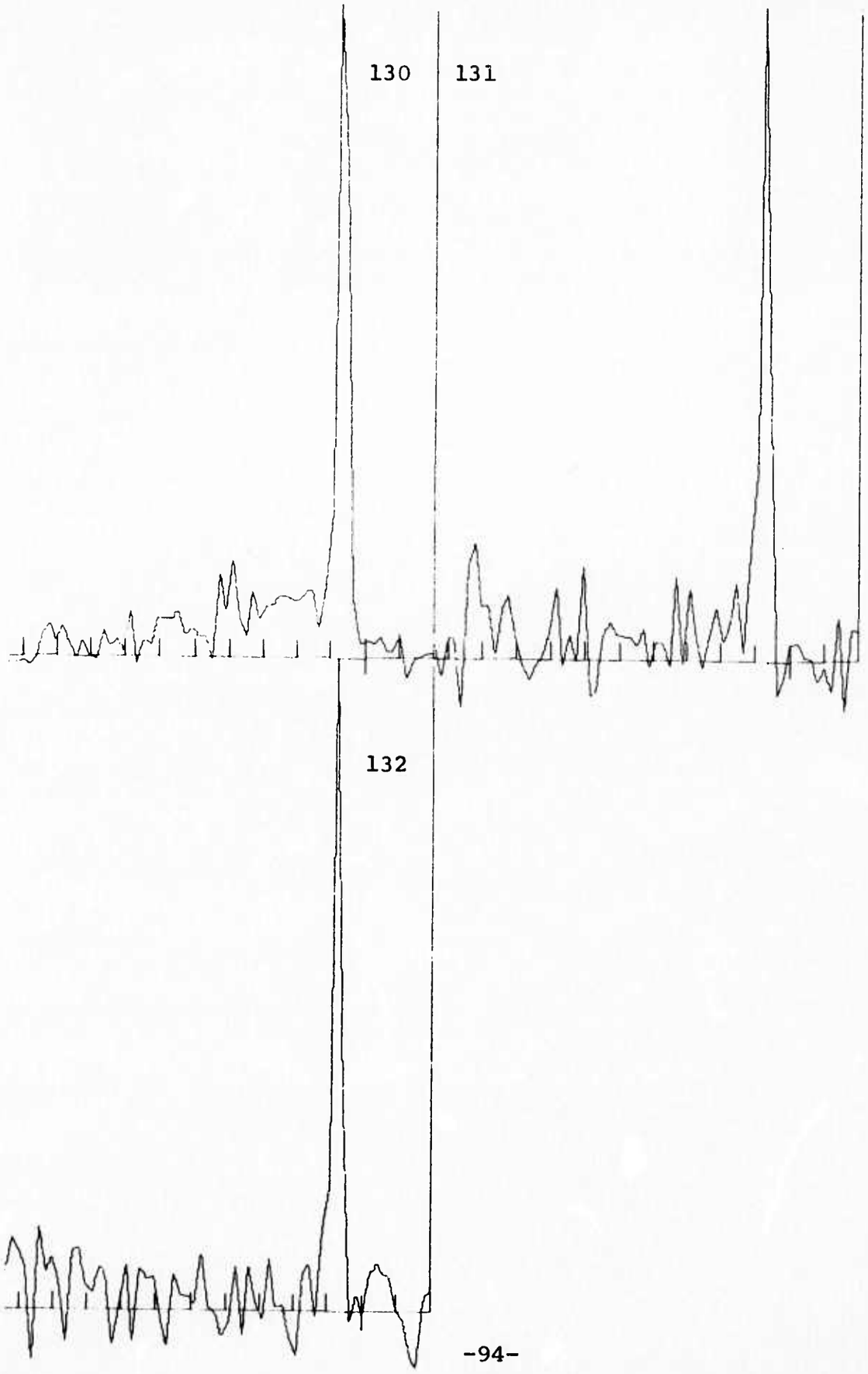
130
131
132

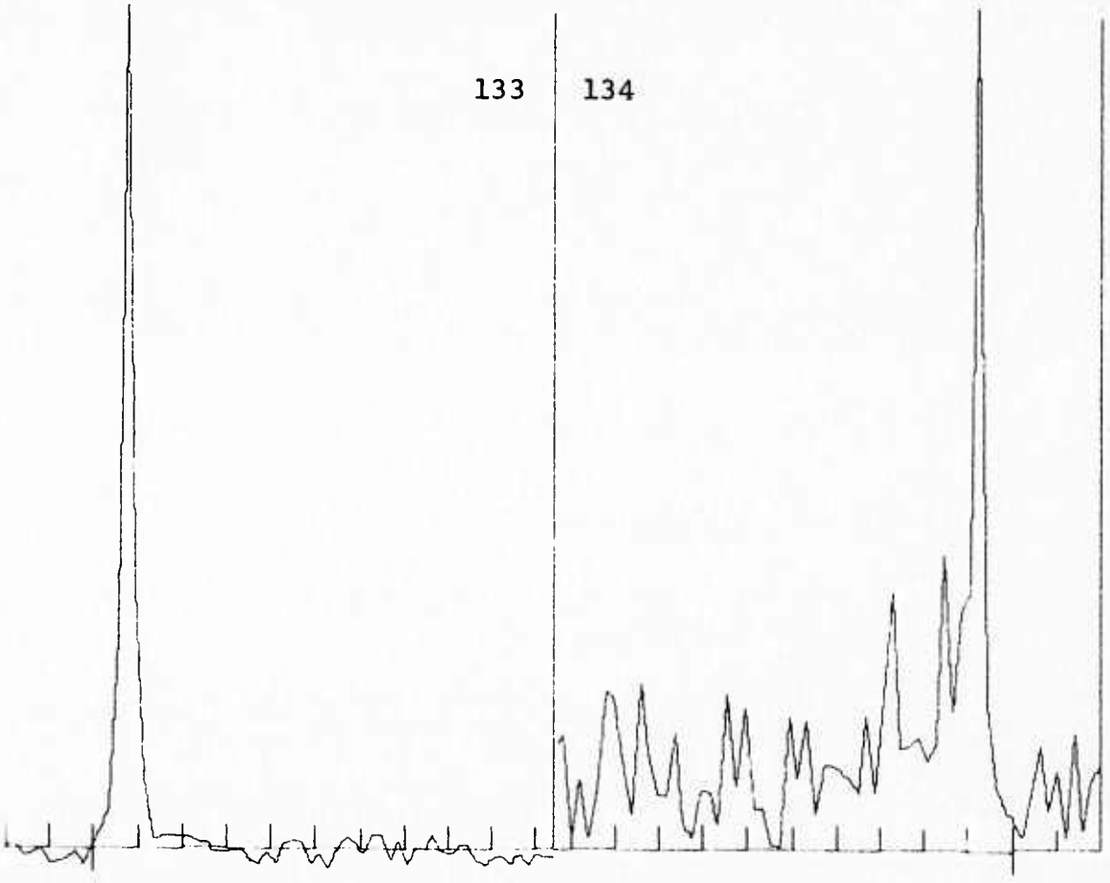
133
134

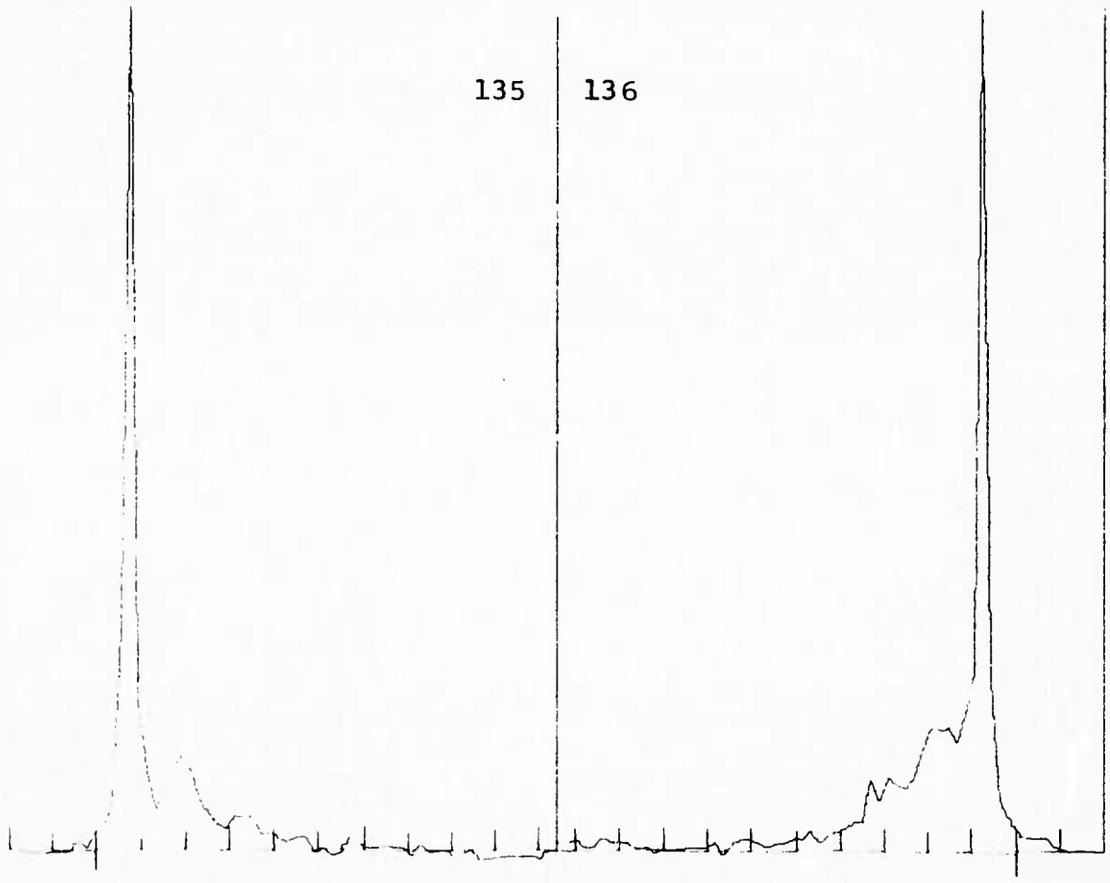
135
136

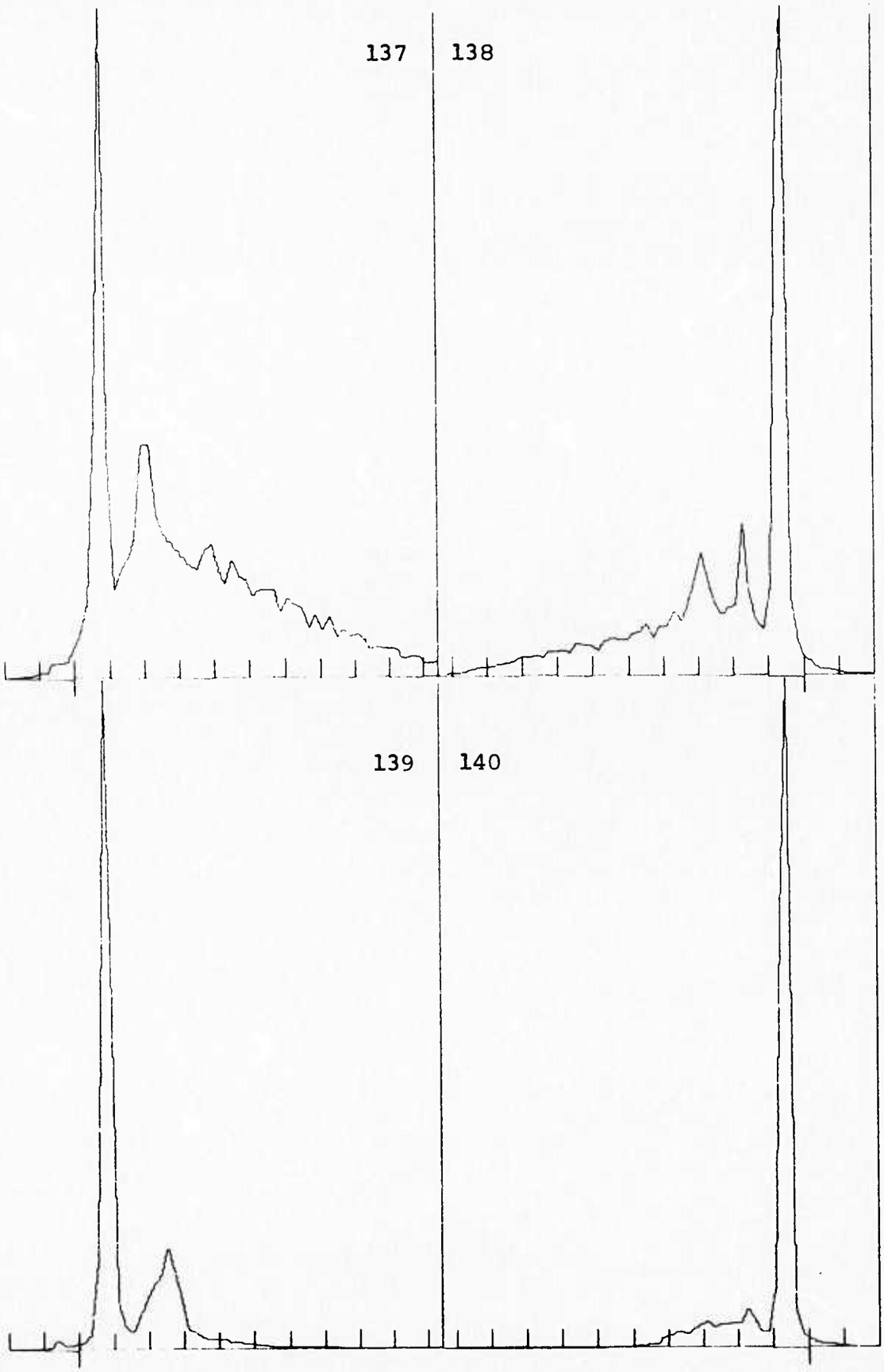
137
138
139
140

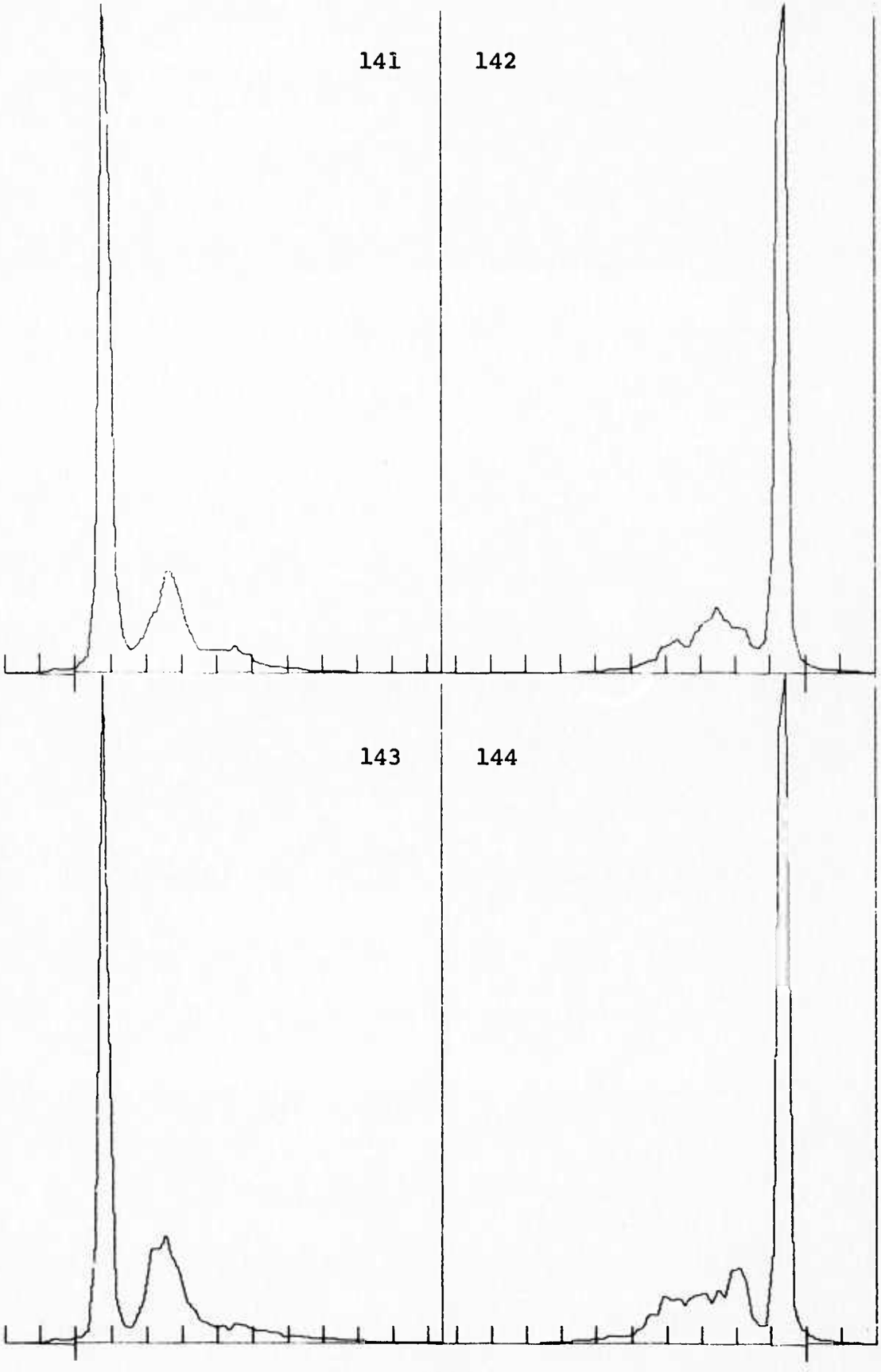
141
142
143
144

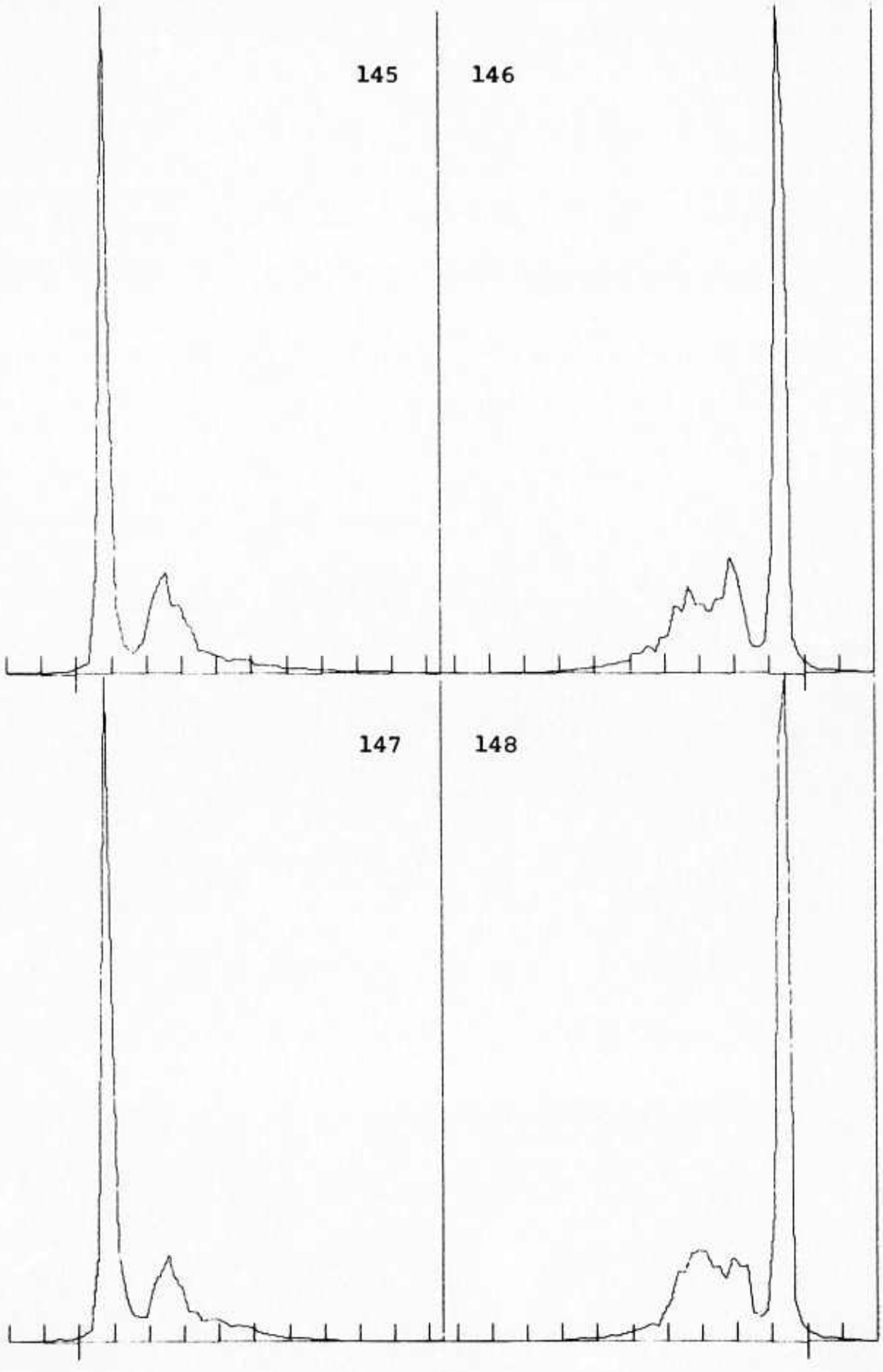
145
146
147
148

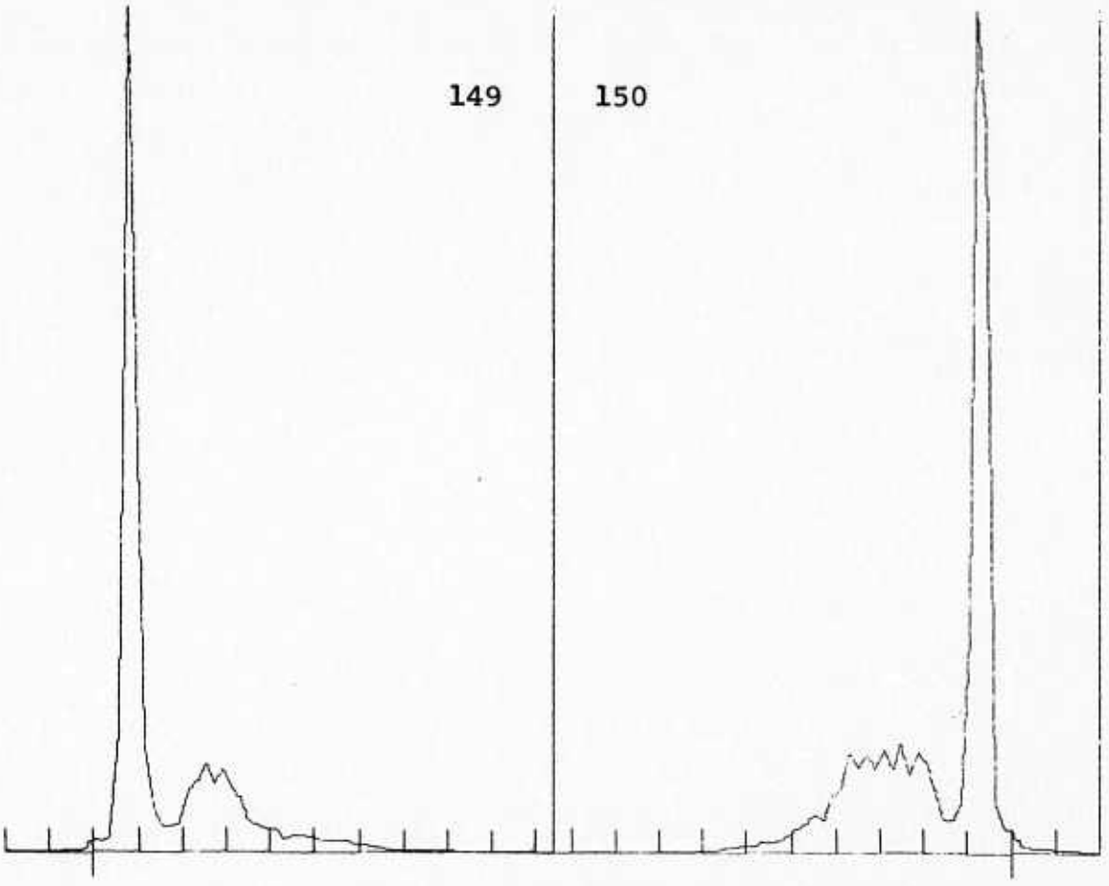
149
150